CHAPTER 2

GEOCHEMICAL SURVEY

Chapter 2. Geochemical Survey

2–1 Purpose of Survey

Geothermal manifestation which is represented by geysers, fumaroles, and hot water springs as geothermal indications on the surface is considered to be derived from the geothermal energy existing in the aquifer under subsurface condition. This energy can be used in the development of electric power derived from geothermal energy. Chemical compositions of the geothermal fluid which is composed of the water can infer the characteristics of a geothermal system.

Objectives of this geochemical exploration are to study the geothermal indications on the surface of the Puchuldiza geothermal field, to analyze the principal chemical compositions that characterize the hot water taken from the hot springs and exploratory wells, to deduce the temperature of the subsurface geothermal reservoir, and to find out the probable location of the heat source from the distribution of the altered minerals as a consequence of hot water underground circulation. Isotope analyses of the hot water and of the river water had also been made for the consideration of identifying the geothermal system.

2–2 Methods

Chemical analysis of hot water

In order to know the characteristics of the hot water around the area of geothermal manifestation, mapping on the scale of 1: 10,000 has been done for the investigation of present geothermal survey. During the survey, temperature and PH of the water have been measured. Water samples were collected in 1,000 ml polyethlene vessels. These water samples were carried back to Japan and analyzed for twelve principal elements at the Bishimetal Exploration Co. Chemical Laboratory.

Altered minerals

In the investigation of the distribution of clay minerals as product of geothermal activities, microscopic observations, and X–ray diffraction analyses were employed. In order to carry out the study, thin sections of rocks taken from each formation in the area and of some core samples from the exploratory wells were made. Core cuttings and altered rock on the surface were used for the X–ray diffraction analyses.

Equipment used and measurement conditions are as follows:

(1) Microscopic observation

1) Equipment

Orto plan. Vol (Ernst Leiz, PHO (Nippon Kogaku))

Rutomat (Photography, Ernst Leiz)

2) Observation Method

Mineral assembleges, paragenesis and texture were examined by microscopically for each thin section.

Microscopic pictures of the typical part of the samples have been taken with both parallel and cross Nicol prisms.

(2) X–Ray diffraction analyses

1) Instruments used

Philips X–ray diffractometer

2) Test procedure

The collected samples were ground to 50 – 100 mesh in a stainless steel martor. Furthermore, it was ground in the agate martor until no grit is felt by finger tips to produce non-oriented particles.

3) X–ray diffraction Conditions

Target	Cu Kα
Filter	Graphite monochrometer
Voltage	30KV
Current	30mA
Divergence slit	1^{o}
Receiving slit	0.2mm
Scanning speed	1^{o}/min
Chart Speed	1cm/min

2–3 Geothermal indications (Fig. II–2–1)

Geothermal manifestations observed on the surface are scattered in the area 10km^2 at the low places of 4,100m A.S.L in the Puchuldiza geothermal field.

The most strong geothermal activity in the area is represented by the geysers, fumaroles, mud pools and sinter terraces at Puchuldiza and Tuja.

The geothermal manifestations are closely related with the N–S, NW–SE and NE–SW trending faults that control the geological structures of the area.

(1) Puchuldiza manifestation (Fig. II–2–2)

The Puchuldiza manifestation, the biggest in the area, appears at the low place along Puchuldiza river with the reversed L shape south of Tahipicollo hills.

This manifestation is geologically located at the intersection of N–S trend branch faults derived from NW–SE trend.

Hydrothermal solution is considered to rise up to the surface along Condoriri and the NW–SE trending Puchuldiza faults system. The hot springs are in a 1.2km (N–S extension) by 1.5km (E–W extension) along the Puchuldiza river.

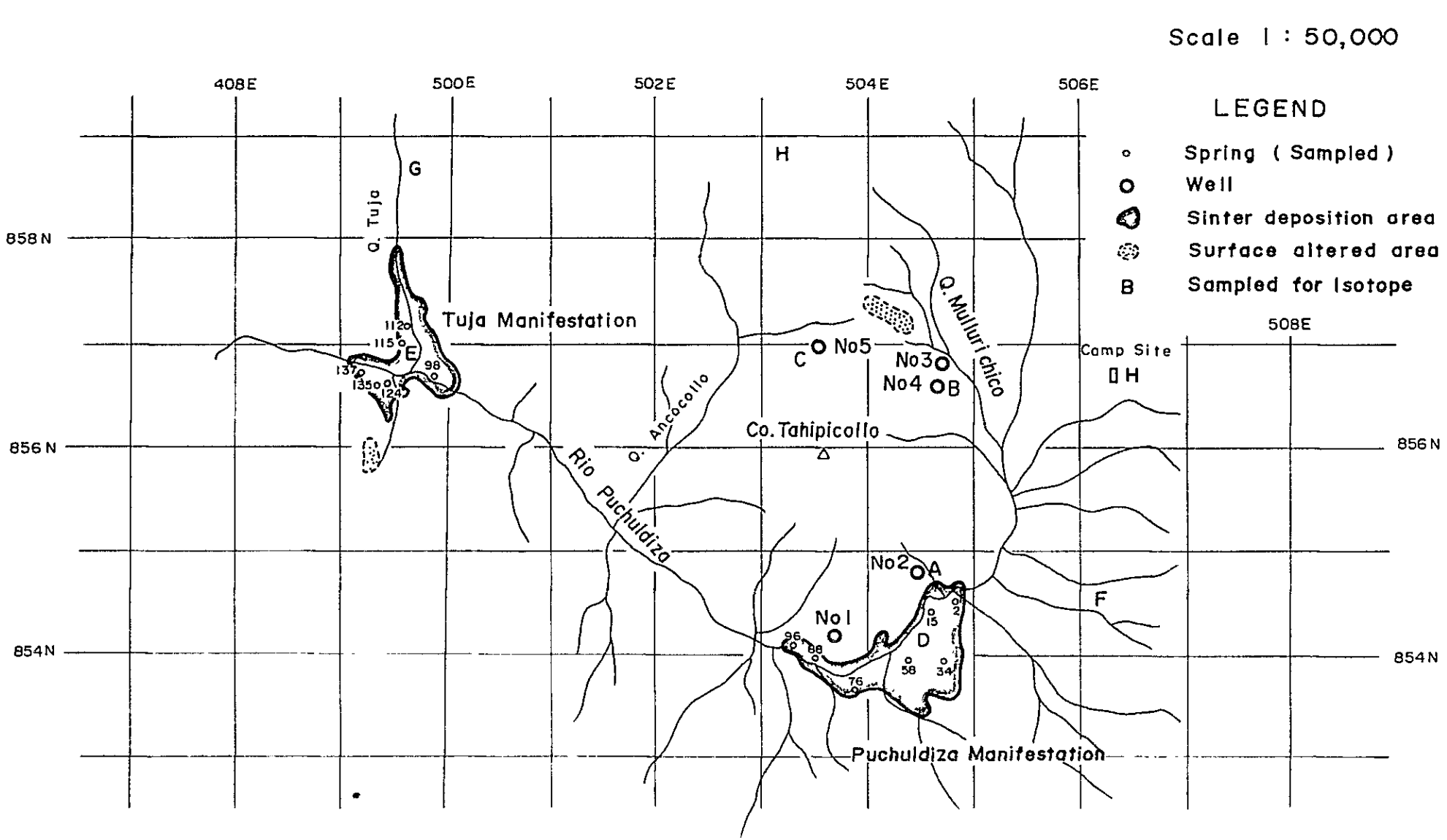

Fig. II-2-1 LOCATION OF SURFACE GEOTHERMAL ACTIVITIES AND EXPLORATORY WELLS

And about 100 geysers or fumaroles were found in the area and the total rate of water flow was measured to be about 40 liters per second at the time of survey. Chloride and silica precipitated from the spring water were found in lower level along the Puchuldiza river. The sinter terrace formed is estimated to weigh about 10 million tons.

(2) Tuja manifestation (Fig. II–2–2)

This is located in the western part of the field and comes second after Puchuldiza manifestation in scale of activity.

The thermal activity is also at the intersection of Tuja fault trending N–S and Puchuldiza fault trending NW–SE. Along the lower portions of the valleys influenced by both faults, fumaroles and geysers more than fifty in number have been observed in area of 700m (N–S extension) by 300m (E–W extension).

The rate of water flow from the geysers has been estimated to be about 20 liters per second. Silica sinters forming terraces precipitated from the spring water is about 3 million tons in weight.

(3) Other geothermal manifestations

Alterations due to the geothermal activities was observed at the low land of Mulluri Chico in the northeastern slope of Mt. Tahipicollo and at the southern extension of Tuja fault.

2–4 Altered minerals

In the geothermal field, various altered minerals have been produced due to the interaction between hot water and host rocks, form the geothermal alteration zone. In general, silicified zone is in the center composed mainly of silicate minerals such as quartz, cristobalite and tridymite surrounded by the argillized zone (mainly composed of kaolinite and montmorillonite).

The zonal distribution of the altered minerals is commonly found in the geothermal field and is understood to reflect the chemical gradient of the hot water coming up.

In this chapter, kinds of altered minerals and their distribution have been discussed based on the microscopic and X–ray diffraction studies on the samples taken for the rock formations and wells.

2–4–1 Altered zone on the surface (Table II–2–1)

Large scale alteration zone was observed in the surrounding area of Puchuldiza and Tuja manifestations while small scale alterations were found in the Mulluri Chico stream and southern part of Tuja.

Minerals detected by X–ray diffraction analyses are α–quartz, tridymite, α–cristobalite, montmorillonite, chlorite, sericite, kaoline minerals, chlorite-montmorillonite mixed-layer and alunite.

Table Ⅱ-2-1 X-Ray Diffraction Analysis of Surface Altered Rocks

Location \ Mineral		Silica			Feld.		Clay						Zeolite		Others		
		α-Qz	Tri	α-Cr	Pl	K Fel	Mon	Chl	Ser	Kao	C-M	S-M	Mor	Lau	Cal	Alu	Py
Puchuldiza N	RP02			+	+	+			+								
N	RP03					+				++							
N	RP04				++												
S	RP06			++	+	+											
E	CP34	+	+	++													
E	S3003	+++		++	+												
Q. Mulluri C	S3007	++		+++	+	+											
Tuja E	RT01		++	+	++	+			+							+++	
E	RT02		++	+												++	
W	RT03		++	++						+						+	
W	RT04		+++	+						++							
S	CT26	+			+	+		+			+						
S	S0303		+				+		+								

Qz : Quartz
Tri : Tridymite
α-Cr : α-Cristobalite
Pl : Plagioclase
K-fel: K-feldspar
Mon : Montmorillonite
Chl : Chlorite
Ser : Sericite
Kao : Kaoline
Py : Pyrite
Mor : Mordenite
Lau : Laumontite
Cal : Calcite
Alu : Alumite
C-M : Chlorite-Montmorillonite Mixed-Layer
S-M : Sericite-Montmorillonite Mixed-Layer

TUJA

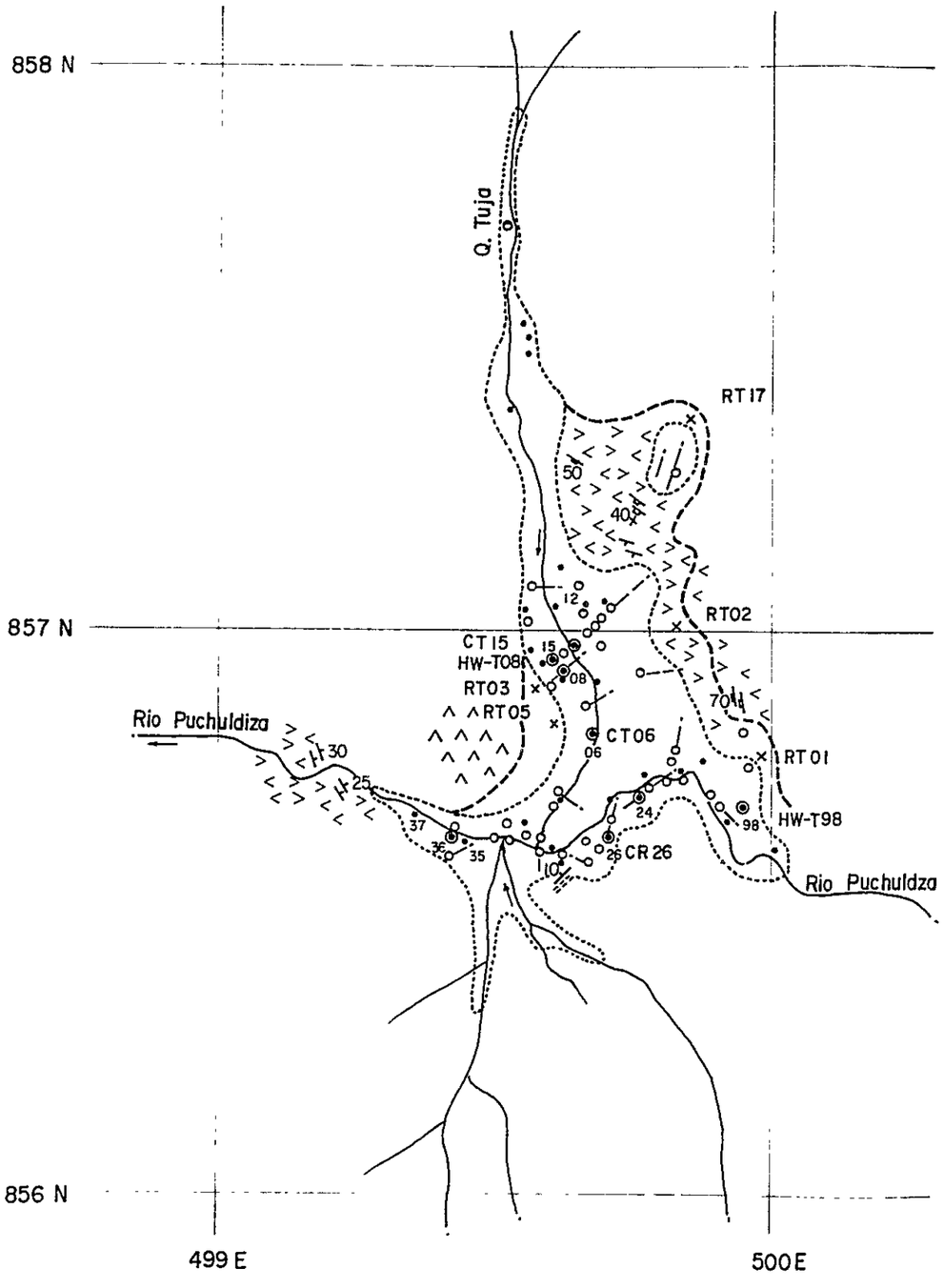

PUCHULDIZA

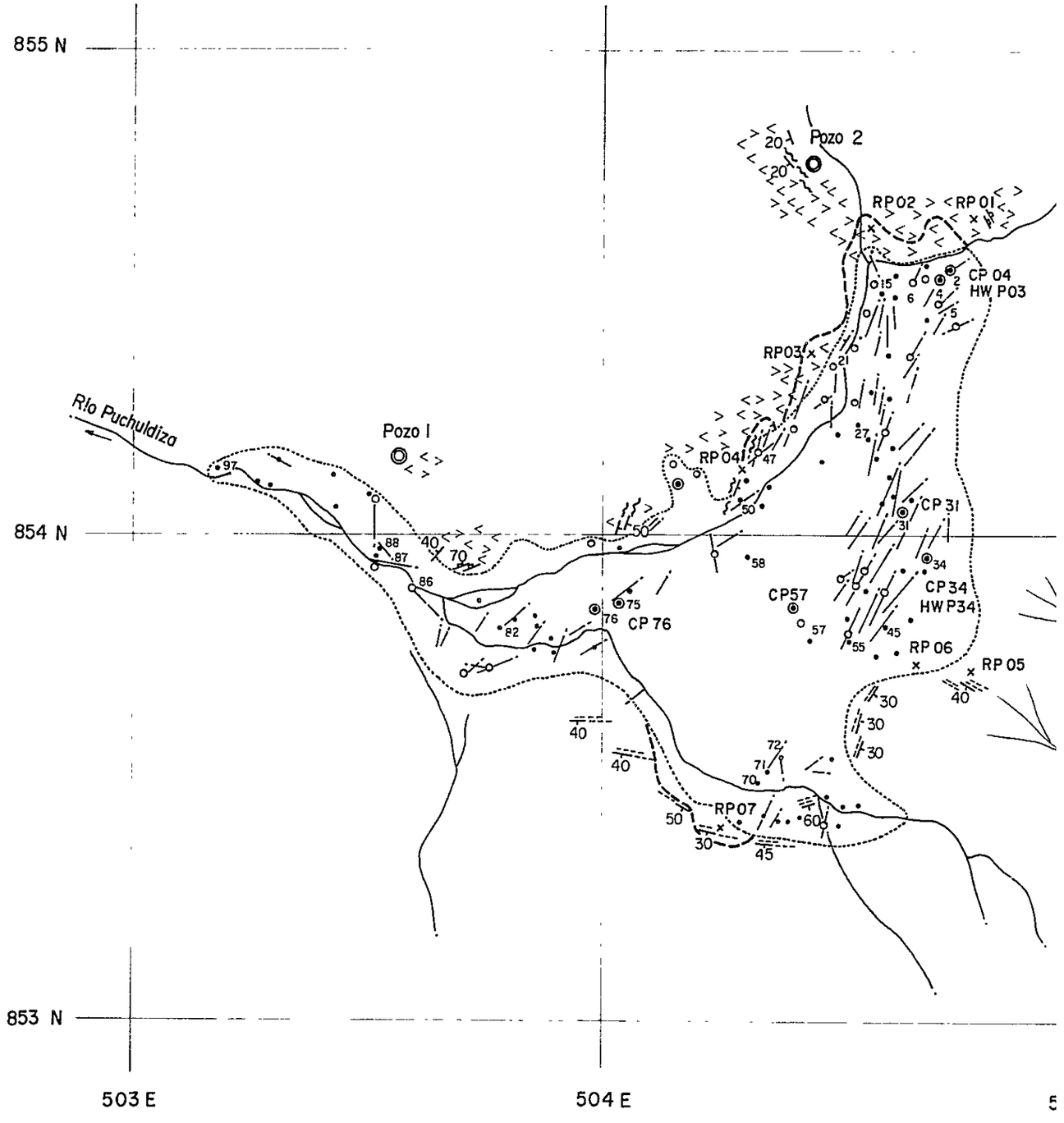

PUCHULDIZA

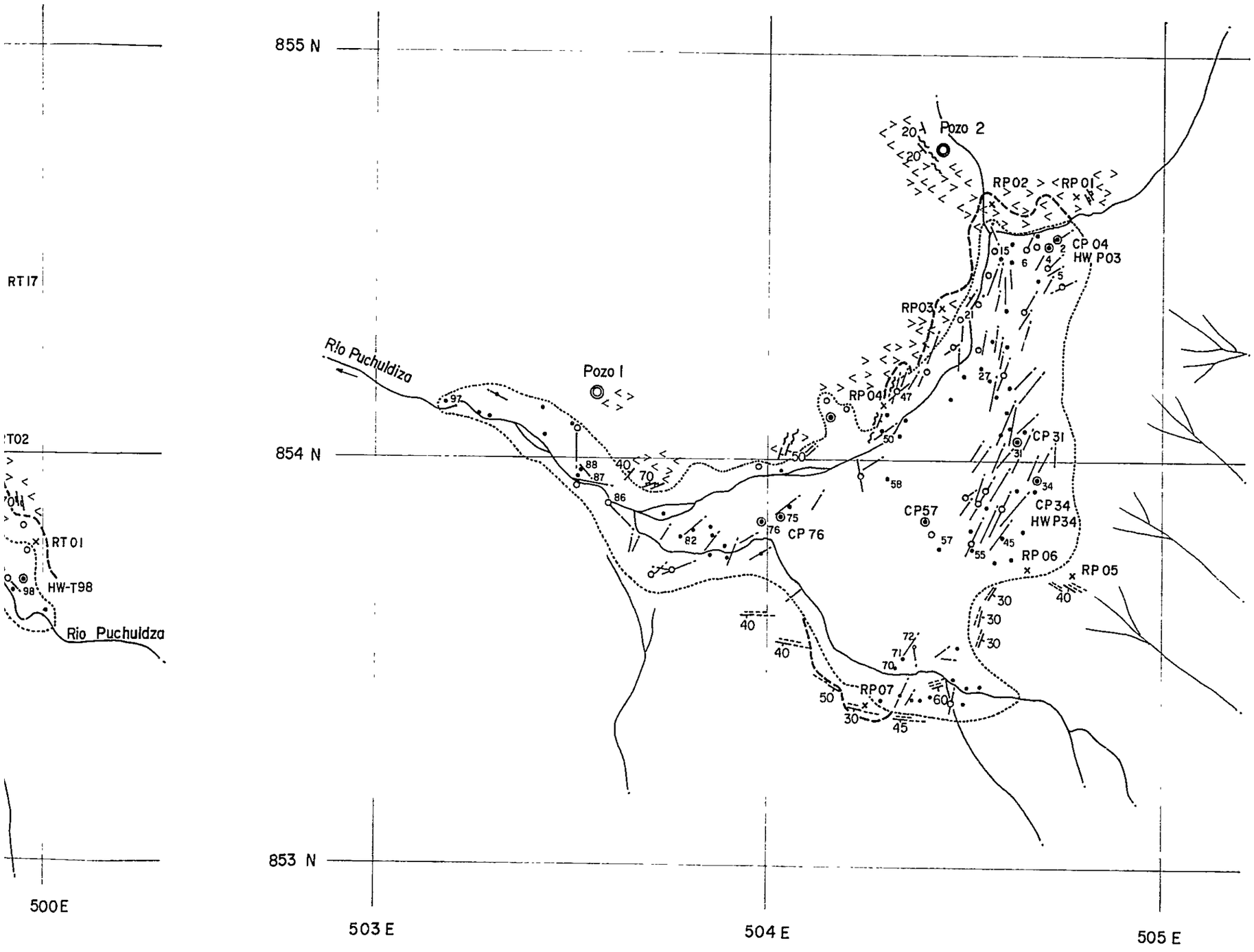

LEGEND

- Sinter deposit
- Hydrothermal alteration zone
- Sinter active strongly
- Sinter active
- Sinter
- Trend of sinter arrangement
- Location of sampling
- Gravel and terrace
- Pleistocene andesite
- Puchuldiza andesite
- Puchuldiza andesitic tuff
- Andesitic ignimbrite

Geothermal Power Development Project
in Puchuldiza
the Republic of Chile

THERMAL MANIFESTATION AT PUCHULDIZA AREA

1 : 10,000

0 500 m

Nov ~ Dec, 1978

Fig. II-2-2

(1) Puchuldiza alteration zone

Rocks derived from Puchuldiza andesite were sampled on the southern slope of Mt. Tahipicollo toward well No. 1 to well No. 2. Altered minerals are α–cristobalite, sericite and montmorillonite mixed layer mineral. No clay minerals were detected in samples taken near the well No. 2.

On the other hand, in the altered zone of Churicollo formation located in the southern slope of the geothermal area, α–cristobalite, montmorillonite and chlorite were found. To the south of the area, α–cristobalite only was detected but no clay mineral.

(2) Mulluri Chico stream alteration zone

α –quartz and α–cristobalite were detected with no clay mineral.

(3) Tuja alteration zone

Silicate minerals such as tridynite and α–cristobalite were commonly recognized with α–quartz in the samples taken from the south and west of the geothermal altered zone. Clay minerals of sericite and chlorite were recognized in the east and south, and kaolinite was noted in the west.

Only in this area was alunite found in association with α–cristobalite. In view of this sulphate activity must have dominated in the past.

(4) South Tuja alteration zone

Tridymite, montmorillonite and sericite were recognized in the area.

2–4–2 Examination of the drilling cores and cuttings

In order to know the mineral assemblages of the altered minerals of the drilling cores and its cuttings, microscopic observation and X–ray diffraction analyses were done except for well No. 3. Core samples were employed for the thin section. Cutting and core samples taken every 100m interval for X–ray diffraction analyses.

(1) Microscopic observation

Due to the scarcity of drilling core, the samples were selected from the deeper portions of the wells for the microscopic observation. White tuff belonging to Condoriri formation is volcanic clastics comprising crystal of quartz, K–feldspar and plagioclase. Alteration is specially seen in volcanic glasses and shows strong sericitization and argillization. Kaolonization and silicification are also observed. Utayane formation occuring in the deeper part of the wells is composed of dacitic tuff. Welded tuff has phenocrysts of primary feldspar but mafic minerals are altered to chlorite, calcite and other green color clay minerals. Groundmass is replaced also by sericite or sericite-montmorillonite mixed layer minerals. Film veins composed of quartz, calcite and sericite have been observed in the thin section.

(2) X–ray Diffraction Analysis (Table II–2–2, Fig. II–2–3 ∿ II–2–5)

In order to know the distribution of altered minerals around geothermal area, X–ray diffraction method has been carried out using drilling cores and drill cuttings.

Churicollo F. Pozo-4 (310m)

Vitric-crystal Tuff
(altered)
x 33
Open nicols

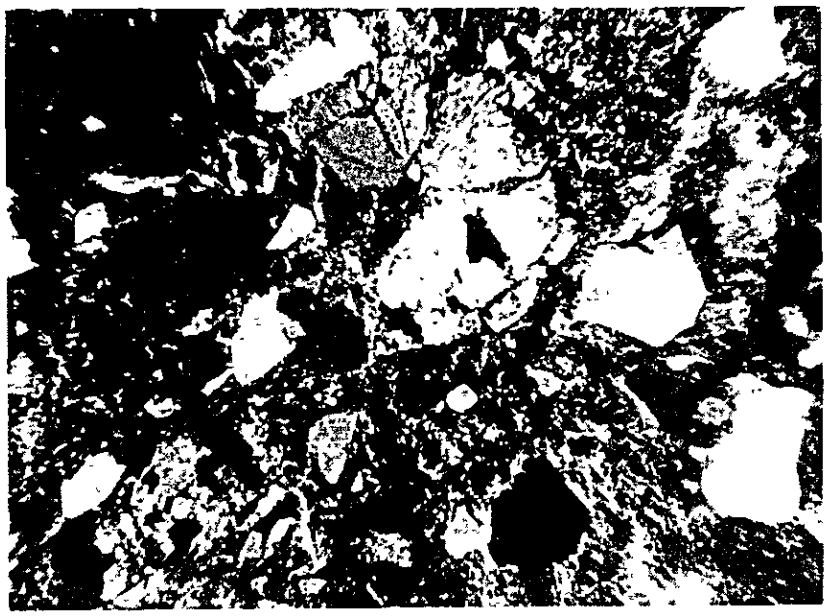

do
Cross nicols

Rhyolitic pyroclastic rock containing crystal fragments of quartz , potash-feldspar and plagioclase. Alteration (sericitic argillization , kaolinization and silicification) is remarkably recognized in volcanic glass.

Photo : Photo is showing mainly sericitic argized part.

Utayane F. Pozo-4 (945m)

Dacitic Welded Tuff

(altered)

x 33

Open nicols

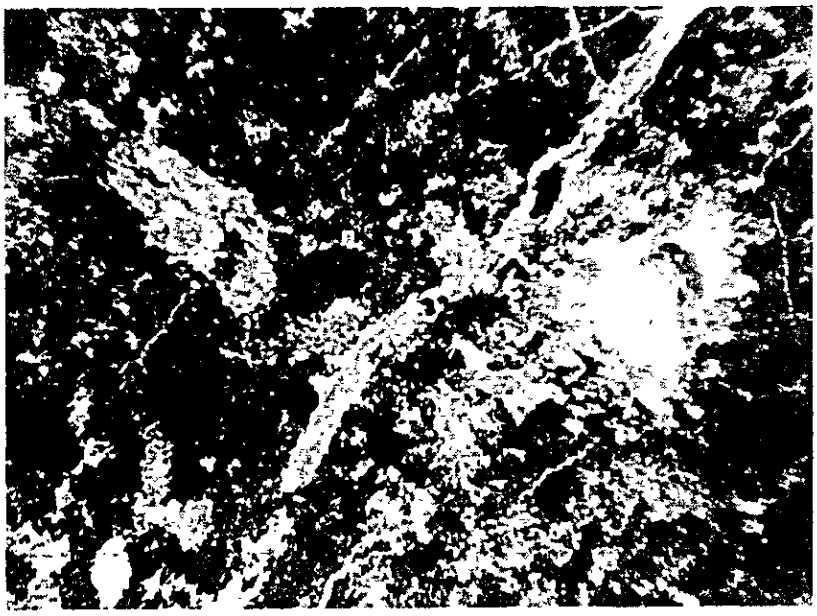

do

Cross nicols

Welded tuff containing crystal fragments of feldsper highly altered into aggregate of sericite and calcite and composed of silicified matrix.

Photo : Phenocryst is altered feldspar, showing the outline of feldsper. Phenocryst on the right contains aggregate of calcite.

Vein is composed of quartz and sericite.

Table Ⅱ-2-2 X-Ray Differaction Analysis of Cores and Sludges from Exploratory Wells

Mine. Well	Depth (m)	Silica			Feldspar		Clay						Zeolite		Others		
		α-Qz	Tri	α-Cr	Pl	K Fel	Mon	Chl	Ser	Kao	C-M	S-M	Mor	Lau	Cal	Alu	Py
No.1	100			+	+	+						+	+				+
	153			+	++	+			+				+				+
	200	+		++	+	++			+	+							+
	300			++	++	+				+		+					+
	400	++		++	+	+				+		+					+
	500	++		++	+	+						+					+
	600	++		++	++	+						+					+
	647	+++				+			+	+							
	695	+++				+			+	+					+		
No.2	100			++	+							+			+		
	200	+++		++		+						+			+		+
	300	+++			+	+		+	+						+		
	400	+++			+	+		+	+						+		
	500	+++			+	+		+	+								
	522	+++			+	+		+	+								
	648	+++						+	+			+					
No.4	100		+		++	+	+								+		
	200	++			++	+											
	300	++	+		+	++			+								
	400	+++			++	+		+	+								
	500	+++			+	+		+	+								
	600	+++			+	+		+	+								
	700	+++			+	+		+	+								
	951	+++				+			+								
No.5	100	++	+	++	++	++											
	200			++	++	+	+										
	300	+++		++	++	+											
	400	+++			++	+			+								
	500	+++			+			+	+								
	600	+++			+	+		+	+								
	680	+++			+	+		+	+								
	850	+++			+			+	+								
	951	+++			+			+	+								
	1012	+++			+	+		+	+								

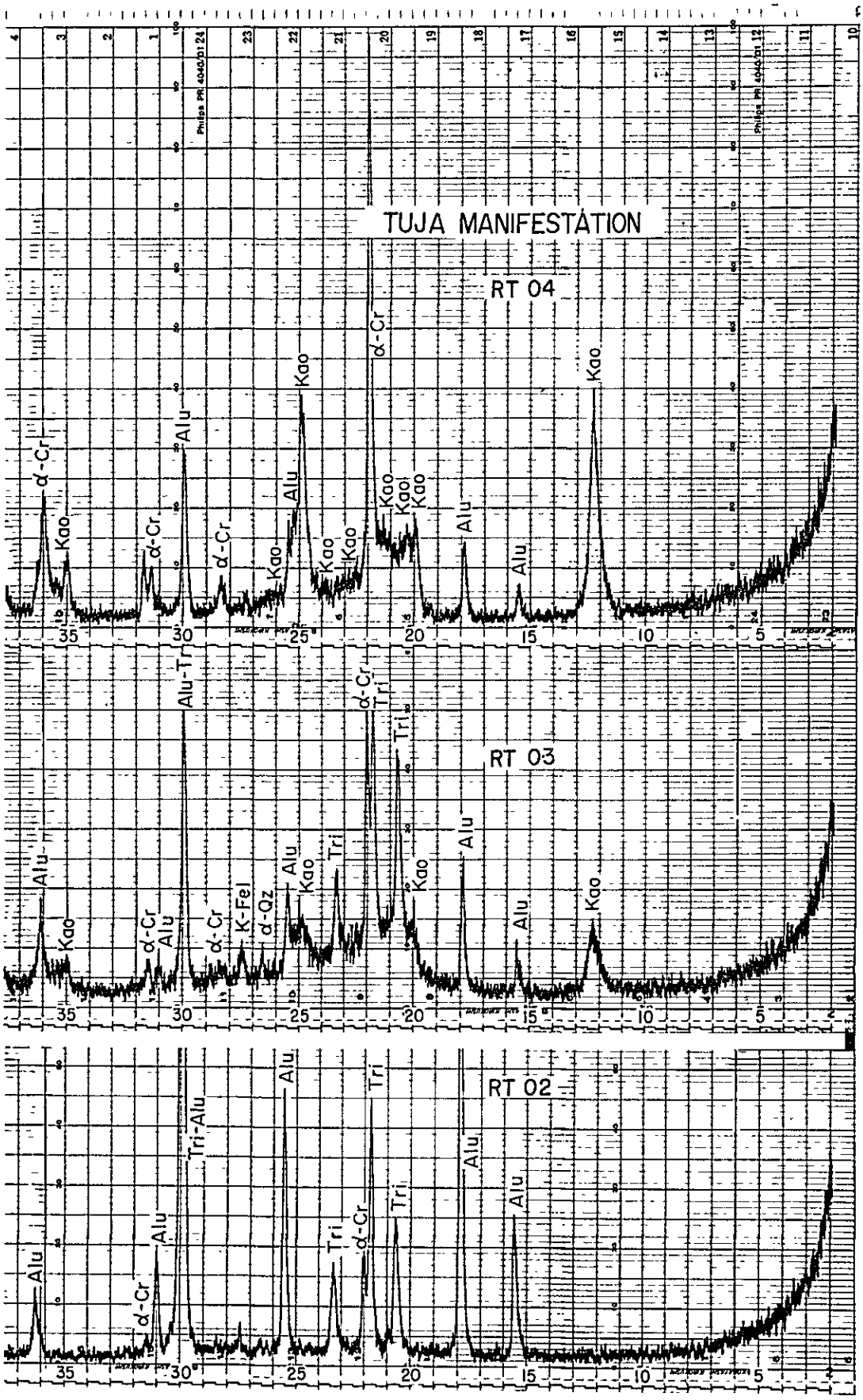

Fig. II-2-3 X-ray diffraction (TUJA)

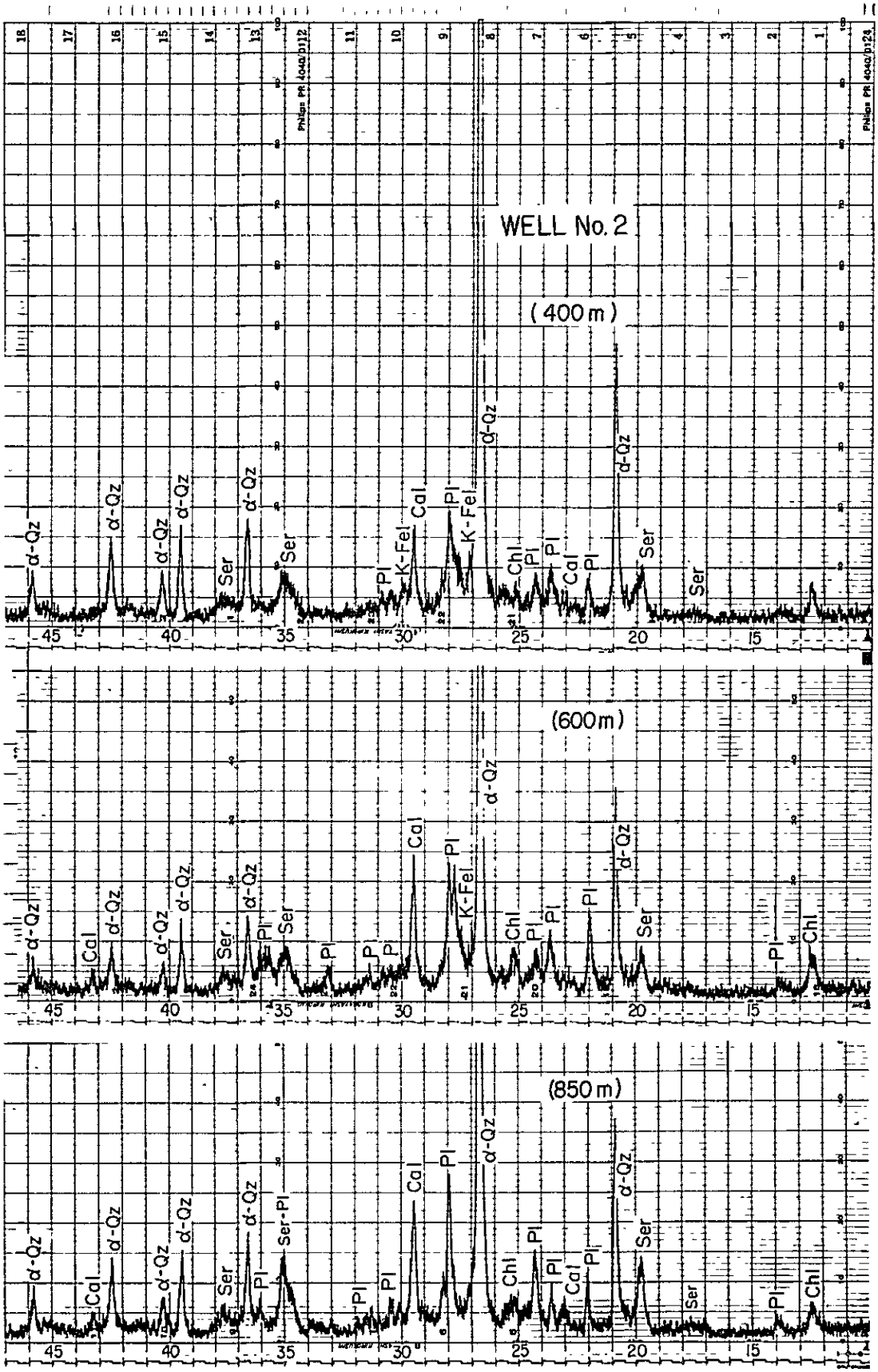

Fig. II-2-4 X-ray diffraction (Well No.2)

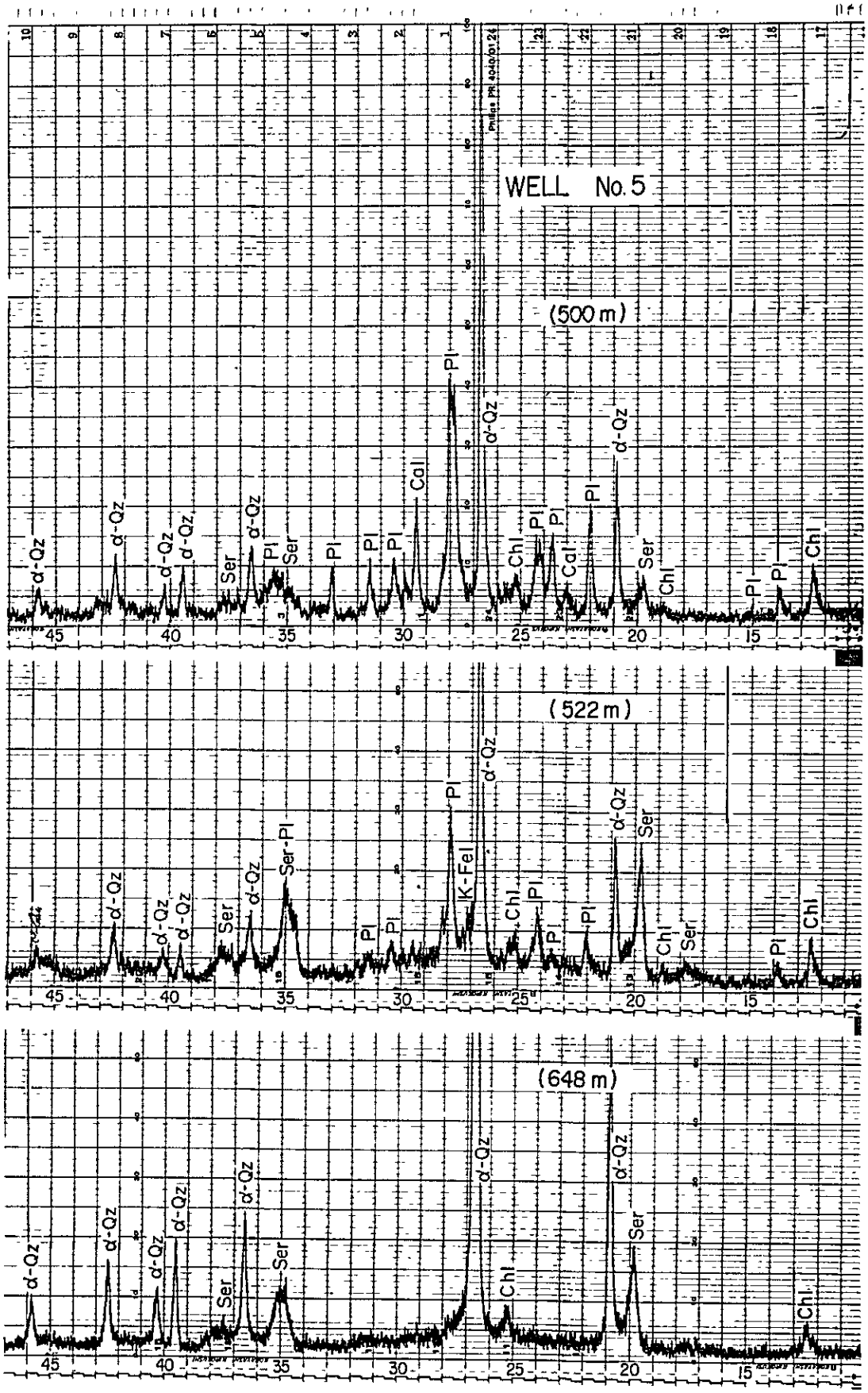

Fig. II-2-5 X-ray diffraction (Well No.5)

Detected minerals are silicate minerals of α–quartz,tridymite and α–cristobalite, and clay minerals of montmorillonite, chlorite, sericite, kaolinite and sericite-montmorillonite mixed layer. Zeolite minerals of mordenite were present in the shllower part of well No. 1. Carbonate mineral of calcite was noted in all wells except well No. 1. Considering from the mode of occurence of altered minerals detected by X–ray diffraction, the aquifer temperature can be estimated.

α–quartz of silicate minerals is commonly seen in the deeper part of the wells but of lesser amount from the surface to 300m depth for well No. 1. The mineral is not detected down to 100m depth for well No. 2 and No. 4.

On the other hand, α–cristobalite which commonly appears in the low temperature altered zone is usually found down to the depth of 600m in well No. 1 and in the shallow depth of well No. 5. Tridymite is slightly recognized in the shallow portion of well No. 4 and No. 5.

Of the clay minerals, montmorillonite is found in the shallow portion of well No. 4 and No. 5 while chlorite and sericite generally appear in all the wells except at the shallow portion of well No. 1. Montmorillonite mixed layer and kaolinite are found in well No. 1 only.

Of the zeolite minerals, mordenite occures in the shallow portion of well No. 1. Lumontite, wairakite, and pyrophyllite which are high temperature altered minerals were not present in all wells.

2–5 Chemistry of hot spring water

Hot spring waters in the area were analyzed in detail by Dr. Herman Cusicanqui and CORFO determination of the chemical composition of the hot spring water. In this survey, the analysis was limited to the main composition in order to check some known data from selected typical samples. In addition to the main chemical composition, As and I elements were examined for comparison with hot water spring in Japan.

As stated in section 2–3, in view of the large amount of silica sinter deposits and the volume of water outflow, it concluded that activity of the present geothermal area would have been very strong in the past. Geyser is located 4,200m above sea level, and therefore, the average atmospheric pressure and boiling point of water are 85.5°C respectively.

Surface rock alteration due to the hot water is observed to be steeply weak as the distance from the water gushing points increases. It is considered that geothermal fluid rise to the surface through the fault zone and are not scattered at random because the surface is covered with less porous and permiable Puchuldiza andesite.

The result of chemical analysis is shown in Table II–2–3. According to the table, the nature of hot spring is classified as neutral NaCl type.

Table II - 2 - 3 Chemical Composition of Hot Water in Puchuldiza Geothermal Area

	No.	Temp. (°C)	pH	TSM	Na (mg/l)	K (mg/l)	Ka (mg/l)	Mg (mg/l)	As (mg/l)	Fe (mg/l)	B (mg/l)	I (mg/l)	Cl (mg/l)	SO_4 (mg/l)	HCO_3 (mg/l)	SiO_2 (mg/l)
Puchuldiza	2	82	7.78		1,380	167	85	2.54			92.6		2,308	114	261	260
	Po 4*	86	7.01	4,905	1,540	205	59.5	3.80	14.41	0.08	66.9	1.04	2,297	219	298	416
	15	86	7.49		1,520	207	35	0.96			99.0		2,462	126	195	320
	34	86	7.49		1,650	223	20	0.30			108		2,704	130	200	363
	58	86	8.06		1,575	208	43	1.10			102		2,543	133	261	347
	76	86	6.66		1,483	164	25	0.70			98.0		2,439	114	154	272
	88	65	6.38		1,487	142	56	1.46			97.0		2,416	115	116	250
	96	50	6.26		1,030	97	47	17.4			70.0		1,720	82	213	205
Tuja	98	86	7.17		1,600	124	82	1.16			115		2,704	94	89	277
	TO 5*	86	7.46	6,435	1,924	177	66.8	4.20	18.93	0.08	95.7	3.86	3,067	204	114	502
	112	86	7.17		1,844	251	50	0.44			137		3,140	113	86	322
	115	86	7.96		1,775	157	62	0.36			125		2,981	114	87	292
	124	86	7.08		1,550	126	71	3.92			111		2,599	92	49	245
	135	86	8.03		1,265	100	53	0.14			87		2,073	82	83	267
	137	86	7.85		1,250	122	70	6.66			89		2,098	76	90	311
Exploratory Well	1		6.32		1,560	70	41	2.70			71		2,198	205	453	203
	2		8.33		1,660	231	18	1.00			88		2,674	120	236	340
	Pz 2*		8.21	5,440	1,754	232	14.6	2.90	14.65	0.07	95.4	4.54	2,718	219	220	584
	4		7.65		1,290	143	25	1.62			60		1,800	237	378	163
	Pz 4*		8.14	4,355	1,460	175	23.1	4.40	12.43	0.27	65.9	3.55	2.242	211	223	348
	5		7.60		1,125	105	42	0.70			55		1,690	162	262	270

* Sampled by Japanese Survey Team

Considering in general that hot water gushing out on the surface comes from the subsurface geothermal fluid and if geothermal fluid is emanated from volcanism, the hot water should be acidic.

Therefore, the presence of neutral NaCl type hot water is more of a product of interaction between acidic hot water and host rocks.

On the genesis of neutral NaCl type hot water, however, there is a theory that huge amount of salt can be dissolved in the water under high temperature and high pressure condition in the depth.

In this area, the difference of main chemical compositions of hot water between Puchuldiza and Tuja manifestations have not been observed. It is seemed, therefore, that the geothermal fluid in both area may have a common heat source and that hot water flowing to the different places in the surface through chemically similar host rocks. Main chemical compositions between the waters from exploratory well and hot spring on the surface have less differences, however, SO_4 and HCl_3 contents are more in the hot water from the exploratory wells.

Where fluids from geothermal convection systems have reached the surface through springs or wells, the chemical and isotopic compositions of these fluids may indicate the subsurface temperature and flow patterns, as well as the recharge source, type of reservoir rock, and other important parameters of the system. Component concentrations or ratios that can be related to subsurface temperature are called geothermometers. According to Ellis and Fournier, quartz of neutral NaCl type hot water in geothermal reservoir is in equilibrium with the surrounding rocks, and therefore, silica content in the discharged water may indicate the geothermal reservoir temperature. Fig. II–2–6 shows that Founier and Truesdell presented a theoretical curve where the underground temperature can be estimated from the solubility of silica dissolved in the heated water. From high temperature experiment of K–Feldspar and Na–Feldspar, the ratio of Na and K is suggestive of the underground temperature.

Na, K, and Ca can be used for geothermometry as a tool for locating and evaluating prospective area for geothermal development. The method employs the results of Founier and Truesdell (1973) who found that Na–K–Ca data can be used to determine the last temperature at which water–rock equilibrium was attained. For most natural waters, Fournier and Truesdell found that a plot of the function F(T) defined as

$$F(T) = \log (Na/K) + \beta \log (\sqrt{Ca}/Na) \quad \ldots\ldots (1)$$

against the reciprocal of absolute temperature in clustered around a straight line. In equation (1), concentrations are expressed in molality and $\beta = 1/3$ of $4/3$ depending

whether the last water rock equilibrium occurred above or below 100°C and F(T) is converted to temperature (°C) using the equation (based on Fournier and Truesdell 1973)

$$T(^{o}C) = \frac{1647}{2.24 + F(T)} - 273.15$$

Thus, the only data required to estimate the temperatures expected in a geothermal system are Na–K–Ca analyses from samples of the geothermal fluid.

From the above mentioned-methods, the temperature of geothermal fluids in the reservoir was estimated as shown in Table II–2–4.

Table II–2–4 Chemical Geothermometer

Location	SiO_2	Na/K	Na.K.Ca
Puchuldiza	190	203	225
	214	220	231
Tuja	190	175	207
	227	177	211
Well No. 2	201	215	227
	238	219	249
Well No. 4	164	205	225
	202	206	234

Lower : Sampled by Japanese survey team

Unit : ^{o}C

2–6 Isotopic Study

Isotopic compositions of geothermal fluids have been used to indicate sources of recharge, time of circulation, fluid mixing, and subsurface temperatures.

On the origin, movement, and mixing of water, the study of D/H and $^{18}O/^{16}O$ plays an important role. Table II–2–5 and Fig. II–2–7 show the data on D/H and $^{18}O/^{16}O$ of the natural water, hot spring water, and discharged water from the geothermal wells.

Table II–2–5 Deutrium: Hydrogen and $^{18}0$: $^{16}0$ Ratios

Sample No.	Location	$\delta\,^{18}0$	δD
A	Well No. 2 (flushing)	–10.5	–90.3
B	Well No. 4 (flushing)	–11.6	–90.5
C	Well No. 5 600mB.G.L.	–12.0	–99.0
D	Hot water from Puchuldiza	–10.4	–89.5
E	Hot water from Tuja	– 9.6	–91.7
F	Stream water from Condoriri	–14.0	–102.3
G	Stream water from Tuja	– 9.9	–81.0
H	Well water at Camp Site	–13.6	–88.9
I	Rain from Co. Blanco (Stagnant water on the surface)	– 4.6	–50.0

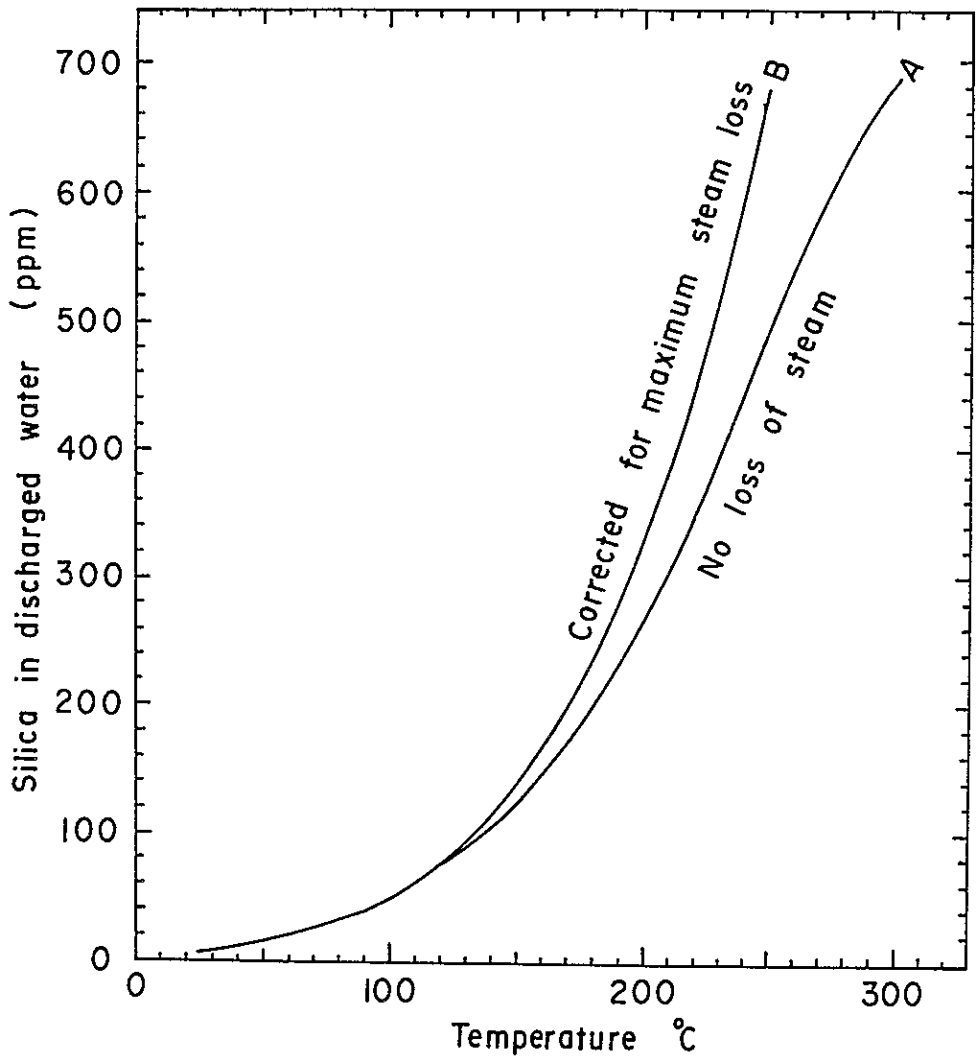

Fig. Ⅱ-2-6

RELATIVE CURVE BETWEEN TEMPERATURE AND SOLUBILITY OF SILICA

(1) Isotopic study of natural water

Sample No. F was taken from the river water on the western slope of Condoriri, and No. H was from the well for potable water at the camp site. The data of these samples lie in coincidence with the line of $\delta D = 8.\delta\ ^{18}0 + 10$. In general, it is difficult to estimate the representative value of surface water in some area, however, sample No. H which is shallow ground water is considered to be representative one. Sample No. 1 is stagnanted rain water taken from a rock pit near the top of Mt. Blanco, highest mountain in the area. In surface water the isotopic ratios increase gradually because of evaporation.

In this case isotopic value moves toward right on the line with gradient 5.0 in the δ D vs $\delta\ ^{18}0$ diagram as shown in Fig. II–2–7.

Sample No. G and No. I are connected to No. F and No. H by the line with gradient 5.4.

As mentioned above, the origin of Sample No. I is considered to be rain water, however, the rain in the low latitude and dry climate area is usually heavier than original ground water because of evaporation effect in downward movement, and is also considerably changed by prolonged evaporation.

(2) Isotopic study of geothermal water

Isotopic ratios of hot waters, as shown in Fig. II–2–7 indicate that geothermal fluid was a product of the interaction of surface water and host rocks in the subsurface. No. C among the hot water samples was taken using KLYEN surface sampler at the 600m depth of the exploratory well No. 5. From the isotopic ratio of this sample, No. C could be considered representative geothermal water in the area, because of no change in δ D. Only a shift in oxygen was noted.

Isotopic ratios of hot water generally change by evaporation.

In the case of 100°C evaporation, change of ratio moves toward up–right direction of the line with gradient of about 2. Due to the evaporation of the steam during sampling, isotopic ratios of Sample No. A, No. B, No. D and No. E had been made heavier than that of No. C which is considered the representative geothermal water in this area.

From the above results, the isotopic ratios of the surface water are as follows;

$\delta^{18}0 \fallingdotseq -14$ ‰

$\delta D \fallingdotseq -100$ ‰

The geothermal fluid is the product of the interaction between the surface water and the host rocks, as shown by 1.7 ‰ of oxygen shift in No. C.

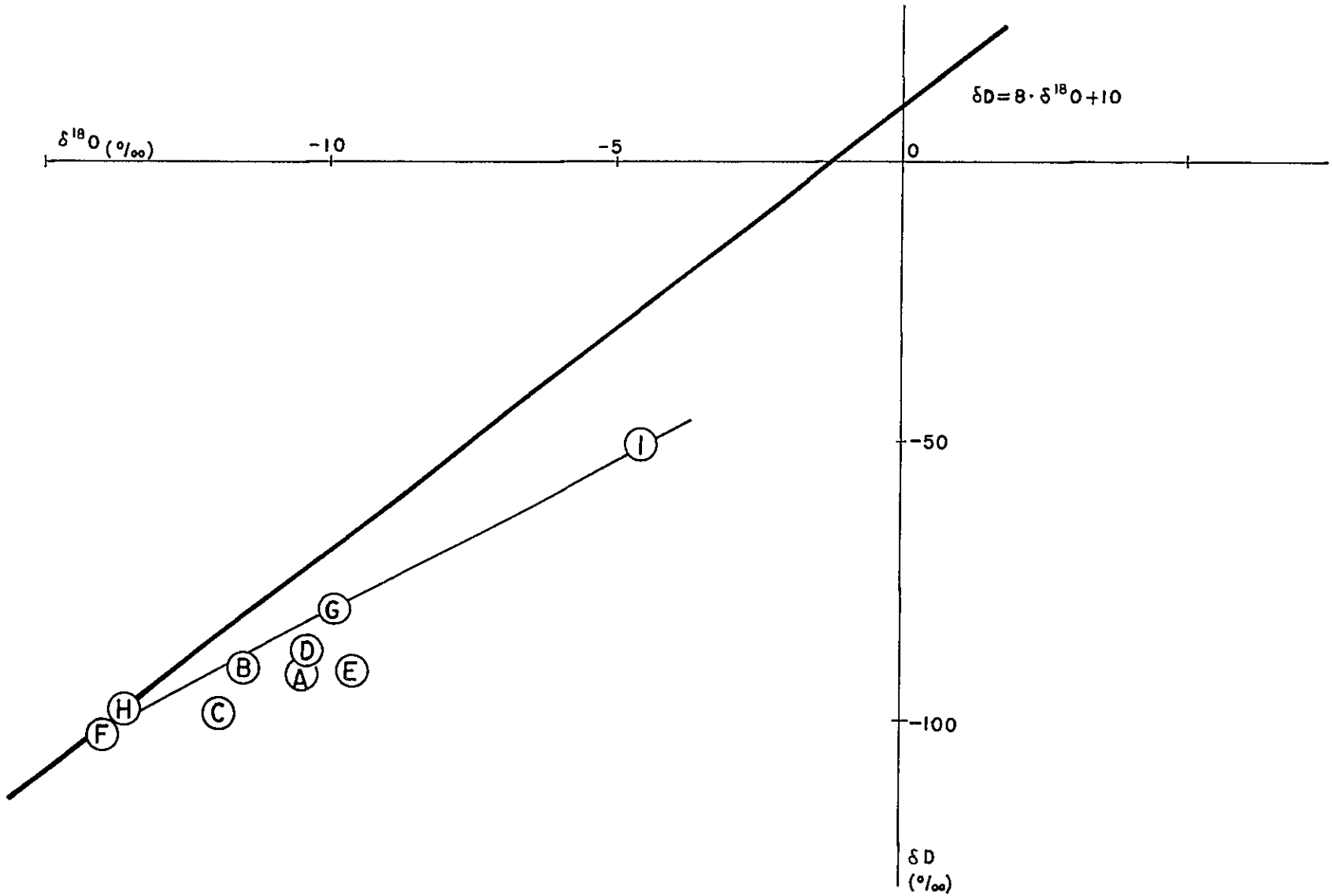

Fig. II-2-7 D/H AND $^{18}O/^{16}O$ RATIOS

CHAPTER 3

GRAVITY SURVEY

Chapter 3 Gravity Survey

3–1 Preface

Gravity surveys are conducted in order to determine the subsurface structure such as the basement structure, faults, and intrusive rocks with the moderate assumption in their densities.

Furthermore gravity surveys are utilized to confirm the structure interpreted by geological surveys and other means of geophysical exploration.

Recently gravity surveys have been frequently utilized in regional geothermal explorations. Japan is famous throughout the world for its hot springs. These hot springs are seen all over the country and many of them are located at or adjacent to large scale gravity lows. This observation has largely been a theoretical knowledge during the past years but the relationship between gravity anomaly and geothermal resources is becoming an established fact due to the numerous regional gravity surveys utilized for geothermal energy exploration.

That is, among the operating geothermal power plants in Japan, OHNUMA, KAKKONDA, ONIKOBE, OHDAKE and HACHOOBARU, 5 geothermal power plants except MATSUKAWA were proved to have relationship with large scale gravity lows.

Such large scale low anomalies suggest the presence of grabens and depressions at depths and are very effective in furnishing information about geothermal conditions.

On the other hand, in the case of the Imperial Valley of U.S.A. and Broadland in New Zealand, it is reported that local high anomalies are caused by rocks of higher density due to geothermal alteration.

According to these reports, residual maps are highly appraised and that the positive correlation with high anomaly and geothermal manifestations are confirmed.

Also, in Japan it is reported that geothermal areas are distributed in a manner that can be associated with very local high anomalies and that some of them are along the structural faults deduced by gravity survey.

Therefore, in addition to furnishing information regarding the general underground structure, a gravity survey will be useful in determining the targets for the subsequent detailed survey.

In Wairakei, New Zealand, movement of geothermal fluids at depths are said to be inferable from the continuous observation of gravity readings.

In Japan, the same study of long-term gravity measurement is going to be made in the TAKINOUE geothermal area. It might be difficult to make all kinds of study through this survey because of the area and the periods, but judging from the patterns and distributions of the anomaly, it could be possible to interpret data not only from the geological but also from the geothermal structure.

3–2 Method of Survey

3–2–1 Abstract

The earth's gravity is a composite force combining the attraction due to the earth's mass and the centrifugal force due to the earth's rotation.

If the earth was perfect sphere and its density distribution was spherically symmetrical, the gravity value would be the same anywhere on its surface.

Centrifugal force is maximum on the equator and zero on both poles, direction of action is always opposite that of gravity. Therefore, gravity becomes maximum on the poles and minimum on the equator, this is a difference of 0.3% from the maximum gravity value so that is almost negligible.

A body on the surface of the earth has a 'weight' which results from the gravitational attraction of the entire earth. If the body is allowed to fall, it is accelerated by this weight. The unit of acceleration is the gal, named after Galileo and 1 gal is simply 1 cm/sec^2.
The average acceleration on the earth's surface is about 980cm/sec^2=980 gals (but increases by about 0.5% from equator to pole).

Gravitational anomalies are only very small fractions of the earth's field, and a smaller unit is needed. The unit commonly used is the milligal or mgal which is 0.001gal. Anomalies from local geologic structures are commonly of the order of one to ten mgals.

3–2–2 Survey Planning

Observation stations are shown on the Location map (Fig.II–3–1) made by the JICA survey team. Planned stations were 500 points but the actual obsevation stations are 517. Among these, altitudes of 260 points were measured by leveling, and the rest of the 257 points were measured by microbarometer.

The number of the station are 1 to 517 continuously and a gravity station Bg. 1000.

The surveyed area is about 140 km^2, and the standard station interval is 500 m. But along two E–W lines and three N–S lines the interval is 250 m. The survey were made by using transit, pocket compass and clinometer.

Topography is not very gentle but since vegetation did not pose any problem, no delay in scheduled was experienced.

3–2–3 Gravimeter

Two La Coste G type gravimeters were used.
Each specification and function are listed below,

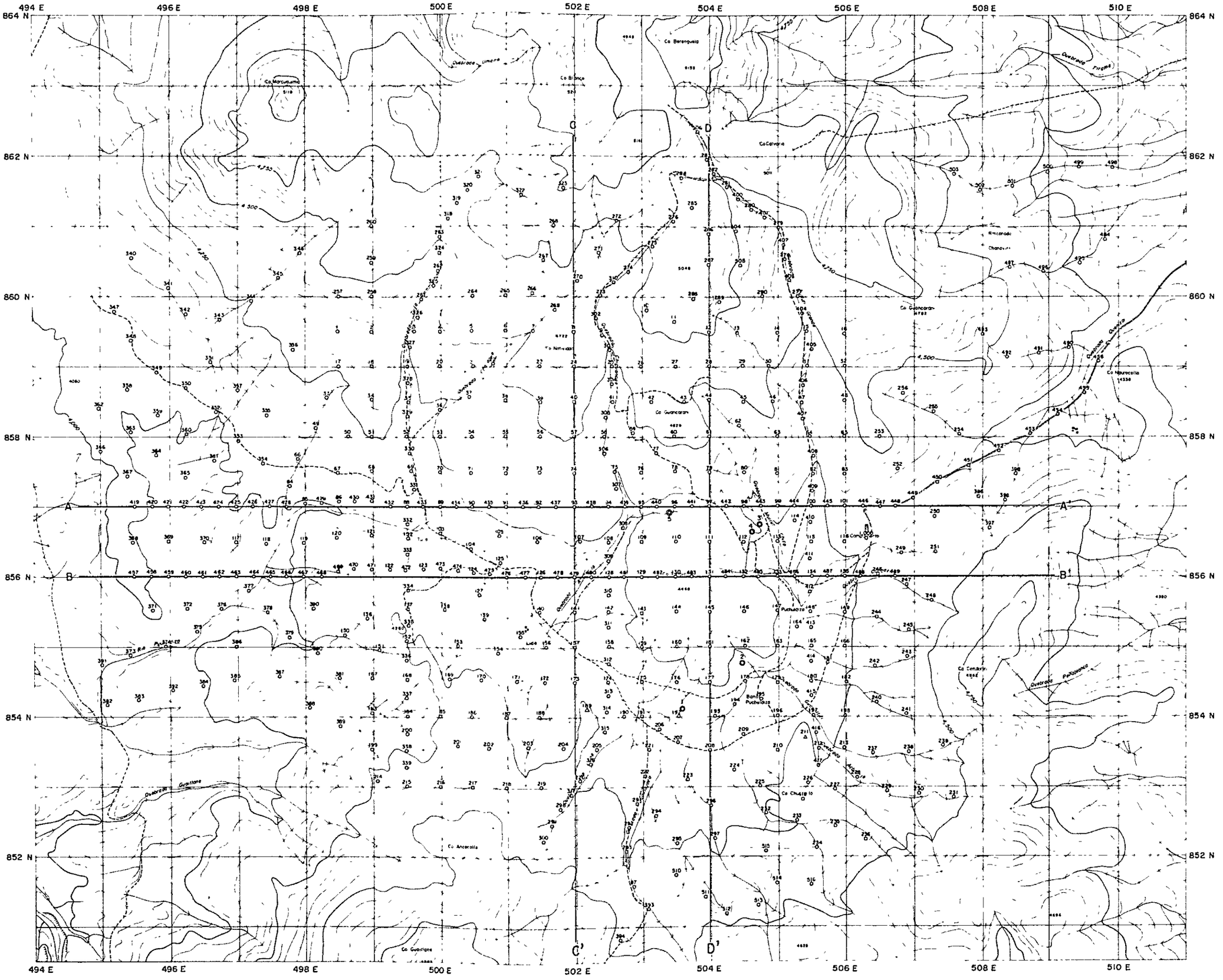

Geothermal Power Development Project
in Puchuldiza
the Republic of Chile

LOCATION OF GRAVITY OBSERVATION POINTS

1 : 50,000

0 1,000 2,000 3,000 m

Nov ~ Dec, 1978

Fig. II-3-1

Name of Instrument	La Coste G type	
No. of Production	G–204	G–236
Operating Range (mgal)	0.0 – 7261.530	0.0 – 7440.760
Temperature of heater (°C)	52.5	47.5
Reading line	3.10	2.60
Date of production	Feb. 1969	Jul. 1970
Dimensions (cm)	14 x 15 x 20	
Meter weight (kg)	8.6	
Made by	La Coste S. Romberg (U.S.A.)	

La Coste gravimeters are characterized by their world-wide range without the need of resetting and their negligible drift is normally less than 0.5 mgal/month. It becomes possible then to measure the gravity both in Japan and in Chile without resetting.
To obtain gravity values in milligals from the reading of the counters, the following table was prepared for each gravimeter.

3–2–4 Comparison of Standard Gravity

In Northern Chile there is no standard point for gravity comparison, so that simple relative observation was planned in the beginning.

But at the survey area situated on the Andes above 4,000m, very low negative Bouguer anomalies were expected due to the theory of isostacy.

In order to confirm the real Bouguer anomaly, it is necessary to compare values with the international gravity value. In this case, the gravity comparison was made with the known gravity station in Japan.

The results of comparison are shown on Table II–3–1 and the gravity standard set in front of Puchuldiza camp Bg 1000 are calculated by those data. All gravity data are based on the standard value of g= 977.414185gal and where BM7470 of the first order level point located at TOHMA town, KAMIKAWA–GUN, HOKKAIDO and JGSN71 is the gravity standard point set by Japan Geographical Institute, MEGURO–KU, TOKYO.

The drift value is only 1.211mgal for more than 113 days so that the average drift rate becomes 0.0004mgal/hr and the gravity difference tetween BM4470 and Bg1000 is about 3000mgal. The procedure for the calculation of Table II–3–1 are as follows:

a. By adopting the several corrections on the observed value A,B,C, corrected gravity values D,E,F, are calculated.
b. G and H are the known gravity values officially published.
c. Gravity difference I between BM7470 and JGSN71 is obtained by G–H=I.
e. Drift L on JGSN71 is obtained by I + J=K, F – K=L.

Table Ⅱ-3-1 Calculation of Gravity Standard Value

	BM 7470	Bg 1000	JGSN 71
LATITUDE (DEG.MIN.)	N 43°53'20"	S 19°23'12"	N 53°38'60"
LONGTITUDE (DEG.MIN.)	E 142°32'00"	W 68°56'39"	E 139°41'30"
Y.M.D.	1978.10.04	1978.11.28	1979.02.05
TIME (HOUR,MIN.)	15.03	20.36	14.21
READ	A 4010.255	B 1006.414	C 3286.595
INSTRUMENT H. (CM)	20	27	21
X.FACTOR (MGAL)	4156.448	1041.169	3404.713
EARTH TIDE CORRECTION	-0.040	0.012	-0.027
INSTRUMENTAL CORRECTION (MGAL)	0.062	0.083	0.065
CORRECTION (MGAL)	D 4156.470	E 1041.265	F 3404.751
DRIFT CORREC. (MGAL)	0	M -0.540	L -1.211
CORRECTION VALUE (MGAL)	J 4156.470	N 1040.725	K 3403.540
GRAVITY DIFFERENT (MGAL)	0	O -3115.745	I -752.930
GRAVITY VALUE (GAL)	G 980.529930	P 977.414185	H 979.777000

Drift M on Bg 1000 is calculated from L by time proportion allotment.

f. Gravity value P on Bg 1000 is obtained from E + M = N, N − J = O and G + O= P.

g. Then, K−J=I and G + I=H.

3−2−5 Leveling

The direct leveling method is adopted for 260 points by Auto level B−2 of SOKKISHA, Japan.

Basement of leveling are two triangular points as follows.

	Lupe	Tahipicollo
Latitude	S19°24'36"90	S19°24'24"66
Longitude	W68°56'54"13	W68°58'44"83
Altitude	4305.28m	4263.08m

Main roads were used for the leveling route.

The surveys were made by 2 teams, one Chilean and Japanese, although most of it were done by Chilean surveyors.

3−2−6 Survey by Microbarometric Altimeter

Altitudes of 257 points were measured by microbarometer made by American Paulin, U.S.A.. Two field altimeters model MM−1, were used one as moving barometer and one as Base Barograph for the base point measurements.

Each altimeter has a minimum accuracy of 1 m, ranging from 0 to 5,000m A.S.L..

Continuous records were taken at Bg 1000 where the altitude is known. On each readings the following corrections such as temperature, pressure and closed error correction were made.

a. Temperature correction

Air column correction for the reading are determined by the following formula

$$\delta H = 0.00204 \cdot \Delta H (F - 50.0)$$

where, δH : Temperature correction value of two diffrent points

ΔH : Altitude difference of two different points

F : Average temperature of two different points (°F)

The American Paulin System Altimeter is calibrated to measure directly the density of the air at 50°F.

A temperature above or below this value will involve a change in density of the column of air being measured.

b. Barometric Correction

In most cases, after a traverse has been made and the altimeter correction have been

applied, temperature and elevation corrections and the true elevation at the base station should be noted. In this survey, a base barograph was used for the barometric correction.

c. Closure error correction

Just like a leveling, a traverse starts from a point of known elevation and closes on the same point. The error of the traverse is time-alloted on each readings after making the above-mentioned corrections.

3–3 Gravity Correction

Several corrections should be made on the observed gravity value to know the real Bouguer anomaly.

3–3–1 Flow of Correction

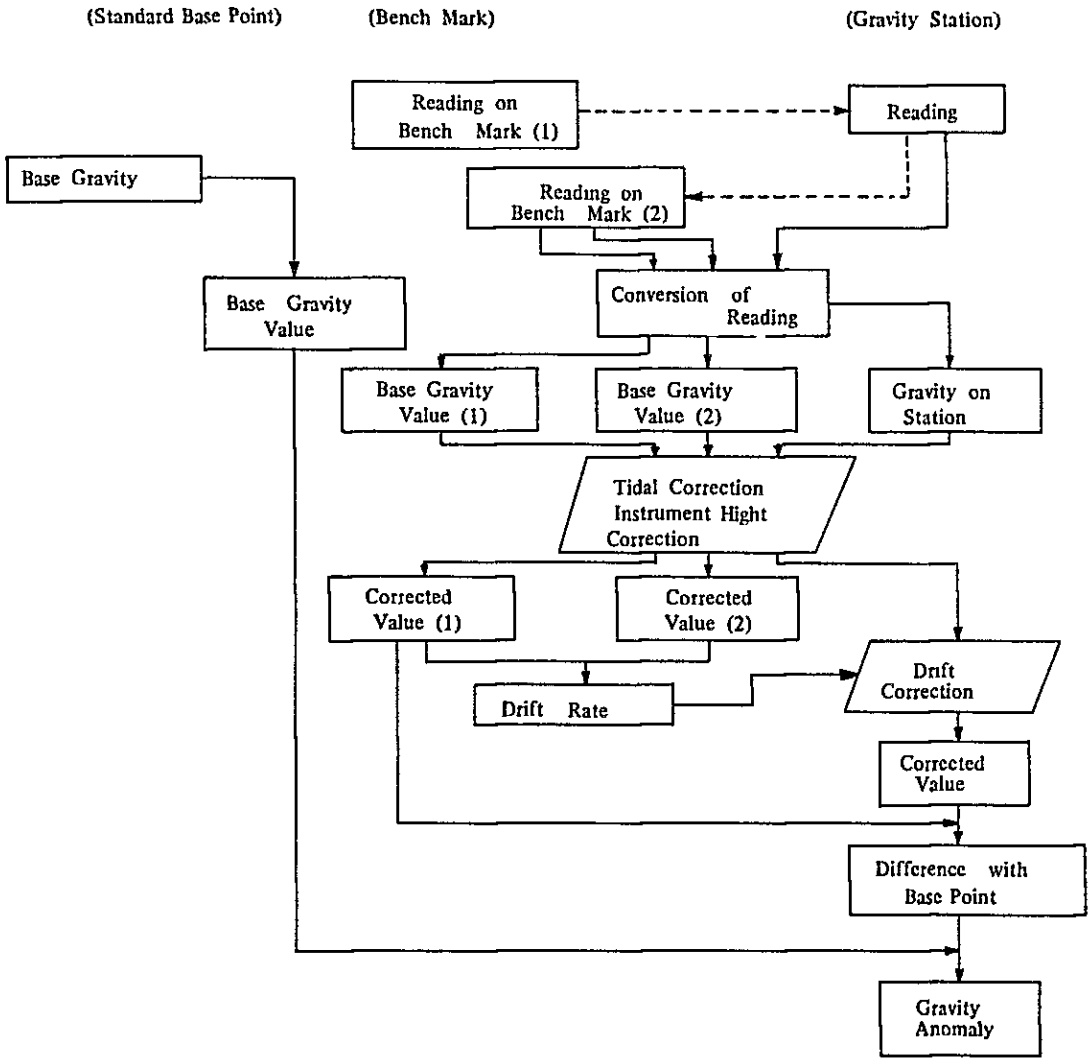

a. Conversion

To obtain gravity values in milligals from the reading of the counter and dial, a table for conversion is employed. In the table, the value of gravity in milligal is given for each 100 units of the counter. By use of this table, and the corresponding factor, the value of gravity for any reading of the counter may be obtained.

b. Tidal correction (Fig. II–3–11)

Tidal forces are due to the fact that the attraction of sun and moon at the earth's surface deviate in direction and intensity by time and place of observation.

Tidal force due to sun and moon are caluclated by the following formula;

$$Vet = -\Sigma u$$

$$u = -\frac{3}{2} \cdot G M \frac{a}{r^3}\left\{ 3(\sin^2 \delta - \frac{1}{3}) \cdot (\sin^2 \psi - \frac{1}{3}) + \sin 2\delta \cdot \sin 2\psi \cdot \cos \theta \right.$$

$$\left. + \cos^2\delta \cdot \cos^2\psi \cdot \cos 2\theta \right\}$$

Where,

Vet: Tidal correction

u : Tidal force of the planet

G : Gravitational constant

M : Mass of the planets (sun and moon etc.)

a : Distance from center of earth to observation point

r : Distance between earth and planet

δ : Declination of the planet (angle from equator to south or north)

ψ : Latitude at observation point

θ : Angle of the planet (angle between terrestrial and planetary meridian plane)

In order to check the tidal correction gravity observations on a constant station have been made. Gravity values on the constant station changes only due to tidal force, so that the tidal force variation can be confirmed by observing changes for more than 12 hours.

Two peaks and bottoms were observed for 20 hours 30 minutes from 9:30AM, 11 Nov. to 6:00AM, 12 Nov. 1978.

Good agreement between values is seen for the period with a slight scattering of 0.165 mgal on the peak and −0.077 mgal on the bottom. The error is only less than 0.008 mgal. Even on the high Andean field results show an accurate correspondence between observed and theoretical values.

c. Instrument height correction

This correction is used to adjust the instrument height from the station elevation surveyed by leveling.

$$Vhi = 0.3086 \cdot hi \times 10^{-2}$$

Where,

Vhi : Correction of instrument height

hi : Height from station level to top of gravimeter

d. Drift correction

Drift is an inherent characteristic error of a gravimeter which changes proportionally with time. The change rate of drift is not always constant as it depends upon the characteristic of a gravimeter, temperature and pressure of the atomosphere and the way of handling. So, in this survey the closure error was regarded as drift and distributed by time allotment.

e. Gravity value

Correction on the observed value are obtained as follows;

$$Vc = Vrk + Vhi + Vd$$

Where,

Vc : Corrected gravity value

Vrk : Observed gravity value

Vd : Drift correction value

The gravity value (g) is obtained by adding a difference (Dg) of corrected gravity (Vc) and the corrected gravity of bench mark (Vg) with a base point gravity (Bg), which has the same value as the international standard gravity.

$$Dg = Vc - Vg$$

$$g = Bg + Dg$$

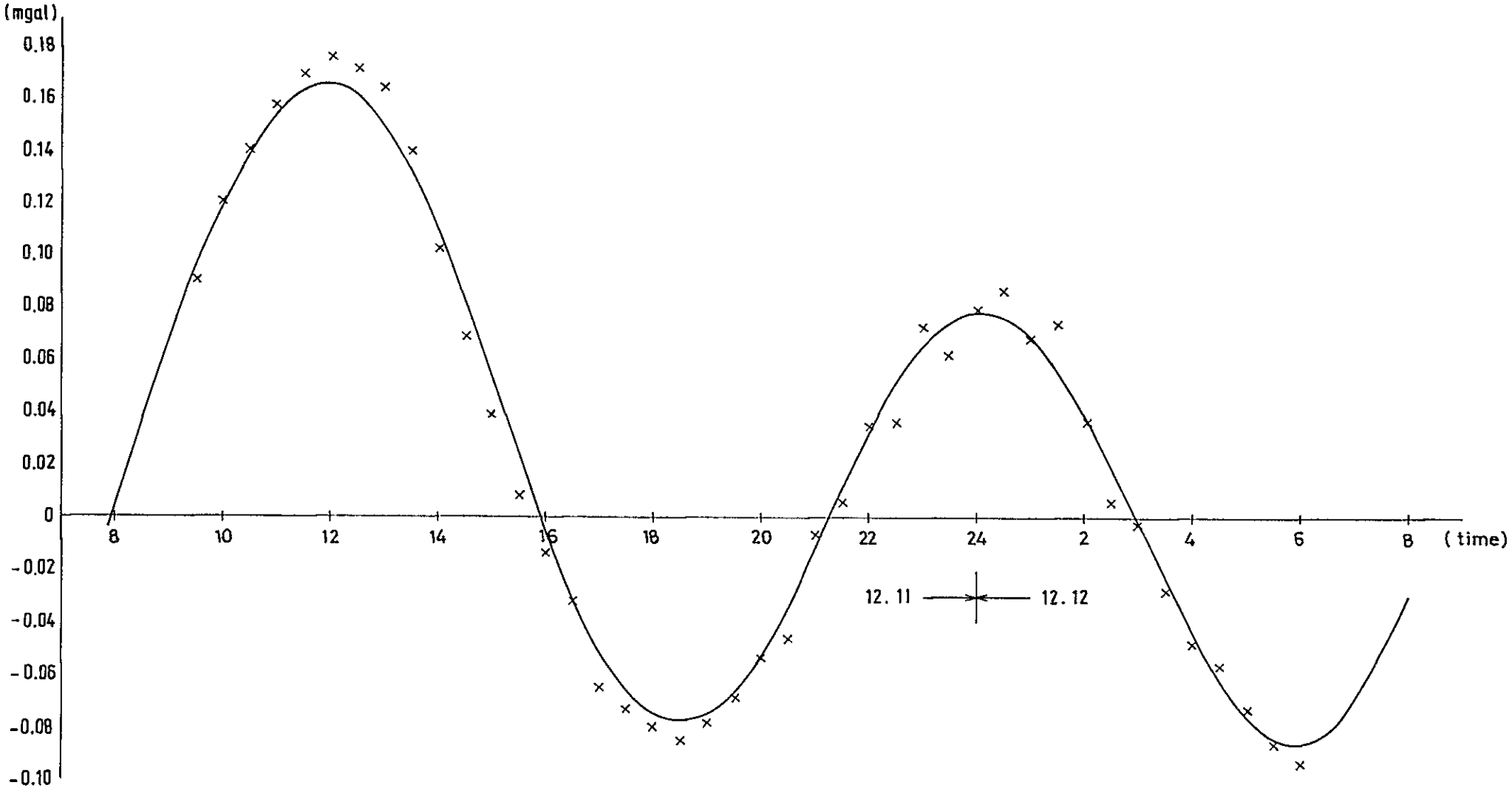

Fig.Ⅱ-3-11 DIURNAL VARIATION AT GRAVITY STATION

3-3-2 Correction of Gravity

A flow chart of various corrections from a reading to a Bouguer anomaly is shown below.

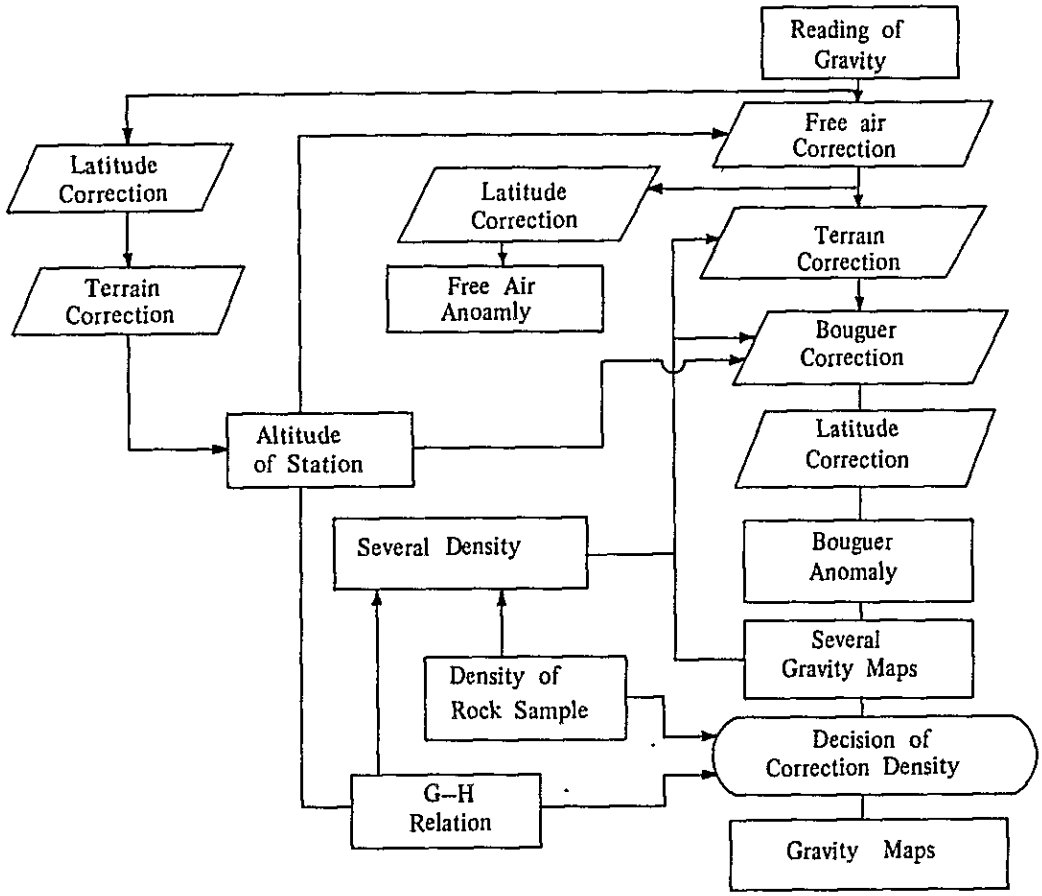

Free Air correction

This is a correction for the elevation of a gravity measurement required because the measurement was made at a different distance from the center of the earth.

The first term of the free air correction is 0.3086 mgal/m. This is called the height correction together with Bouguer correction.

$$\delta g = 0.3086 \cdot H .$$

Where,

H: Altitude of the station (m)

Terrain Correction

A topographic irregularity (hill, knoll, slope, etc.) will exert an attraction directly proportional to its density. The vertical component of this attraction will be directed upwards and reduce the gravity.

A term of this magnitude must therefore be added to the measured value of gravity. A station near a valley is a negative mass and the vertical component of its attraction will also be directed upwards leading again to an additive topographic correction.

The topographic correction is calculated by dividing the area around a station in compartments into 5 groups, namely, "far ", "medium", "near", "neighbor" and "close".

The range and size of grid are as follows,

Kinds of correction	range (Km)	grid interval X(m)	grid interval Y(m)	topographic map
far	105.00 x 74.00	5250	3700	1/50,000
medium	21.00 x 14.80	1313	925	1/50,000
near	5.25 x 3.70	328.1	231.3	1/25,000
neighbor	0.98 x 0.69			1/25,000 – 1/10,000
close	0.04 x 0.04			sketch.

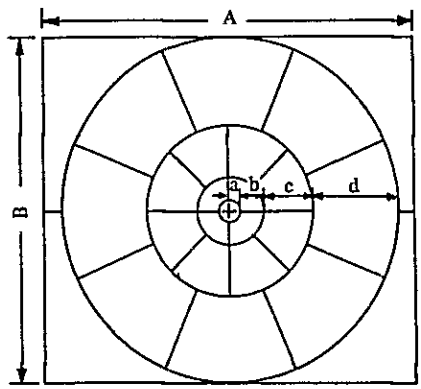

A = 980m
B = 690m

a = 20m
b = 50m
c = 100m
d = 175m

Terrain Correction (neighbor)

The range of correction is the outer square of the terrain correction with an observation station as its center and without overlapping.

Corrections of "neighbor" are based on the altitude of a cartesian co-ordinate but for a "close" correction, a circular plate shown above was used in order to make the correction more accurate.

This plate is divided into 24 compartments for the correction with an exception of a center which has a diameter of 40 m named "close".

The average altitude of each compartment is used for the correction. The "close" correction is obtained by a table composed of two dimensional topographic section calculated in many cases.

The correction due to the attraction of the material in such a compartment is

$$\delta g0' = 2\pi \cdot G \cdot Sx \cdot Sy\rho\Sigma \left(\frac{1}{R} - \frac{1}{\sqrt{R^2 + H^2}}\right)$$

Where,

$\delta g0$	:	Topographic correction
ρ	:	Correction density
G	:	Gravitational constant
R	:	Distance between station and grid
Sx	:	Grid length X
Sy	:	Grid length Y
H	:	Difference of altitude between station and average height of grid

Bouguer correction

Bouguer correction is a height correction due to the attraction of the rock mass between the station and the sea level for the mass that is absent between the station and the sea level.

Bouguer correction is given as follows:

$$\delta g0'' = -0.0419 \times \rho H(m)$$

Where,

H(m)	:	altitude of the station
ρ	:	specific gravity (density) of the intervening rock

Latitude correction

The attraction of gravity on earth decreases towards the equator and increases towards poles because of the centrifugal force resulting from the earth's rotation and of the earth's radius due to polar flattening.

So it is the function of latitude ψ and the International Gravity Formula adopted in 1930 by IUGG (International Union of Geodesy and Geophysics) is,

$$\gamma 0 = 978.049\,(1+0.0052884\sin^2\psi - 0.0000059\sin^2 2\psi)$$

but later in 1967 IUGG recommended to use the Normal Gravity Formula, as shown below,

$$\gamma = \frac{a \cdot \gamma_E \cdot \cos^2\psi + b \cdot \gamma_p \sin^2\psi}{\sqrt{a^2\cos^2\psi + b^2\sin^2\psi}}$$

a = 6,378,140m

b = 6,356,180m

γ_E = 978.032 gal

γ_p = 983.218 gal

In this gravity survey the above formula was used for the calculation of standard gravity. The differnence between International gravity Formula (γ_I) and Normal Gravity Formula (γ_N) is $\gamma_N - \gamma_I = 17.2 + 13.6 \sin^2\psi$

Bouguer anomaly

The difference between the corrected gravity value resulting from the above-mentioned corrections and the standard gravity is called Bouguer anomaly,

$go' \fallingdotseq g + \gamma go' + \gamma go'' - \gamma o$

go'' : Value of Bouguer anomaly

The Bouguer anomaly depends on rock densities.

Six anomaly maps presented here (densities of 1.80, 2.00, 2.10, 2.20, 2.30 and 2.40) were corrected for density and terrain. On the appendix are the lists of corrections for the case of density 2.40.

3–4 Method of Analysis

Results of this investigation are qualitatively interpreted using normal structure of residual gravity detected by running mean method and the result of surface fit analysis together with its residual map. Two-dimensional section analysis is performed as a quantitative way of interpretation.

3–4–1 Density Assumption

Although only one assumption is necessary in the analysis of data derived from a gravity survey, it is very difficult to describe geologic structure by using only density data. In the past the assumption on the density was necessary for terrain corrections. Recently however, upgraded precision of analysis requires assumption of detailed density structure underground.

a. Density of Rock Samples

In this survey, 47 rock samples were collected on the ground surface and their dry and wet densities were measured. The method and results of density measurements will be discussed later in Chapter 6.

Tab. II–3–2 shows the average and distribution of density of the rocks that were measured. There is no significant difference between the averages and the distribution of measured densities because the values are considerably spread wide over a number of samples except for the cretaceous rocks.

Average density is 2.48 for the Quaternary and Tertiary volcanics, 2.32 for the Tertiary sedimentary rocks, and 2.40 for the Cretaceous sedimentary rocks making up a three-layered structure with an intermediate layer of lower density. The overall average density is 2.41. The density difference between the layer of the Cretaceous sedimentary rocks which is

considered to be the high density basement, and its upper layer is very small, $\Delta\rho$ =0.08, thus resulting in a difficulty in determining the proper density model.

Table II–3–2 Average Density of Rock Samples

Period	Rock Name	Average			Density 2.0 2.2 2.4 2.6 2.8
Quaternary	Andesite	2.49	2.48	2.41	2.31 – 2.62
Tertiary	Andesite	2.46			2.30 – 2.60
	Basaltic An.	2.46	2.32		2.00 – 2.40
	Dacitic Tuff				
	Rhyolitic Tuff	2.34			2.14 – 2.50
	Dacitic Welded Tf.				
Cretaceous	Rhyolitic Tuff	2.40			2.39 – 2.40
	Dacitic Welded Tf.				

b. G–H Correlation

Gravity decreases with the altitude of measurement. The rate of decrement is nearly equal to the coefficient of altitude correction, 0.3086–0.0419 ρ . Therefore, when the gravity data are plotted as the altitudes on one axis and latitude corrected gravity on the other axis, the inclination of the line fit to the plots represents the average of rock density in the survey area. Fig. II–3–10 shows the G–H correlation for this case and the density was estimated as ρ =2.39 by least square method.

c. Determination of Correction Density

The correction density was determined to be 2.40 from the average density 2.41 of rock samples and the derived density 2.39 from G–H correlation. Rough Bouguer anomaly maps were drawn for two cases of density ρ =2.30 and ρ =2.40, and better correlation with the geological map was observed in the case of ρ =2.40.

3–4–2 Residual Gravity

For the purpose of selective detection of gravity anomaly of a certain scale, a residual map was derived from the Bouguer anomaly map by use of running mean method. Residual gravity value of normal structures is derived by SEYA's formula as follows.

$$\Delta g(x_j, y_j) = \frac{1}{2(2\alpha+1)} \left[\sum_{k=i-\alpha}^{i+\alpha} g(x_k, y_j) + \sum_{n=j-\alpha}^{j+\alpha} g(x_i, y_n) \right] - \frac{1}{2(2\beta+1)} \left[\sum_{k=i-\beta}^{i+\beta} g(x_k, y_j) + \sum_{n=j-\beta}^{j+\beta} g(x_i, y_n) \right]$$

where $\alpha < \beta$ and for Bouguer anomaly $\alpha = 1$ and $\beta = 3$.
Grid interval was determined as 500m for gavity reading. The theoretical dominant wavelength for the detection of Bouguer anomaly will be about 3 km and gravity anomaly of this scale will be most clearly depicted.

3–4–3 Surface Fit Analysis

Surface fit analysis shows the general trend of gravity distribution which is known to express gravity anomaly due to deep structures around the survey area.
Gravity trends of decreasing Bouguer anomaly values from west to east is observed in the Bouguer anomaly map of the survey area. The first, second and third order surface fit analyses were carried out with the following formula.

1st order surface fit

$$g_1(x, y) = -279.14 - 0.315x + 0.142y$$

2nd order surface fit

$$g_2(x, y) = -276.54 - 0.0502x - 0.455y - 0.00565x^2 + 0.00410xy + 0.0104y^2$$

3rd order surface fit

$$g_3(x, y) = -281.94 + 0.196x + 0.0900y - 0.000311x^2 - 281.94 + 0.916x + 0.0900y - 0.000311x^2 + 0.000476x^2 \cdot y + 0.0000224x \cdot y^2 + 0.000215y^3$$

The higher the order of surface fit analysis, the shorter the wavelength of gravity anomaly it expresses. Here coordinates (x, y) are expressed in a cartesian coordinate system whose origin is at (495E, 862N) and its x–axis lies along the east and y–axis along the south.
The grid interval was 250 m for gravity reading.

Residual gravity map of a surface fit analysis is obtained by substructing the surface fit from the Bouguer anomaly map, i.e.

1st order residual gravity = $G(X, Y) - g_1(X, Y)$
2nd order residual gravity = $G(X,Y) - g_2(X,Y)$
3rd order residual gravity = $G(X,Y) - g_3(X,Y)$

3–4–4 Two-Dimentional Section Analysis

In two-dimensional section analysis, Bouguer values calculated from an assumed density structure are compared with observed Bouguer values. The density structure is modified until the calculated Bouguer values fit well with the observed values.

Calculation of Bouguer values is performed by an electronic computer using Talwani's formula, taking the effect of topography into consideration.

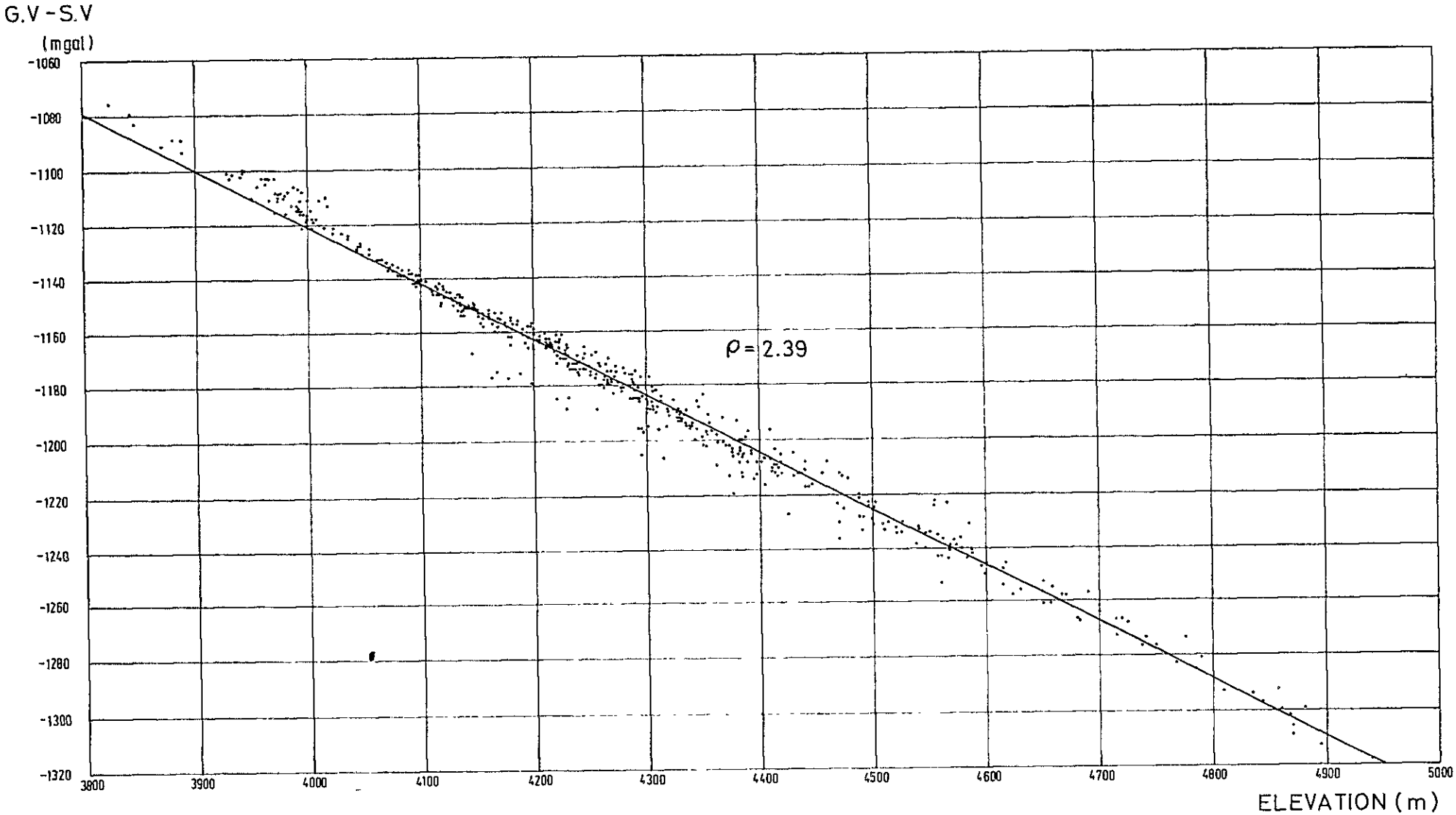

Fig. II-3-10 RELATION BETWEEN GRAVITY AND ELEVATION

$$\Delta g = 2G \cdot \Delta\rho \sum_i Zi$$

$$Zi = Ai \sin\psi i \cos\psi i \left[\theta_i - \theta_{i+1} + \tan\psi_i \log \frac{\cos\theta_i(\tan\theta_i - \tan\psi_i)}{\cos\theta_{i+1}(\tan\theta_{i+1} - \tan\psi_i)}\right]$$

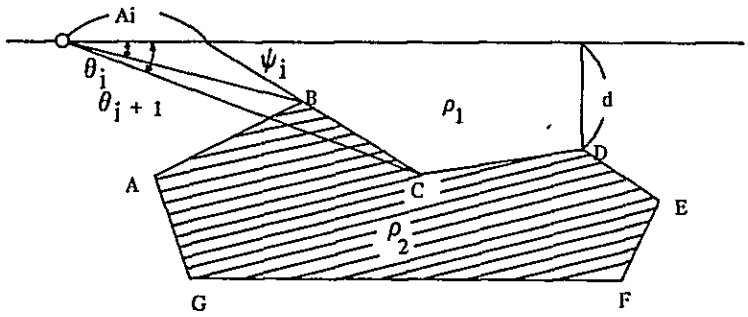

Talwani's way for interpretation

For relatively simple geological structure, this analysis will give well fit results. In this survey, along the four cross-sections of Bouguer anomaly map drawn for density correction $\rho = 2.40$, the method of depth estimation was applied.

3–5 Interpretation

Data of this gravity survey are qualitatively and quantitatively treated in the following interpretation maps.

3–5–1 Bouguer Anomaly Map

Fig. II–3–2 shows the Bouguer anomaly map obtained with density correction $\rho = 2.40$. Distribution of gravity in this map shows a variety of anomalies. Equi-gravity contours run irregularly and curve complexly. Bouguer anomaly values varying from –307 mgal to –273 mgal, shows that the area investigated seems to be situated in a typical negative Bouguer anomaly area.

A gravity trend of decreasing Bouguer anomaly from the west to the east of the area is observed, which is more obvious in the surface fit interpretation maps shown later. High gravity anomalies defined as Bouguer anomalies greater than –280 mgal are developed in the northern part and at the south and west end of this area. Low gravity anomalies which show lower Bouguer anomalies than –290 mgal are developed in the central part and at the northeast and southeast end of the area.

In the north of the area, three high gravity anomalies are localized in closed contours and are bundled together in a large scale anomaly zone featured by –285 mgal contour.

The high gravity anomaly zone around H_4 at the south end of the area has two typical bay-shaped anomalies H_5 and H_6. At the west end, a high gravity anomaly zone is represented by H_7. These high gravity anomaly zones appears as domes of basements due to high density. The two dimensional section analyses described later have shown large-scale uplifts of the basement.

The large, low gravity anomaly zone at the center of the area estimated from the −285 mgal contour is composed of L_1, L_2, L_3, L_4, and L_5 has a bay-shaped anomaly of L_6 aside. The two-dimensional section analyses have suggested a subsidence of the basement with some localized uneveness in it. The low gravity anomaly zone of the east end around L_7 sharply juts out at L_8. L_9 represents the low gravity anomaly zone at the southeast end.
From the scale of these low gravity anomalies, a continuous subsidence of basement from L_7 to L_9 through L_8 is expected.

Localized low gravity anomalies of L_{10}, L_{11}, L_{12} in the western part of the surveyed area from a small gradient N–S trend of low gravity anomaly zone. The small gradient observed in the low gravity anomaly zone at the center is also characteristic of this surveyed area.

A curved, continuous low gravity anomaly zone is also seen from L_7 to L_{10} through L_3, L_2, L_1 and L_6, which suggests a large scale of graben. A further garvity survey on the northeastern and the northwestern regions outside the map will show more information on this suggested graben. This area of survey shows a dominance of low-gravity values and similarity is found in typical geothermal areas in Japan.

The high gradients of gravity surrounding H_1, H_2, H_3 or at the west fringe of L_7 and L_9 or at the south fringe of H_7 seem to show fault structures. Many fault structures frequently found in the two-dimensional section analyses described later implies the occurrence of large block movement by dislocations in this area. The remarkable negative Bouguer anomaly distributed in this area is considered to be an influence of isostacy.
A typical example is isostatic negative Bouguer anomaly is the one across North America in which cross-sections show positive correlation with Mohorovicic discontinuity and negative correlation with topography. In this example −100 mgal to −200 mgal of negative Bouguer anomaly values are observed in highlands of Nevada, Juta and Colorad, one of extreme observations in Juta is a −193 mgal Bouguer anomaly value at the altitude of 1,000 m above the sea where the Mohorovicic discontinuity is expected to be at 47.7 km deep.

In a published observation of gravity surveys across South America at lat. 32°S in the Andean near the border between Chile and Argentina, are marked negative Bouguer anomaly of −300 mgal observed at the highland as high as 4,000 m above the sea, while almost no Bouguer anomaly is observed on the plain of about 100 m to 200 m above the sea in Argentina and Uruguay. As in the case of North America, positive correlation to Mohorovicic depth and negative correlation to the topography are clearly recognized in two-dimensional section

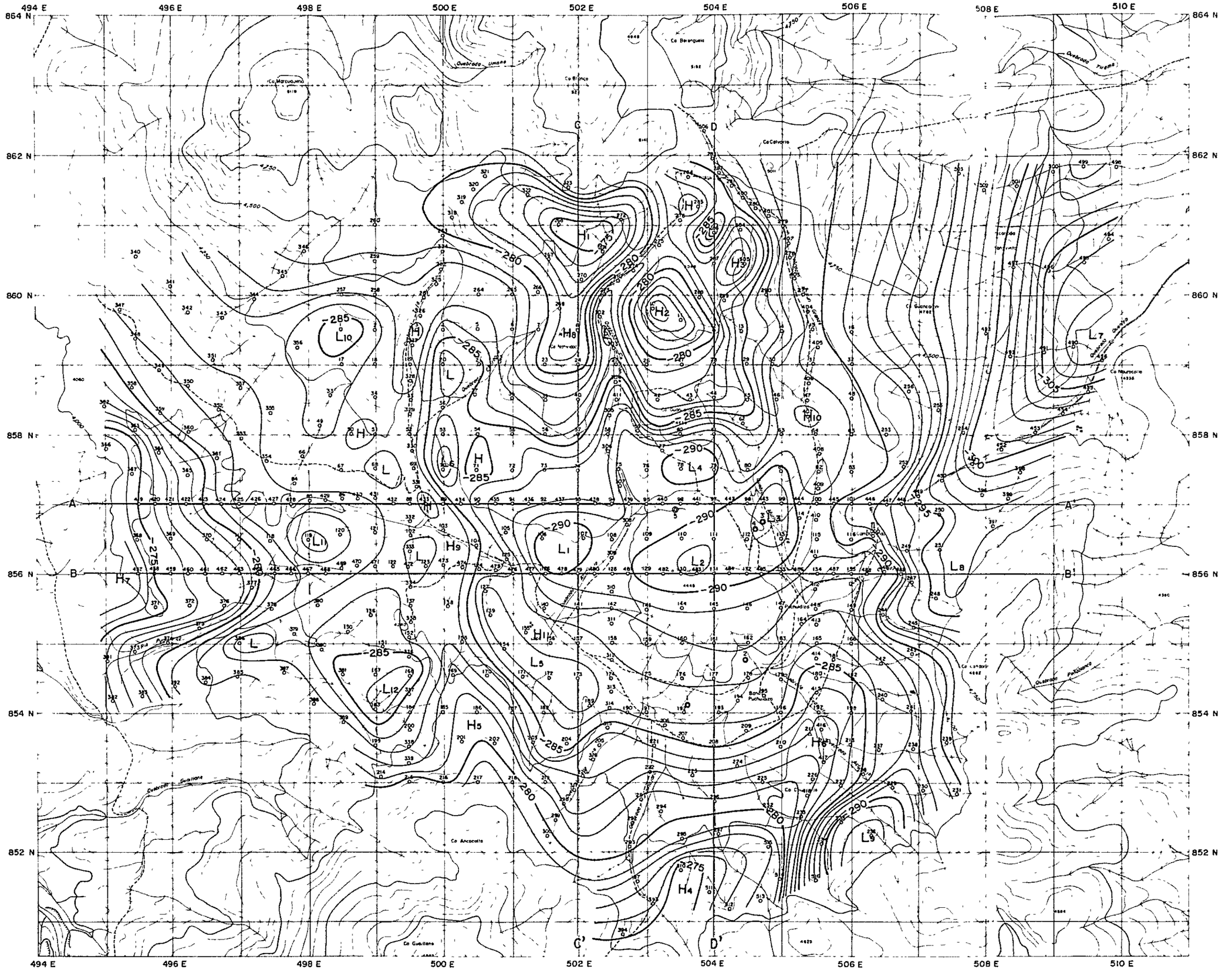

Geothermal Power Development Project
in Puchuldiza
the Republic of Chile

BOUGUER ANOMALY MAP

1 : 50,000

0 1,000 2,000 3,000 m

Nov ~ Dec, 1978

Fig. II-3-2

analysis of the Bouguer anomaly of South America, in which the Mohorovicic discontinuity is estimated to be at 59 to 75 km under ground in highland areas and at 31 to 33 km in plains.

Isostatic negative anomaly values are observed in many mountain ranges in the world, −300 mgal along the Andean, −500 mgal at the altitude of 5,000 m in Tibet plateau, and −150 mgal at the altitude of 2,000 m in the Alps are well known negative Bouguer anomaly as influence of isostacy.

Bouguer anomaly value in this area ranges from −300 mgal to −270 mgal, while free air anomaly value ranges from + 110 mgal to + 200 mgal. It is characteristic of isostatic gravity anomaly in high grounds that the Bouguer anomaly is negative while free air anomaly positive.

3−5−2 Normal Structure Map (Fig. II−3−3 ∿ II−3−7)

In the normal structure map of Fig. II−3−3, broken contour lines correspond to negative anomaly values. Gravity anomalies near the frame of the map like H_1, H_3, H_4, H_7, L_7 and L_9 are not shown, since the calculation cannot be performed on the edge of the area surveyed.

The low gravity anomaly zone represented by three divided anomalies L_1, L_4, and L_5 is closed in the middle of the area. Negative anomalies L_6 and L_{10} in the northwest, L_{12} in the southwest and L_7 and L_8 in the east emphasize the localized low gravity anomaly zone shown before in Bouguer anomaly map. Negative anomalies L_{13} in the northeast, L_{14} in the southeast, L_{15} in the southwest and L_{16} in the west show low gravity anomalies which were not obvious before, while some low gravity anomalies seen in the Bouguer anomaly map are now vague or have completely disappeared.

As for high gravity anomalies, H_2 in the north of the area is now a clear positive anomaly, and fringes of bay-shaped garvity anomalies H_5, H_6, and H_7 are now very distinct with closed contours. Positive anomaly H_8 in the north of the area emphasizes the jut-out of high gravity anomaly. Positive anomalies H_9 in the west, H_{10} in the northeast and H_{11} in the middle of the area correspond to indistinct high gravity anomalies in the Bouguer anomaly map. There are observed continuities from H_5 to H_8 through H_9 and from H_6 to H_{10}, and they form together with H_2, an array of positive anomalies surrounding negative anomalies in the middle of the area surveyed. Among these positive anomalies, H_{10} and H_{11} have been detected as localized high gravity anomaly components and imply high density rocks.

The existence of graben represented by L_7, L_3, L_2, L_1, L_6 and L_{10} is also observed in this normal structure map as a continuous negative anomaly zone.

3−5−3 Surface Fit Map

Although in this course of survey, all the first, second and third order surface fit analyses were examined, only the first order and the third order surface fit maps are shown.

a. First Order Surface Fit Map

Fig. II–3–4 is the first order surface fit map, which show a dominant gravity trend that Bouguer anomaly value decreases from –274 mgal in the southwest to –297 mgal in the northeast, and gravity contours of N70°W develop with about 5 mgal/km gravity gradient.

b. Third Order Surface Fit Map

Gravity trends as seen in the first order surface fit map where Bouguer anomaly decreases from southwest to northeast of the area is also observed in the third order surface fit map shown in Fig. II–3–5. Bouguer anomaly is distributed in the range between –267 mgal and –307 mgal. It should be noted that a curved arc of low gravity anomaly zone runs from the northeast end to the northwest end, passing through the middle of the area in this map. This seems to correspond to the low gravity anomaly zone which lies in the same manner in the Bouguer anomaly map described before.

3–5–4 Residual Map

First order and third order residual maps are shown in Fig. II–3–6 and Fig. II–3–7, respectively, where negative anomaly is distinguished by broken contour lines. Although first order, second order, and third order residual maps were drawn and examined for this survey, no remarkable difference is found between them and therefore, we discuss here only the result shown in Fig. II–3–6.

The low gravity anomaly zone in the middle of the area is divided into three negative center L_1, L_3 and L_5, and as in the normal structure map, L_1 is again emphasized here in this map to show different pattern from Bouguer anomaly map. L_7, L_8, L_9, L_{12} and L_{15} are negative anomalies corresponding to low gravity anomalies in the Bouguer anomaly map. Negative anomalies L_6 and L_{11} slightly emphasize their corresponding low gravity anomalies. L_{10}, L_{13}, L_{14} and L_{16} which are detected in the normal structure map and L_2 and L_4 which are seen in the Bouguer anomaly map are not clear now in this first order residual map.

High gravity anomalies H_1, H_2, and H_3 in the northern area, H_4 and bay-shaped H_5 and H_6 in the southern area, and H_7 near the west edge form very distinct positive anomalies. On the other hand, H_8, H_9, H_{10} and H_{11} which are all distinguished in the normal structure map are only vague jut-out of a positive anomaly zone.

In this first order residual map, positive anomalies are grouped into northern, southern and western groups, while negative anomalies in the northeastern and central groups represent large scale anomalies of basement structure. The continuity of negative anomalies L_7, L_3, L_2, L_1, L_6 and L_{10} is most clear in this map and the existence of a graben is well expected.

3–5–5 Two Dimensional Section Analysis

Two-dimensional section analysis on the first order residual map where the Bouguer anomaly values decrease gradually from the western area to the eastern area have been removed. As for density model, although the three layered model with the first layer of ρ=2.40 of

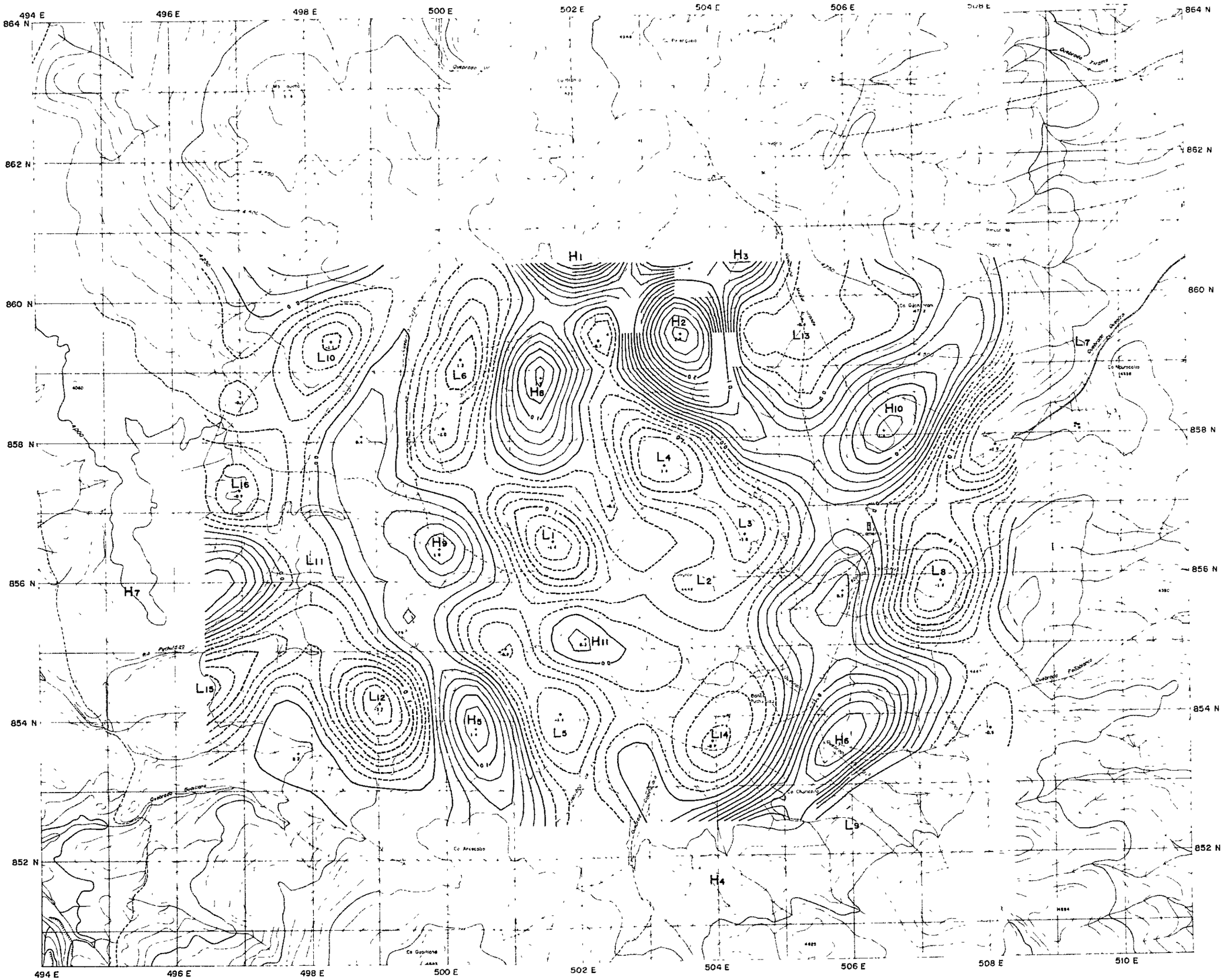

Geothermal Power Development Project
in Puchuldiza
the Republic of Chile

RESIDUAL GRAVITY MAP

1 : 50,000

0 1,000 2,000 3,000 m

Nov ~ Dec, 1978

Fig. II-3-3

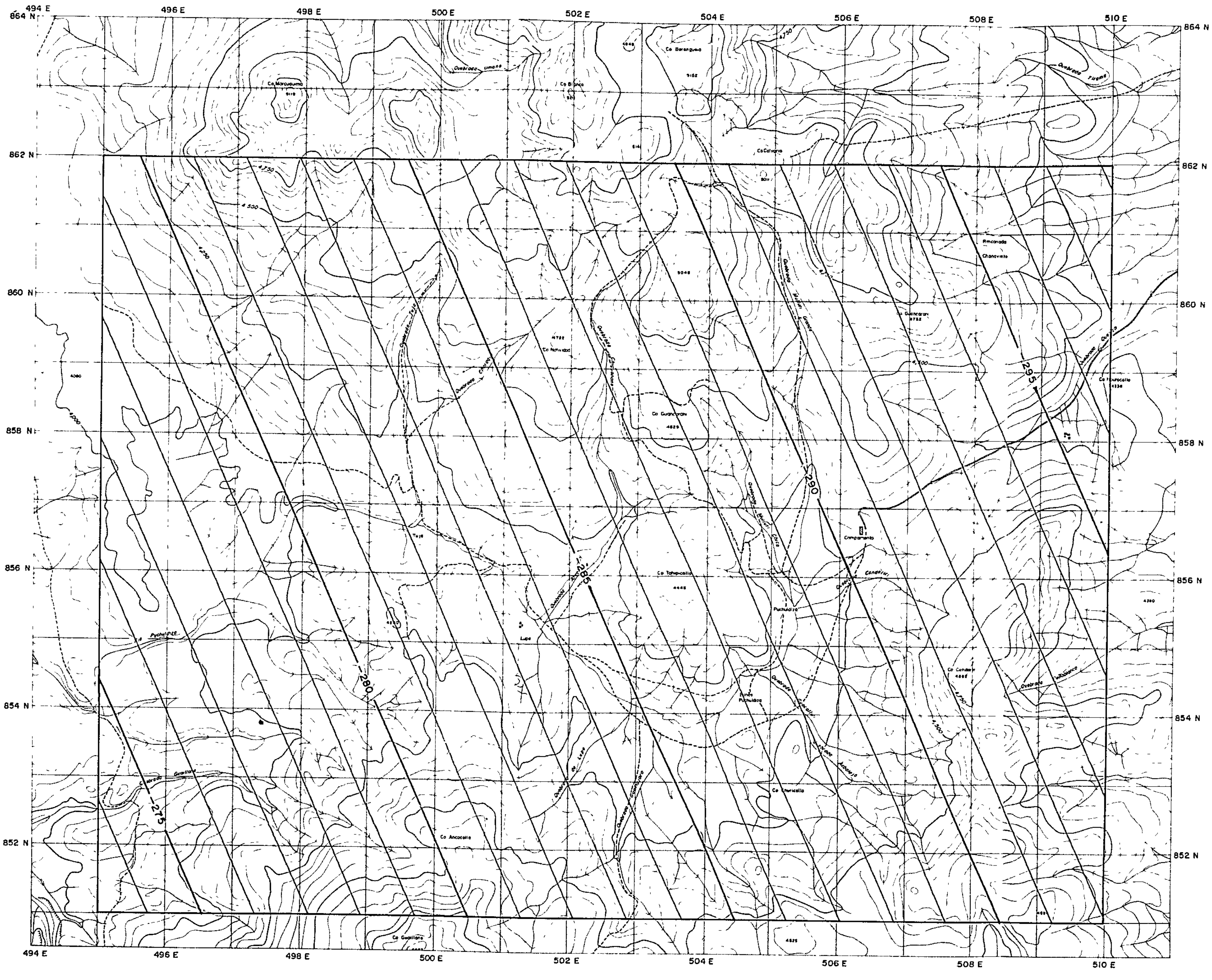

Geothermal Power Development Project
in Puchuldiza
the Republic of Chile

FIRST-ORDER SURFACE FIT MAP

1 : 50,000

0 1,000 2,000 3,000 m

Nov～Dec, 1978

Fig. II-3-4

494 E 496 E 498 E 500 E 502 E 504 E 506 E 508 E 510 E

864 N 862 N 860 N 858 N 856 N 854 N 852 N

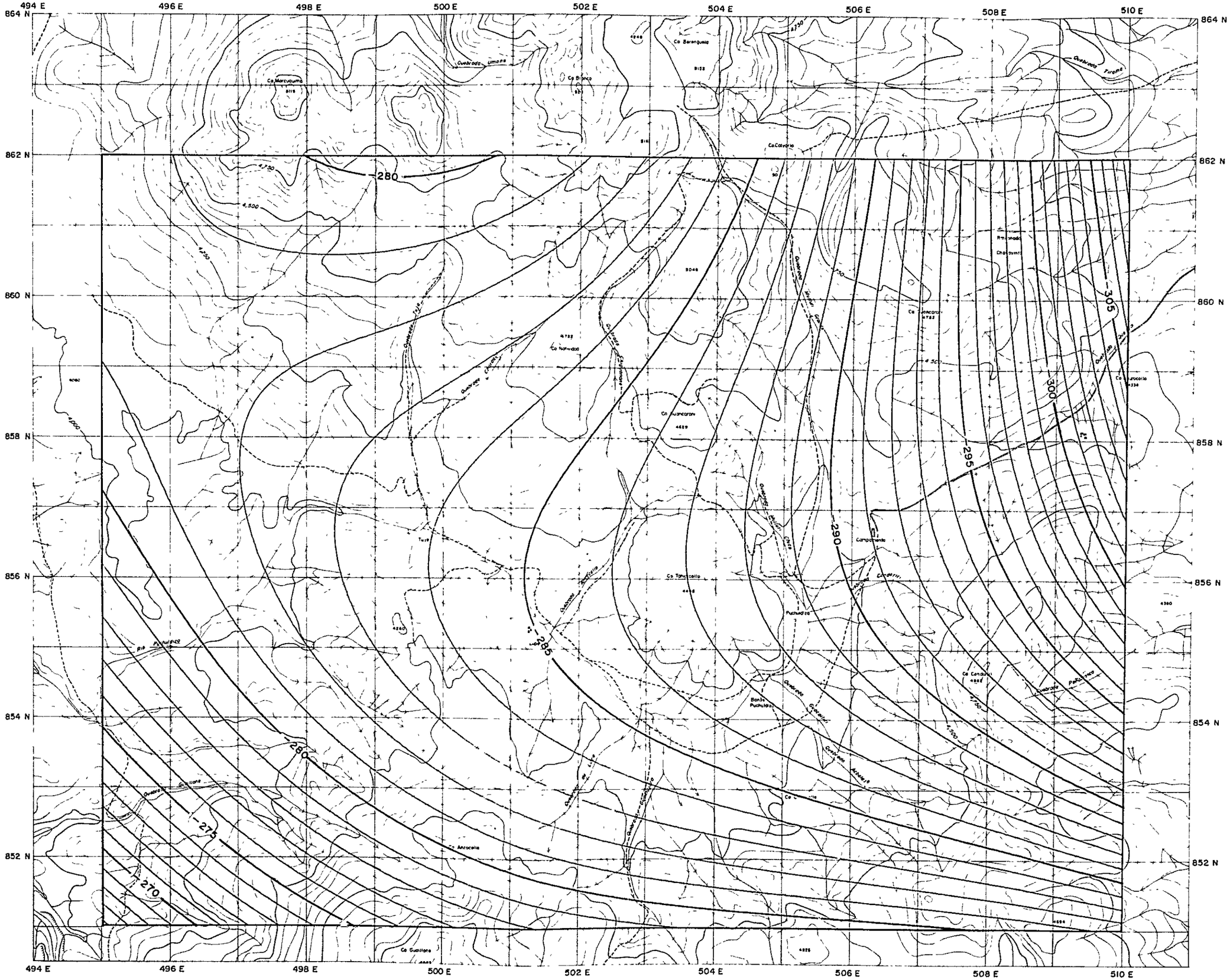

Geothermal Power Development Project
in Puchuldiza
the Republic of Chile

THIRD-ORDER SURFACE FIT MAP

1 : 50,000

0 1,000 2,000 3,000 m

Nov ~ Dec, 1978

Fig. II-3-5

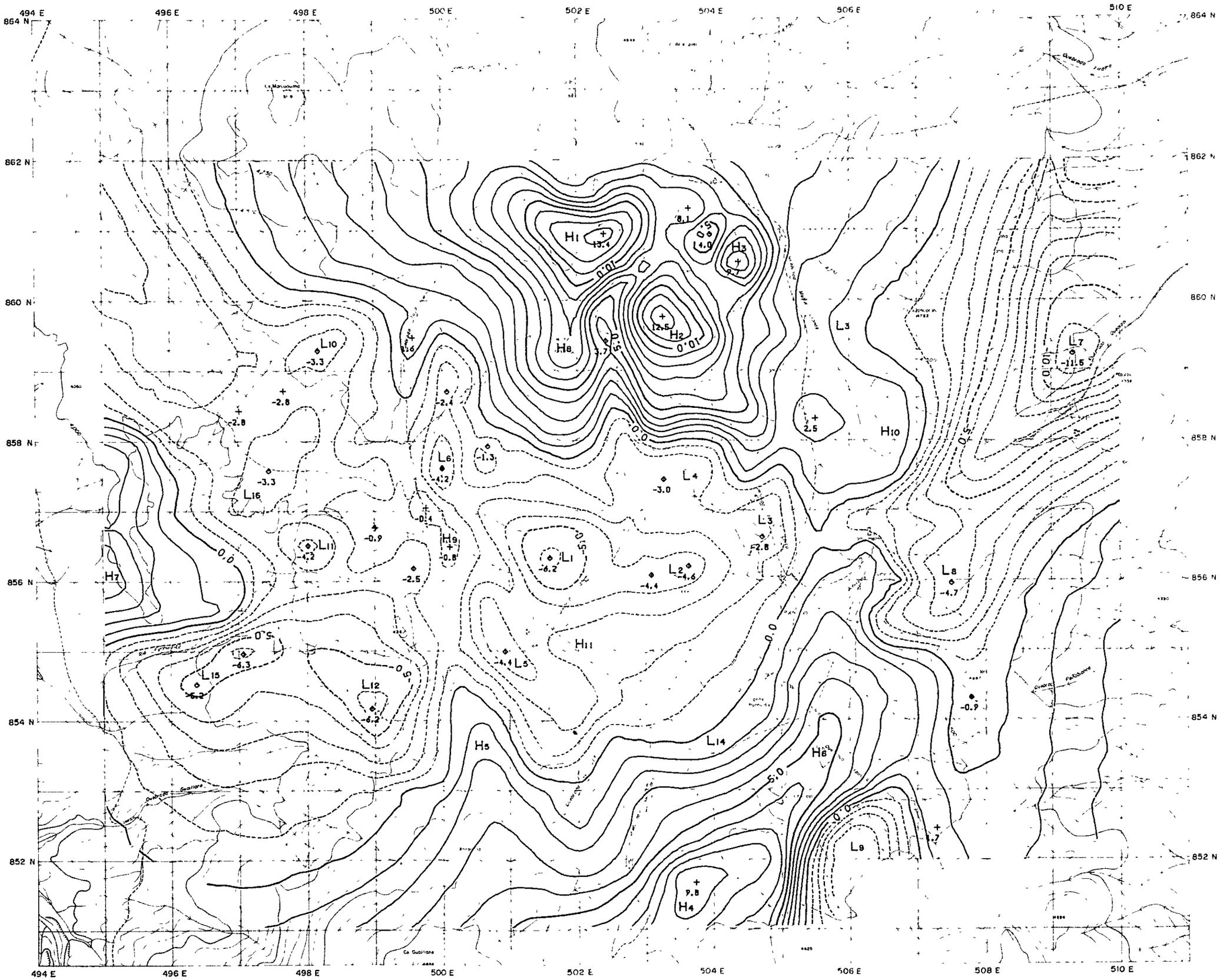

Geothermal Power Development Project
in Puchuldiza
the Republic of Chile

FIRST-ORDER RESIDUAL MAP

1 : 50,000

0 1,000 2,000 3,000 m

Nov ~ Dec, 1978

Fig. II-3-6

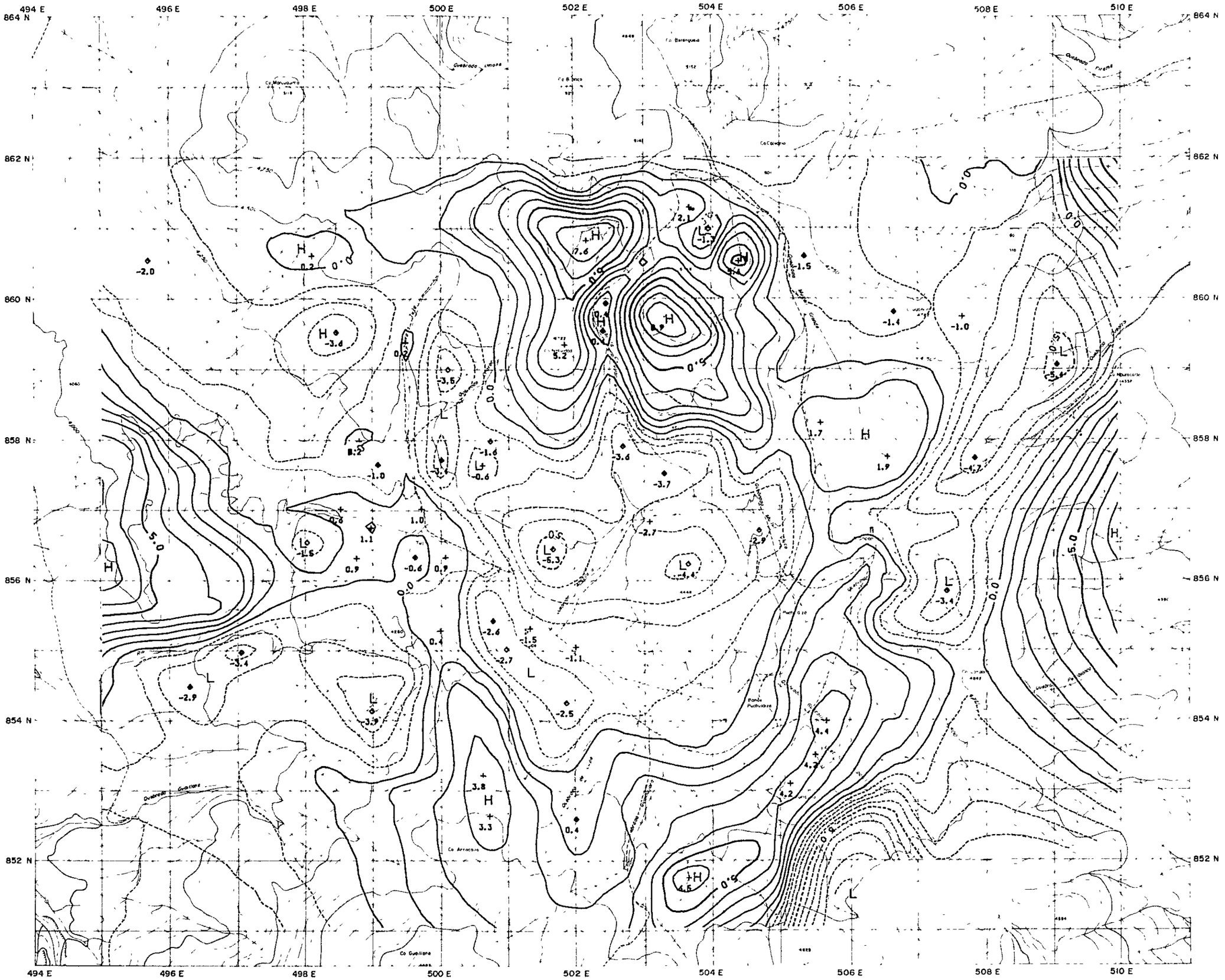

Geothermal Power Development Project
in Puchuldiza
the Republic of Chile

THIRD-ORDER RESIDUAL MAP

1 : 50,000

0 1,000 2,000 3,000 m

Nov ~ Dec, 1978

Fig.Ⅱ-3-7

Quaternary and Tertiary volcanics, the second layer of $\rho = 2.30$ of Tertiary sedimentary rocks, and the third layer of $\rho = 2.40$ of Cretaceous sedimentary rocks is considered reasonable as compared with densities obtained from rock samples. A two-layered model with density difference of $\Delta\rho = 0.15$, where andesitic rocks are almost homogeneously destributed in the first layer, was applied to estimate the upper boundary of Cretaceous sedimentary rocks. The density difference of $\Delta\rho = 0.15$ is applied to correct the very unnatural structure derived for $\Delta\rho = 0.10$ taken from measurements on rock samples. For approximation at the north end of C–C'cross-section and both at the south and north ends of D–D'cross-section, a lower formation of density difference of $\Delta\rho = 0.3$ is assumed as a Paleozoic layer. It must be noted, however, that the structure aimed at in this analysis is Cretaceous sedimentary basement rocks.

In cross-sections shown in the descriptions, Bouguer anomaly values and normal structure values are plotted together with the first order residual values and were applied to the analysis. Calculated values marked as "o"were derived from Cretaceous sedimentary rocks and values marked as "x"were the results of lower formation correction.

As a result of section analyses, many dislocations were observed and constrained geological structure dislocations were to be expected. The lower formation assumed in the south to north sections as shown in C–C'and D–D'sections does not appear in the east to west sections of A–A'and B–B', since it is almost horizontal in the east to west sections. Therefore, the structure of lower formation of paleozoic may correspond to a large scale graben like depression which is narrow in N–S direction and broad in E–W direction. Because of a very small difference in density, $\Delta\rho = 1.5$, some irregular unevenness is seen in the result of analysis. These unevenness were later slightly retouched in geological structure map presented.

a. A–A' Cross-Section

The measure point No. 100 where the outcrop of the basement is exposed was used as the control point in the calculation of A–A' section whose result is shown in Fig. II–3–8. The uplift observed in the east end corresponds to the bay-shaped positive anomaly H_{10} with dislocations expected at both east and west wings.

In the middle of the area, around the measure point No. 89, an uplift corresponds to the positive anomaly H_9 is calculated, and the one near the west end corresponds to H_7. Dislocations are expected in all the wings of these uplifts, especially in the eastern wings, middle and east end of the uplifts. Step faults are also expected to exist.

In the middle and western area, subsidences are developed and are connected with the uplifts through faults. The subsidence structure in the middle of the surveyed area corresponds to negative anomalies L_1 and L_3 and ranges about 5 km to the west gradually increasing in depth with slight up and down internal dislocations. From the measure point No. 90 to No. 437, about 1.5 km extension of localized graben-like depression is estimated with wings both constrained by dislocations.

This depression, corresponding to the negative anomalies L_1, has maximum depth of about 1,500 m at the measuring point No. 91 in this cross-section. The depression in the west corresponds to the negative anomaly L_{11}. It has a monocline structure to the west, and shows the deepest point near measure point No. 425 at the west end. The uplift corresponding to the positive anomaly H_7 is not fully described here, since it is situated at the edge of the survey area.

b. B–B′ Cross-Section

Fig. II–3–8 shows B–B′ cross-section. Assuming that the basement is latent shallow at the east end of the area, measure point No. 486 is used as the control point in the analysis of B–B′ cross-section. In this case also, as shown in A–A′ cross-section, the uplifts are observed in the east end corresponding to the bay-shaped anomaly H_6, in the middle corresponding to H_9 and in the west end corresponding to H_7. Faults are expected to exist in the wings of these uplifts except in the west wing of the middle uplift. Step faults are expected in the east wing of the middle uplift and in the west of the east end uplift.

Subsidence of the basement rocks are developed in the middle and in the west end, and again as in the case of A–A′ cross-section, adjoining the uplifts through dislocations except near the west wing of the middle uplift.

The subsidence in the middle, corresponds to the negative anomalies of L_1 and L_2, ranging about 4 km, has dislocations that gradually increases with depth towards the west with some undulation. The graben-like localized depression with both wings constrained by dislocations is observed equidistant about 1.3 km between the measure points No. 476 and No. 48. This depression corresponds to the anomaly L_1 and its maximum depth of 1,600m is calculated near the measure point No. 478. The subsidence in the west end simply inclines to the west and its maximum depth is near the measure point No. 467.

c. C–C′ Cross-Section

In C–C′ cross-section of Fig. II–3–9, the point of interception with A–A′ cross-section is selected as the control point. In the middle of the figure, a subsidence of the basement corresponding to the negative anomalies L_1 and L_5 is shown with its maximum depth estimated to be 1,600 m on the measure point No. 479. A localized uplift, with both south and north wings constrained by dislocations in the middle of this subsidence, corresponds to the positive anomaly H_{11}. The uplift corresponding to the positive anomalies H_8 and H_1 is adjacent to the north wing of the subsidence with step faults at the border. For approximation purpose, the lower Paleozoic formation is assumed in this region. An uplift is observed in the south corresponding to the bay-shaped positive anomaly H_4, but dislocations are expected at its border with the adjacent subsidence structure.

d. D–D′ Cross-Section

Fig. II–3–9 shows D–D′ cross-section which is calculated using No. 208 as its control

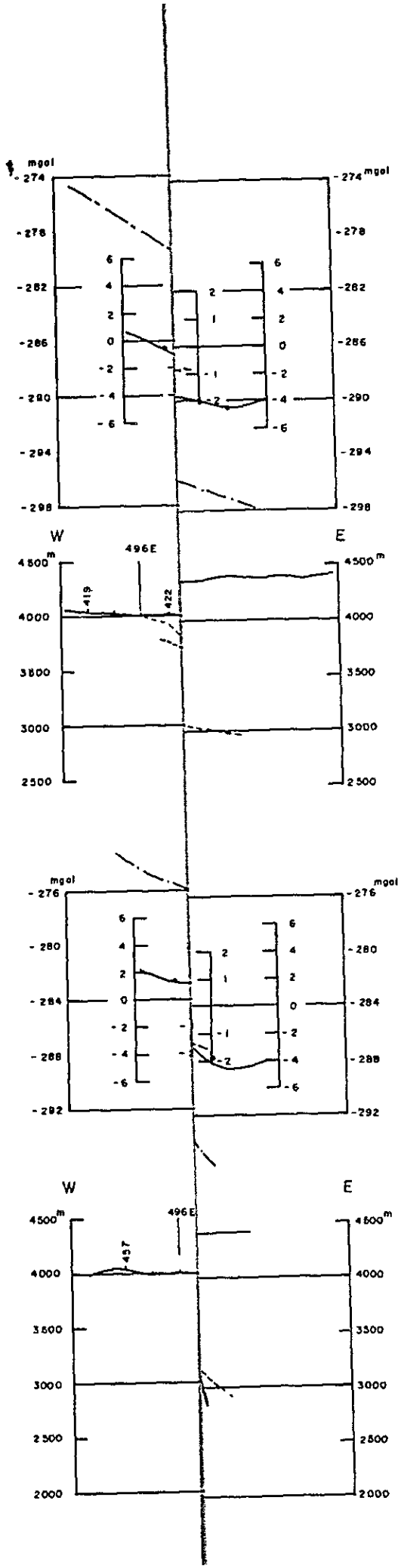

Geothermal Power Development Project
in Puchuldiza
the Republic of Chile

CROSS-SECTION OF A-A', B-B'

1 : 50,000

0 1,000 2,000m

Nov～Dec, 1978 Fig. II-3-8

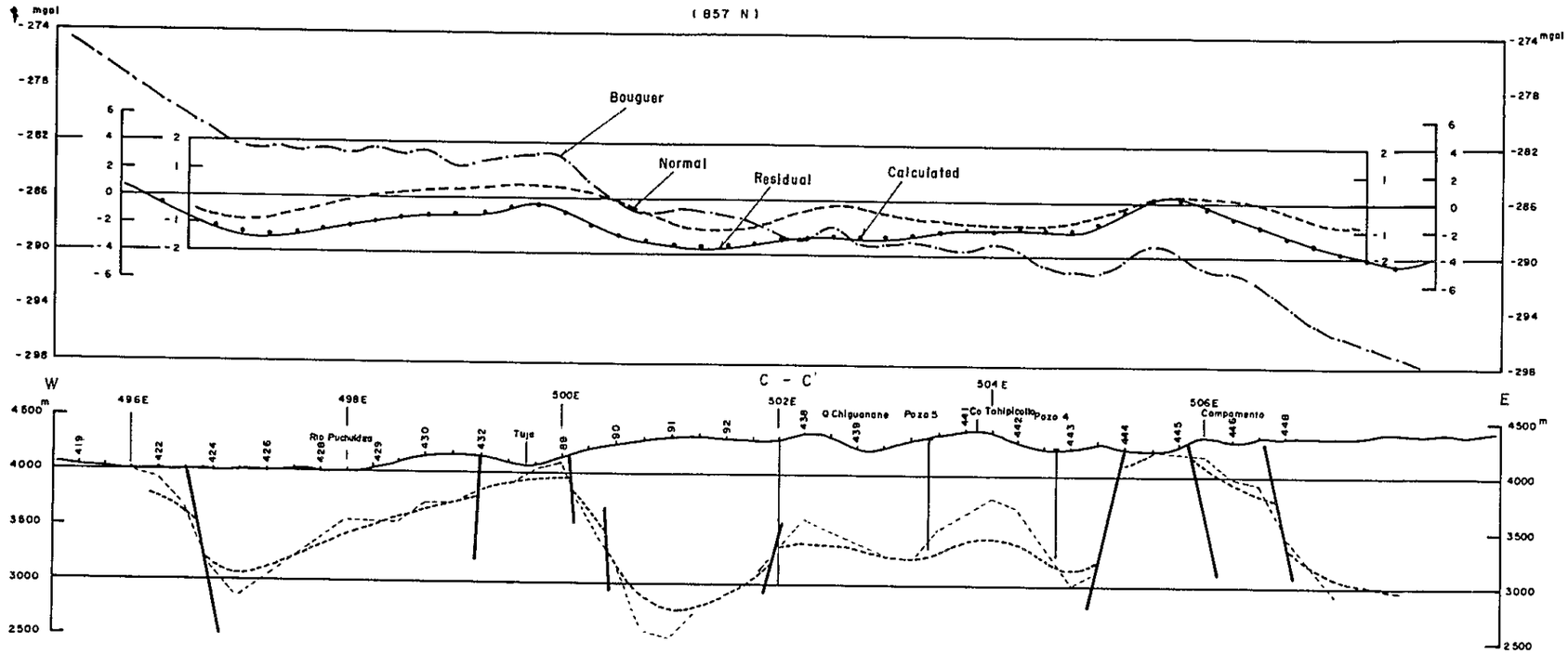

Geothermal Power Development Project
in Puchuldiza
the Republic of Chile

CROSS-SECTION OF A-A', B-B'

1 : 50,000

0 1,000 2,000 m

Nov ~ Dec, 1978 Fig. II-3-8

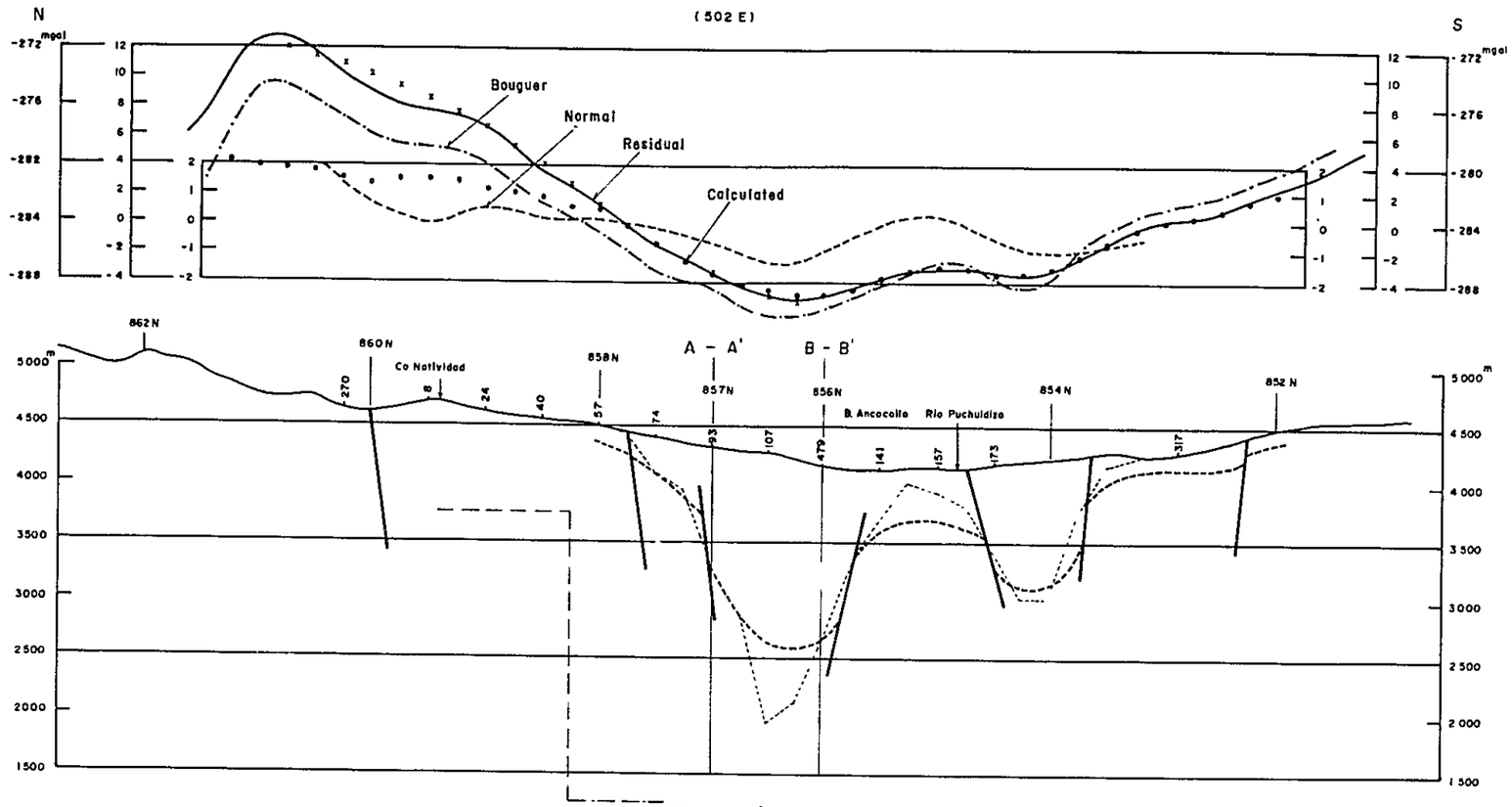

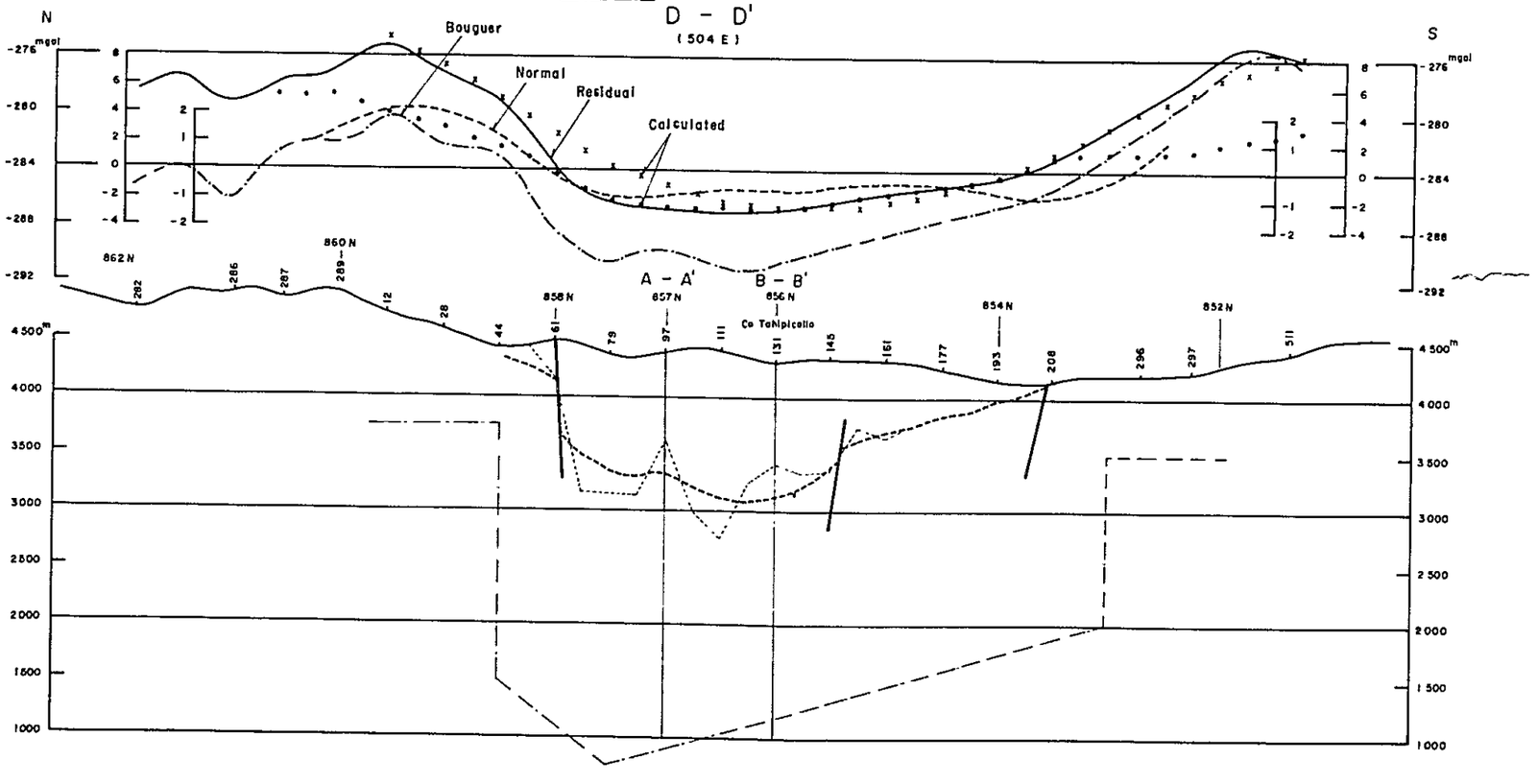

Geothermal Power Development Project
in Puchuldiza
the Republic of Chile

CROSS-SECTION OF C – C', D – D'

1 : 50,000

0 1,000 2,000 m

Nov ~ Dec, 1978

Fig. II-3-9

point. The maximum depth of the subsidence of the basement rock corresponding to the negative anomaly L_2 is estimated 1,300 m near the measure point No. 111. An uplift block which is constained and localized by dislocations is also present in said subsidence, although smaller in scale than that shows in C–C′ cross-section.

A dislocation is presumed in the south wing of this subsidence. As the basement decreases its depth and shift gradually to the uplift structure corresponding to the positive anomaly H_4. The north wing of the subsidence touches the dislocations with the uplift corresponding to H_2 in the north.

Approximation is done for this cross-section analysis with the assumption of a large scale subsidence in the lower formation.

CHAPTER 4

ELECTRICAL SURVEY

Chapter 4. Electrical Survey

4–1 Purpose of Survey

Generally in the geothermal fields, the resistivity of the geothermal reservoir as well as the geothermal fluid itself show extremely low. Also in the Puchuldiza geothermal area, a wide and low resistivity zone less than 10 Ωm has been confirmed by Comite Geotermico, CORFO. But the electical survey method used in the early stage was the constant spread Schlumberger method with fixed electrode spacings of 250, 500 and 1,000m.

A distribution of low resistivity zones by the use of this method has been utilized to roughly delineate an interesting area but it contributes little to the analysis of the underground structure.

A more detailed survey by means of Vertical Electrical Sounding (VES) was employed to determine the resistivity of the structure at depths by increasing the electrode spacing continuously.

As the area between Mt. Tahipicollo and Tuja seem to be the most interesting, a study of the relation between the geothermal reservoir and its resistivity is the subject of this survey.

4–2 Method of Survey

4–2–1 Resistivity Method

Rocks and layers, of which the earth is composed of, have specific electrical properties (resistivities) each under different geological environments (i.e. the porosity and saturated water etc.). The resistivity method uses the resistivities of such layers and rocks for geological mapping of concealed structures. Especially, as the low resistivity zone of an area can be detected in the geothermal area, this method has been widely utilized in the geothermal field exploration.

By the variety of the location of current and potential electrodes at the ground surface, there have been many types of electrode configurations, like the Schlumberger array (as follows), dipole-dipole array, bipole-dipole array etc. The purpose of these arrays is to get the vertical distribution of the resistivity and moreover, the resistivity distribution at depth by changing the positions of electrodes.

In the case of a two-layer earth that consists of a first layer with a resistivity of ρ_1 and a thickness of h_1 and the second layer of ρ_2 and half-infinite thickness, the potential difference Va is changed dependent on the electrical resistance of the ground between MN. The resistivity is a function of the geometrical configuration of the electrodes and the electrical parameters of the ground (i.e. ρ_1 and ρ_2);

$$\rho a/\rho 1 = f(\rho 2/\rho 1, AB/2h_1)$$

Therefore, the objective of the quantitative interpretation is to determine the thickness of h_1 and the resistivity, ρ_2, of the lower layer from the field vertical sounding curve (VES) which is made by means of progressively increasing current electrode distance.

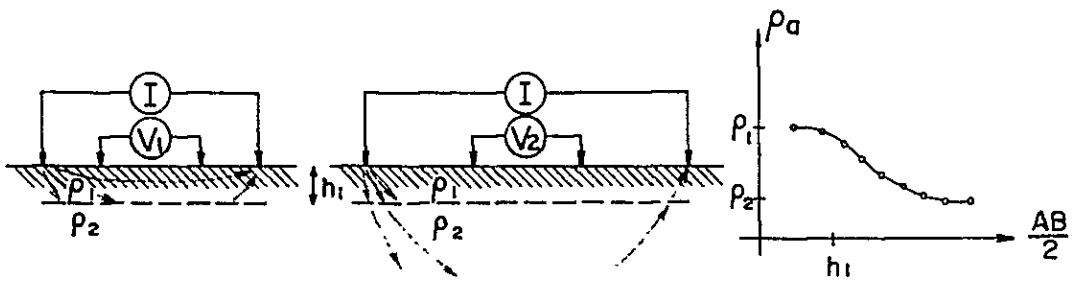

The interpretation is based on comparing the observed curves with the curves obtained theoretically.

Method ; Resistivity method using the Schlumberger electrode array

Electrode distance ; Current electrodes (AB/2) : 10 – 1,500m
Potential electrodes (MN/2) : 2 – 100m

Current ; Constant current of 0.1Hz square wave (0.1 – 2.0A). Current value is read from the current-meter of the out put of the transmitter and the current-wave is monitored by means of pen recorder.

Potential difference ; The potential difference curve bucking out self-potential is recorded by a pen recorder, and then the reading of low noise-level potential difference is read.

Schlumberger electrodes array ;

The points A, M, N, B are taken on a straight line such that the points M and N of potential electrodes are symmetrically placed about the center 0 of the current electrode distance AB as shown below.

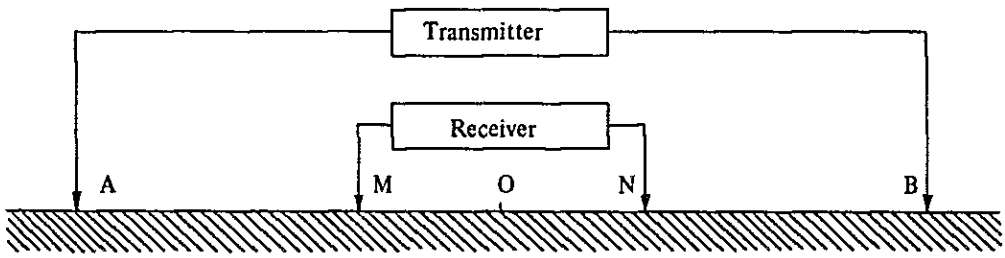

The layout for Schulumberger array used in this survey is shown in Table II–4–1. The VES (Vertical Electrical Sounding) curves was made by means of making twenty-one measurements for each point at the maximum AB/2 of 1,500m except for both end points of the survey line (details are mentioned at 4–3–3).

Table II–4–1 Measuring electrode spacing

No.	AB/2(m)	MN/2(m)	K	No.	AB/2(m)	MN/2(m)	K
1	10	2	75.4	12	200	40	1508
2	15	2	173.6	13	250	40	2392
3	20	2	311	14	375	40	5459
4	30	2	703.7	15	500	40	9755
5	40	2	1253	16	500	100	3770
6	50	2	1960	17	625	100	5979
7	50	10	377	18	750	100	8679
8	75	10	867.9	19	1000	100	15550
9	100	10	1555	20	1250	100	24390
10	150	10	3519	21	1500	100	31590
11	200	40	6267				

Where, K is called a geometrical factor depending on the configuration of the current as well as potential electrodes. K will be given as in the following equation, if AB/2 = L and MN/2 = ℓ;

$$K = \frac{2 \cdot \pi}{\frac{1}{AM} - \frac{1}{AN} - \frac{1}{BM} + \frac{1}{BN}} = \frac{\pi}{4} \frac{AB^2 - MN^2}{MN} = \frac{\pi}{2} \frac{L^2 - \ell^2}{\ell}$$

4–2–2 Survey Lines

It has been suggested that the northern area of five wells already drilled is interesting, according to various past surveys, and the geothermal fluids in Puchuldiza flow down form northern Cerro Blanco.

Therefore, survey line A running in an east-west direction on the low resistivity area north of Tuja and Mt. Tahipicollo, was planned.

By discussing with engineers of CORFO, the second survey line B was planned such that it runs in an east-west direction on the summit of Mt. Tahipicollo through the central part of the area between No. 2 and No. 4 wells, towards the south of Tuja.

An additional survey line C was planned in a north-south direction through Tuja in order to determine the north-south destribution of low resistivity zones by means of the Dipole-Dipole array method.

Location of above-mentioned lines is given in Fig. II–4–1.

Line	Line A	Line B	Line C
Length (m)	6,000	6,000	3,000
Method	Schlumberger array		Dipole-Dipole array
Number of observation point	23	23	44
Distance between observation points(m)	250	250	200
Coordinates	857N ~ 857.5N	856N	499.5E ~ 500E

The opened traverse surveys were done by means of pocket-compass and measuring tape.

The grid points of the coordinates established by CORFO were used as the base points of the surveys, that is, both survey line A and B were spread in an east-west direction from (857.5N, 503.5E, 4380.9mSL) and (856N, 503.5E, 4414.9mSL) corresponding No. 180 respectively as the base points.

The observation points were placed at a horizontal distance of 250m, after setting the auxiliary points at a horizontal distance of 25m. The number of points are given at the distance of 25m from the west end of survey line as 0, 1, 2, ..., 240.

4–2–3 Instruments

Instruments used in the electrical survey and their specifications are as follows:

Transmitting system;

Transmitter — Mitsubishi type power generator Model CH–506A, B (made by Chiba Electronics Inc., Japan)

- Output voltage: 200 – 800V
- Output current: Constant currents of 0.1, 0.25, 0.5, 0.75, 1.0, 1.25, 1.5, 2.0 and 2.5A
- Stability: less than ± 0.5%
- Frequency: 0.1, 0.3, 1, 3 and 10Hz (square wave)

Engine Generator — Model 421 (made by Geotronics Inc., U.S.A.)

- Engine Type: One cylinder, 4 cycle, gasoline fueled.
- Output: 3.9HP at 3428 rpm.
- Generator: Permanent magnet type, 115V, 17.3A, 400Hz, 2KW capacity

Receiving system;

Pen Recorder — Pen Recorder Model EPR200A (made by Toa Electronics Co., Japan)

Type Auto-balance potentiometer type, two pens, ink-writing recorder

Recording range: ± 1mV – ± 100V (sixteen ranges)

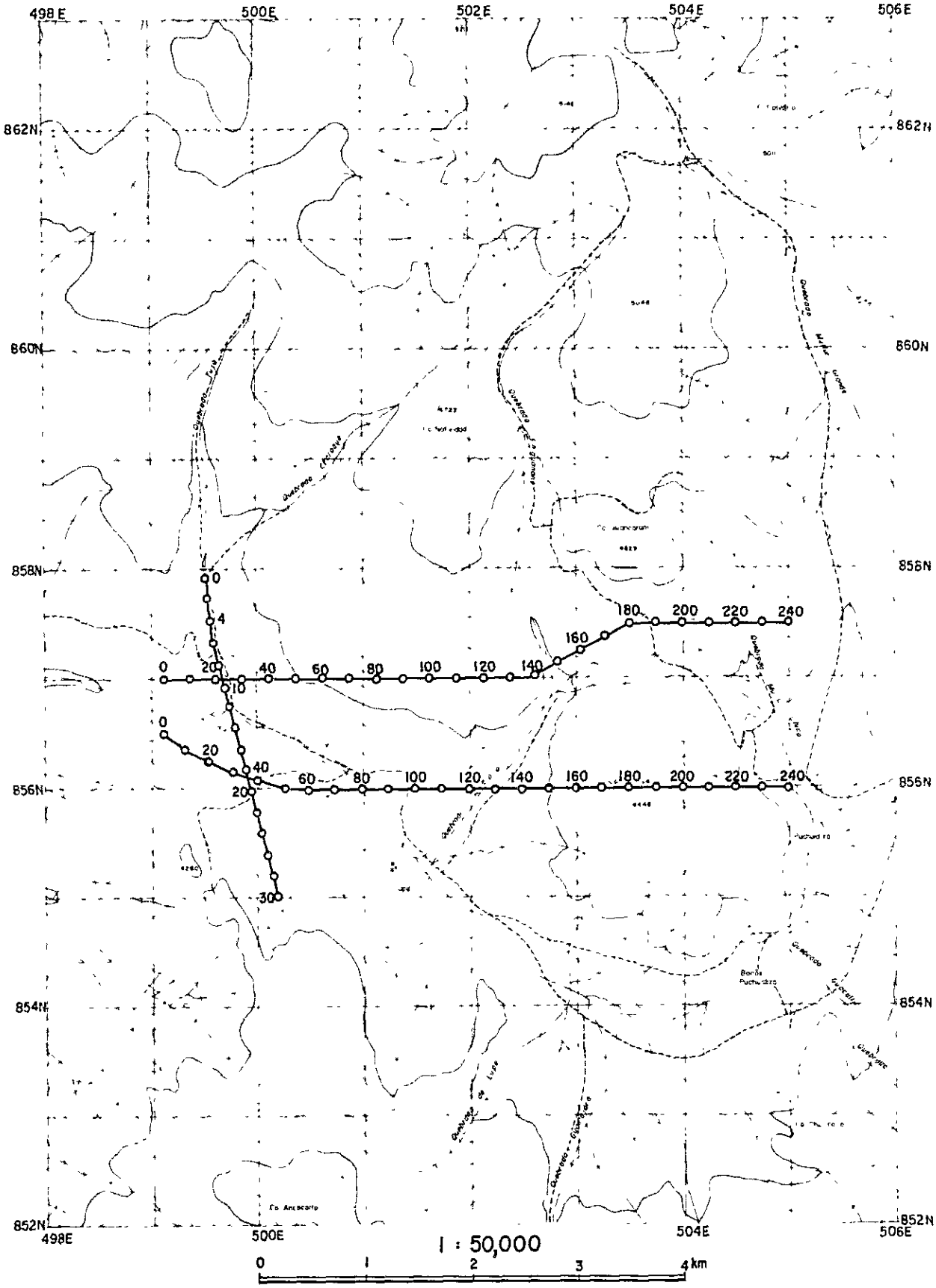

Fig II-4-1

LOCATION OF ELECTRICAL SURVEY LINES

	Input impedance	2MΩ for all ranges
	Chart speed	5mm/H – 320mm/H (thirteen ranges)
	Power	12VDC

Electrode;

Current electrode	Eight stainless steel rods with the diameter of 0.5cm and the length of 65cm.
Potential electrode	Unglazed porcelain pot (non-polarizing electrode) filled with a copper sulfate solution
Wire	Vinyle covered wire, IKIV ($1.25mm^2$)

Block diagram of observation system is as follows.

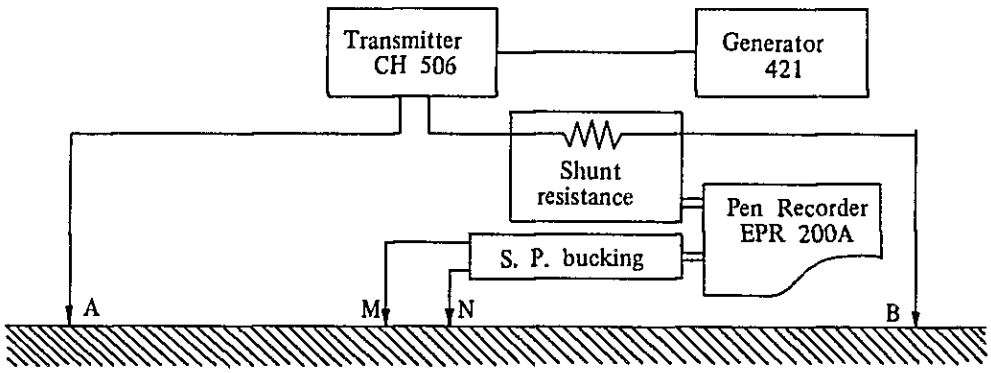

4–3 Method of Analysis

4–3–1 Procedure of analysis

The values of current and potential differences were read out from the waves on recording chart in order to calculate apparent resistivities. Generally, the potential difference waves involve many types of noises such as spontaneous potential, telluric current, current ripples, current leakage, etc., besides signal waves. In this survey, the dignal-to-noise ratio of the potential difference is low as AB/2 is increased, and moreover, the disturbance of waves sometimes occur due to thunder. For these disturbance waves, the values of potential differences are calculated by averaging several point values of wave forms.

Apparent resistivity is calculated from following equation;

$$\rho a = \frac{\pi}{4} \cdot \frac{AB^2 - MN^2}{MN} \cdot \frac{V}{I} \ (\Omega \cdot m)$$

The VES curve is obtained by means of plotting apparent resistivity on the ordinate vs. AB/2 on the abscissa, on the double logarithmic graph.

Observed VES curves are different from the theoretical VES curves due to the effects of topographical changes, mean surface geology and local resistivity distribution, etc. Only the effect of the topography can be corrected quantitatively, using the terrain correction mentioned in following paragraph.

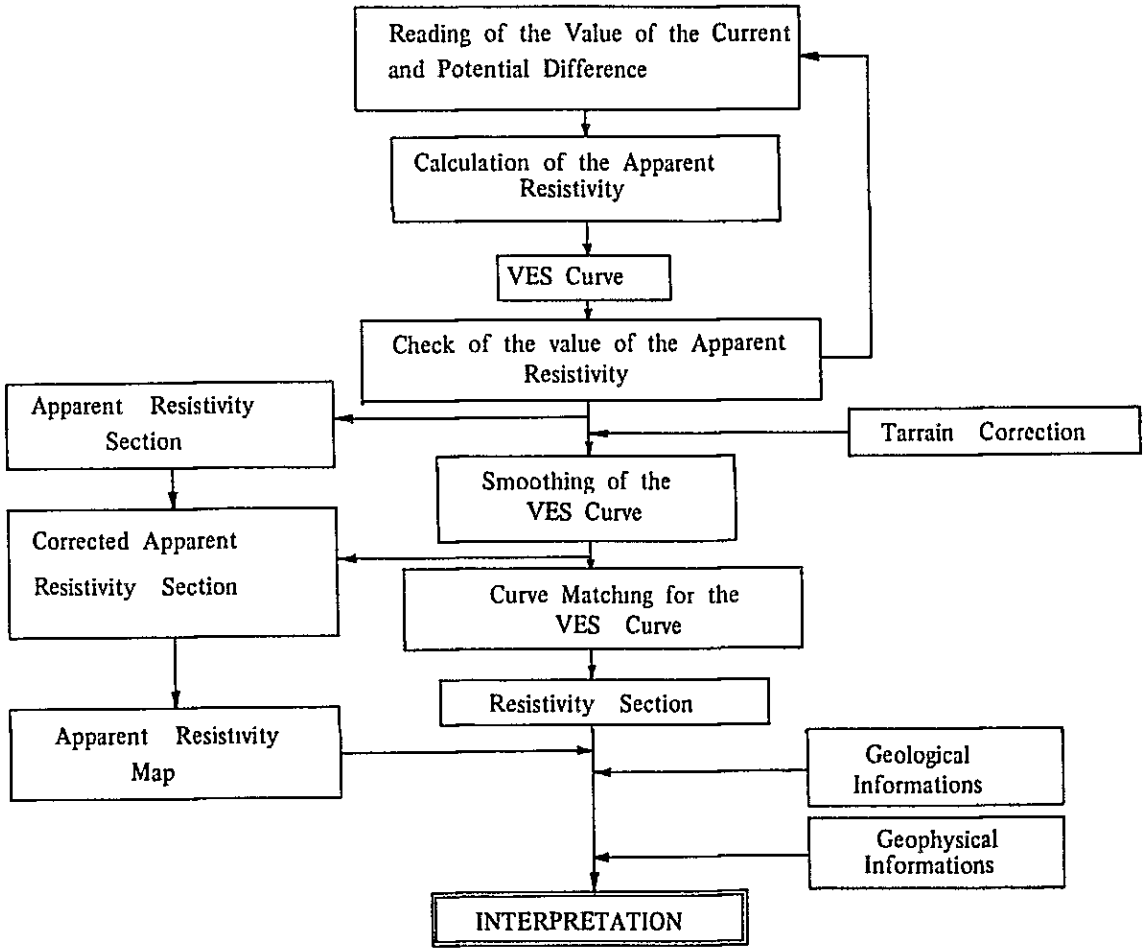

FLOW CHART FOR ANALYSES OF THE ELECTRICAL SURVEY

After the quantitative terrain corrections are made, the smoothed VES curves for making a curve-matching method, are derived by experimental and quantitative corrections by means of comparing the values of neighbouring points for compensating the effect of local resistivity distribution, especially shallow, local distribution which may affect other stations.

The quantitative interpretation for a horizontally stratified structure is made by comparing the smoothed VES curves with the theoretical VES curves, that is, Schlumberger's standard curves of two layers and three layers, and Ono's auxiliary curves.

Sometimes the resistivity structure given by the above-mentioned procedure do not necessarily fit with the geological structure.
In these cases, either the resistivity or thickness of the intermediate layers are changed, and if there is a discontinuity between neighbouring stations, a fault (a discontinuity line of resistivity) is assumed at such point.

4–3–2 Terrain Correction

The VES interpretation is based on the assumption that the measurements are made on a flat surface of a semi-infinite horizontally stratified structure. But as in the mountainous areas, where the observed VES curves are subjected to the effects of the topographical changes, the analysis should be made after the compensation of these effect.

For the method of the terrain correction, there are many types of approximate computation for two and three dimentional topography. As three dimensional computations are very expensive, two dimentional computations are generally made.

It is assumed that there is a semi-infinite, homogeneous earth of the resistivity, ρ_0, and only the variation of the topography causes change in observed resistivities. If, ρ_a is the apparent resistivity measured at the surface, then C is calculated by the equation $C = \rho_0/\rho_a$. C is regarded as the first approximated coefficient for terrain correction and is called as the terrain correction factor. If the values of C are given for each stations, the terrain corrected apparent resistivity, ρ_c for the observed apparent resistivity ρ, is given by the following equation;

$$\rho_c = C \cdot \rho = \rho_0 \cdot \rho / \rho_a$$

For this survey, the terrain correction was made two-dimensionally by means of the conductive paper. It was done for the locations of the considerably rough topography, that is, between No. 130 and No. 180 of Line A, between No. 90 and No. 130, and between No. 160 and No. 200 of Line B, with AB/2 greater than 50 m from the restriction of the accuracy of the scaled section.
The scale of the topographical section is usually 1:10,000 and 1:5,000 for the locations of considerable rough topography.

Instruments for the terrain correction are as follows;

Oscillator	Model E–1011, made by NF Design Block Inc., Japan.
Constant Current Generator	
	Induced Polarization (I. P.) Transmitter,
	made by Geoscience Inc., U.S.A.
Recorder	Model EPR–200A, made by TOA Electronics Co., Japan.
Conductive paper	ANACON Paper, made by Tomoegawa Paper Manufacturing Co.,
	Japan. (resistivity 3 Ω m, 90cm x 50cm x 0.35mm)

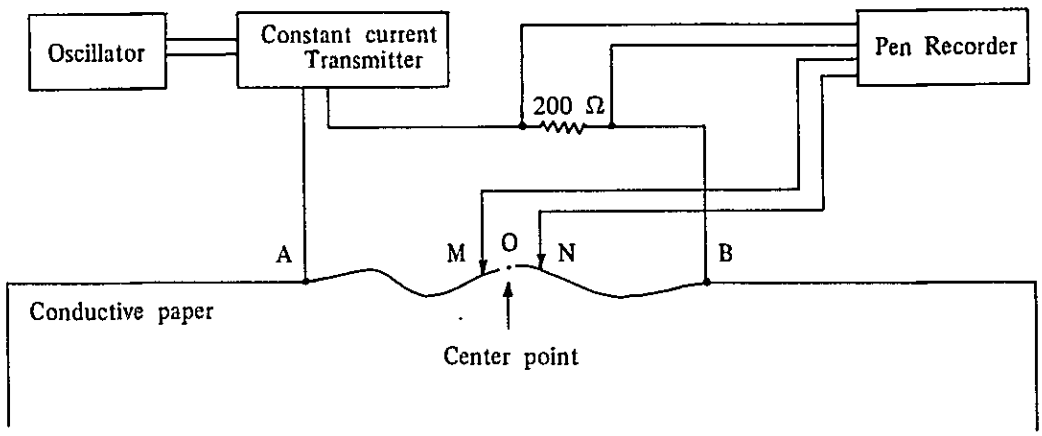

Schematic Diagram for Terrain Correction

As the apparent resistivities, ρ_a on the conductive paper are measured two-dimensionally, ρ_a should be calculated by the following equation;

$$\rho_a = \frac{V}{I} \quad \frac{\pi}{2 \cdot \ell n \left[(L+\ell) / (L-\ell) \right]}$$

where, I is the current, V the potential difference, L=AB/2 and ℓ = MN/2.

Usually, for the Schlumberger electrodes array, the apparent resistivities below the valley are high, on the other hand the ones below the hill are low.

In the figure it can be seen that in this survey the resistivities below the valley are 1.3 times as high as, and the resistivities below the hill 0.8 times as low as the ones below the flat surface.

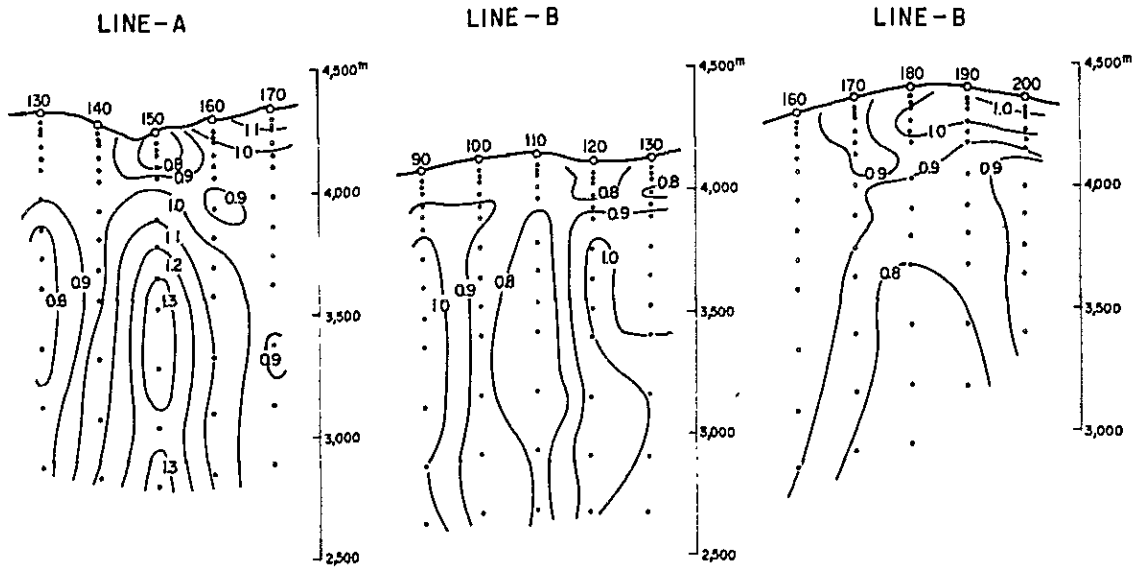

Distribution of Apparent Resistivity on Conductive Paper.

4-3-3 Classification of VES Curves

The smoothed VES curves obtained in this survey are classified into H-type ($\rho_1 > \rho_2 < \rho_3$) and Q-type ($\rho_1 > \rho_2 > \rho_3$) of three-layer type, and KH-type ($\rho_1 < \rho_2 > \rho_3 < \rho_4$) and QH-type ($\rho_1 > \rho_2 > \rho_3 < \rho_4$) of four-layer type which are constructed by combining some kinds of three-layer type curves, as follows:

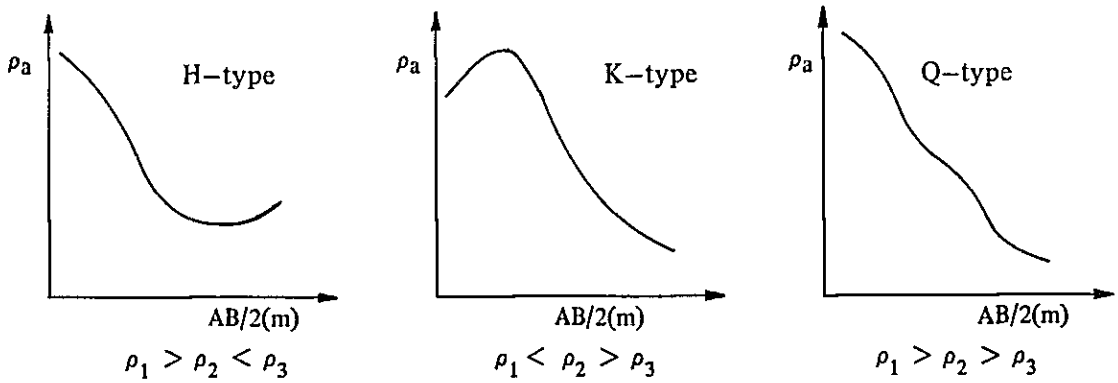

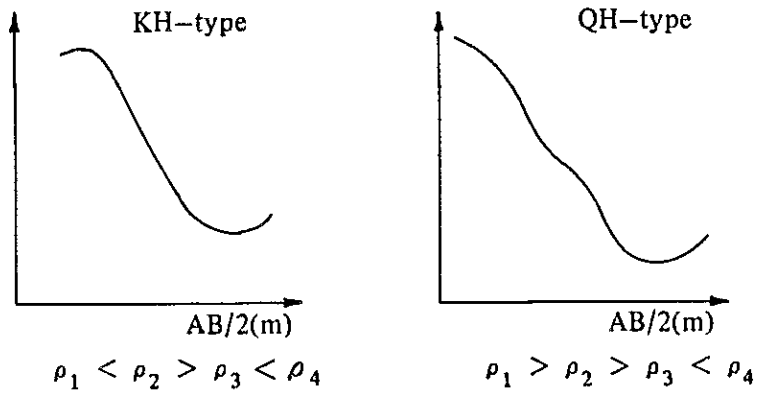

Classification of VES Curves

4–4 Result of Resistivity Analysis

4–4–1 Apparent Resistivity Section

An apparent resistivity section is made by plotting the apparent resistivity read out from the smoothed VES curve at the depth equal to AB/2 from ground surface. From this section, the general vertical distribution can be estimated. The contour pattern at the area of horizontally stratified structure is parallel to the ground surface, but it may be disturbed by lateral changes of layers or rocks, faults, and shallow and local resistivity distributions. An analysis of these effect is therefore necessary.

Line A (Fig. II–4–2)

The low resistivity zone may distribute at depth throughout Line A section, shallow at both ends of the line and deep at the central part of the line.

It is suggested that the high resistivity zone at near surface corresponds to a Quaternary lava and exist as a bed. At the eastern part of No. 150, the overburden of lava may exist as a bed as shown by the low resistivity in many parts of the area. Near a creek at Mulluri Chico, No. 210, the apparent resistivity near the surface tends to increase with depth progressively to the west.

There is a considerably low resistivity zone at the shallow part between No. 20 and No. 30, due to the Tuja fumarole zone.

Disturbances of contour at depth were observed between No. 40 and No. 60, and at No. 110.

These disturbances may be due to local low resistivity distributions.

Line B (Fig. II–4–2)

There are low resistivity zones at both ends of the line as in Line A. A especially distinguishable low resistivity zone exists at east Tahipicollo.

Although the high resistivity layer near the surface corresponds to the Quaternary lava,

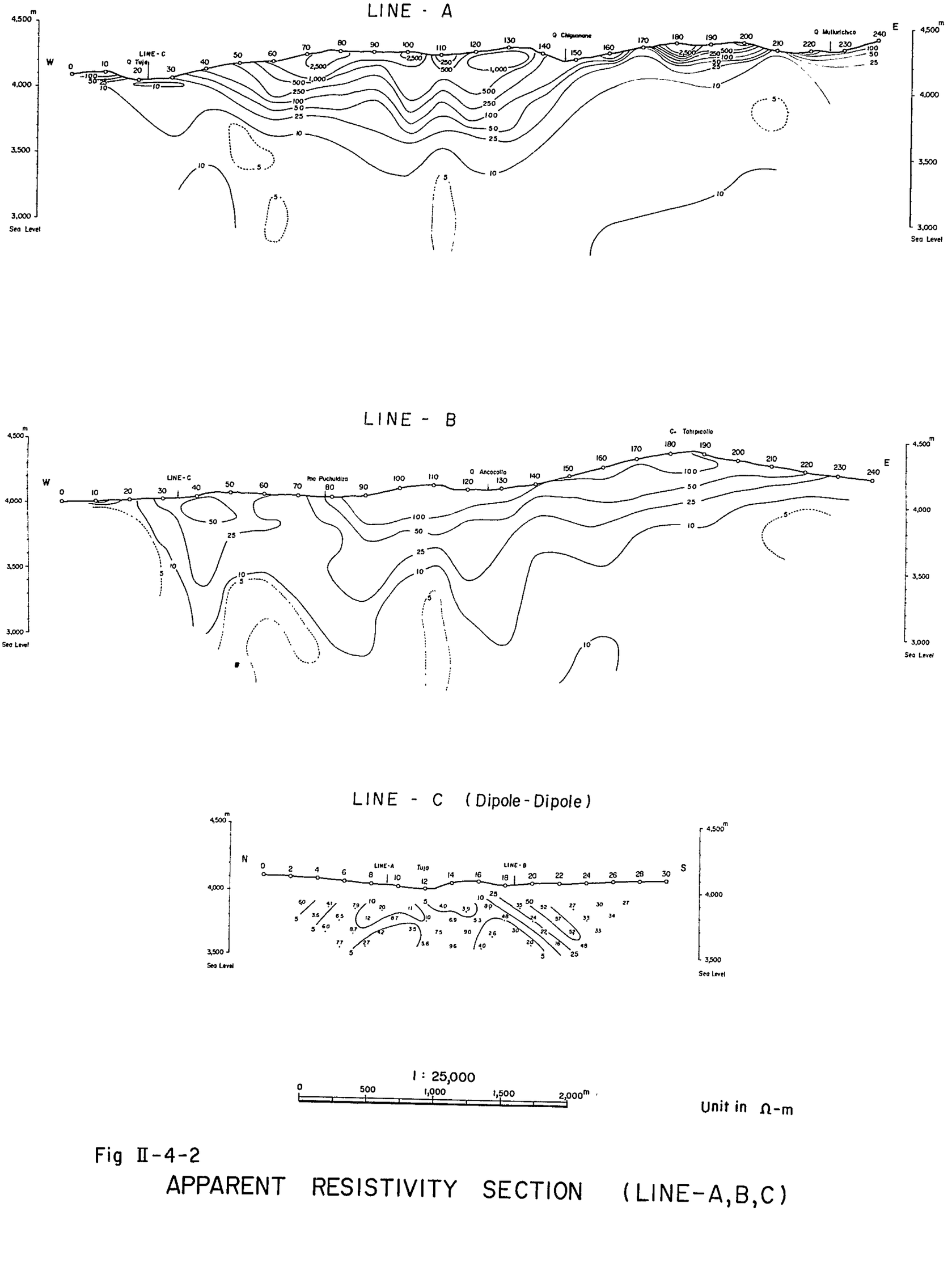

Fig II-4-2

APPARENT RESISTIVITY SECTION (LINE-A,B,C)

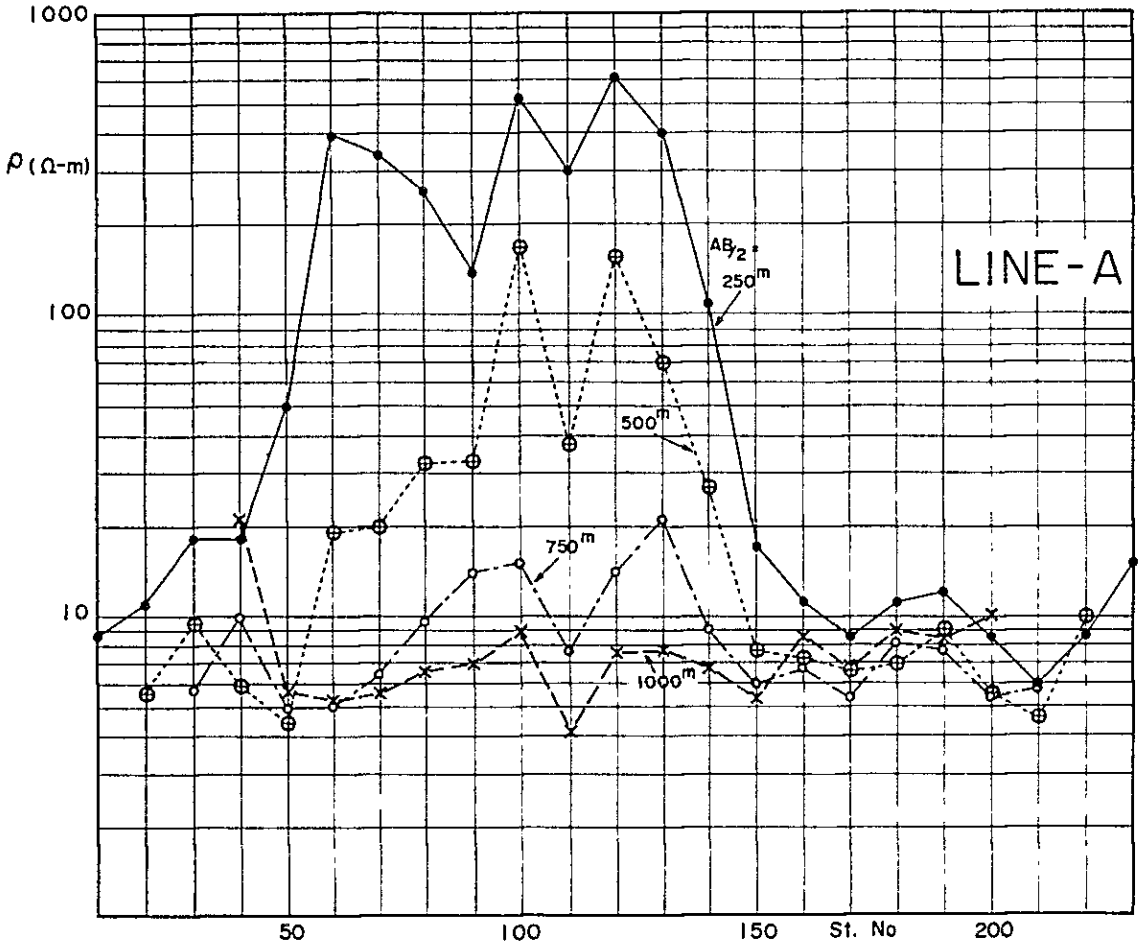

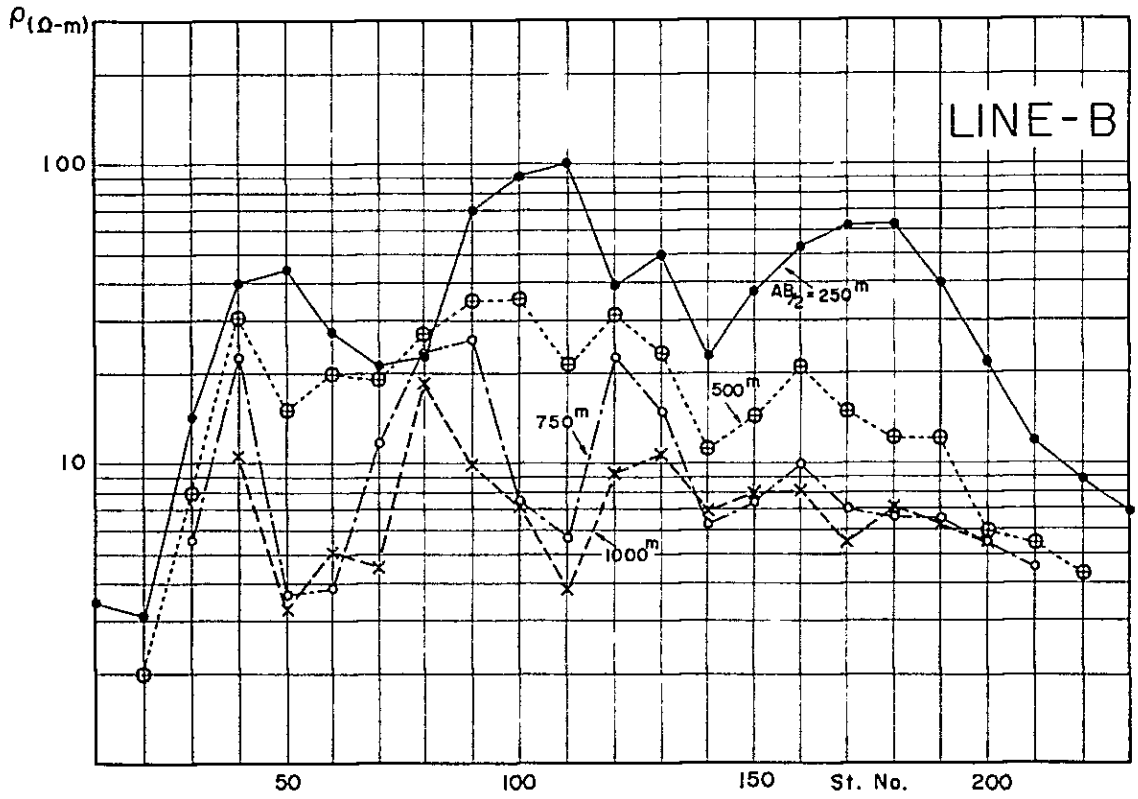

Fig II-4-3

LATERAL CHANGE OF APPARENT RESISTIVITY

its resistivity is one-tenth as low as the one on Line A.

South of Tuja, the apparent resistivity at No. 10 and No. 20 is less than 5 Ω m, and shows the lowest resistivity in this area.

Furthermore, low resistivity zones and disturbances of contour line at depth exist between No. 50 and No. 60, and No. 110.

It seems that the low resistivity zone, less than 5Ω m, around No. 200 may correspond to shallow hydrothermal reservoir. The exploratory wells of No. 3 and No. 4 are located approximately 700m north of this location, and No. 2, about 1200 m south.

4–4–2 Apparent Resisitivity Map (Fig. II–4–4, II–4–5)

These maps were made by incorporating the survey results of early maps. Although there may be a little difference between the apparent resistivity and the resistivity at each station, the apparent resistivity map may show an idea of the surface variation of resistivity within a certain depth.

AB/2 = 500m (Fig. II–4–4)

At the west ends of both lines, there are distinguishable low resistivity zones with N–S strickes, which may correspond to the Tertiary pyroxene andesite and the Quaternary lapilli deposits.

Although there is a NW–SE geotectonic line running near No. 150 of Line A which extends to No. 190 of Line B, the apparent resistivities at the north and east sides of Mt. Tahipicollo, that is, the north-east side of this line, is lower than other areas.

At the Mt. Natividad, there is a high resistivity zone at the central parts of both lines which may corrspond to the Quaternary amphibole sericite andesite.

AB/2 = 1,000m (Fig. II–4–5)

On the map of AB/2 = 500 m, there are two N–S, low resistivity zones extending to the north from Puchuldiza and the other running through Tuja. In this map, the two low resistivity zones were combined to one broad low resistivity zone of 6 km in NW–SE and 3 km in NE–SW directions. In this broad zone, the interesting one is a low resistivity zone (less than 6 Ω m) between No. 50 and No. 70 of both lines.

Although the resistivity is not large, this may indicate that a deep geothermal reservoir exist.

4–4–3 Resistivity of Rocks and Water

The resistivities of thirty-three rocks sampled at the site were measured as shown in Table III–2–1. The transmitter and receiver used are similar to those employed for terrain correction. Cubic rock samples measure 4 cm x 4 cm x 3 cm while core samples have the following dimensions of 4 cm in diameter x 4 cm in length. The samples were prepared by diamond cutter. The resistivities of these samples were measured on the wet condition after being saturated in 0.1 N–KCl solution (resistivity of 50 Ω m, temperature of 15°C) for 48 hours.

The current supplied into the rock samples was the constant current square wave of 2μA with 0.1 Hz. The potential electrodes used were the spiral copper lines contained in KCl solution which were recovered by using filter paper.

The resistivity of rock samples is given by the following equation:

$\rho = (s/l) \cdot (v/I) \times 1/100$

s : section area of rock sample (cm^2)

l : length of rock sample (cm)

v : potential difference (mv)

I : supplied current (mA)

The observation system of the resistivity of the rock sample is as follows

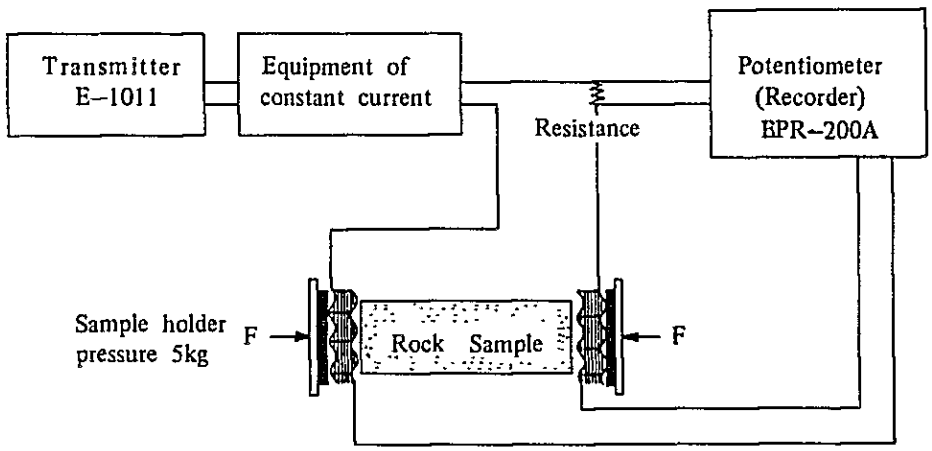

Block diagram of the Resistivity measurement of rock sample.

The result of the observations were classified according to the geological rock type, as shown in the list below.

Rock type	Average		Deviation (Ω m)
Quaternary Andesite	(1.2	±	0.2) x 10^3
Tertiary Andesite	(3.2	±	1.0) x 10^3
Andesitic Welded Tuff (Quaternary)	(0.5	±	0.2) x 10^3
Dacitic Welded Tuff (Tertiary)	(1.9	±	0.9) x 10^2
Dacitic Tuff (Quaternary)	(1.3	±	0.5) x 10^2
Rhyolitic Tuff (Cretaceous)	(1.8	±	0.5) x 10^2

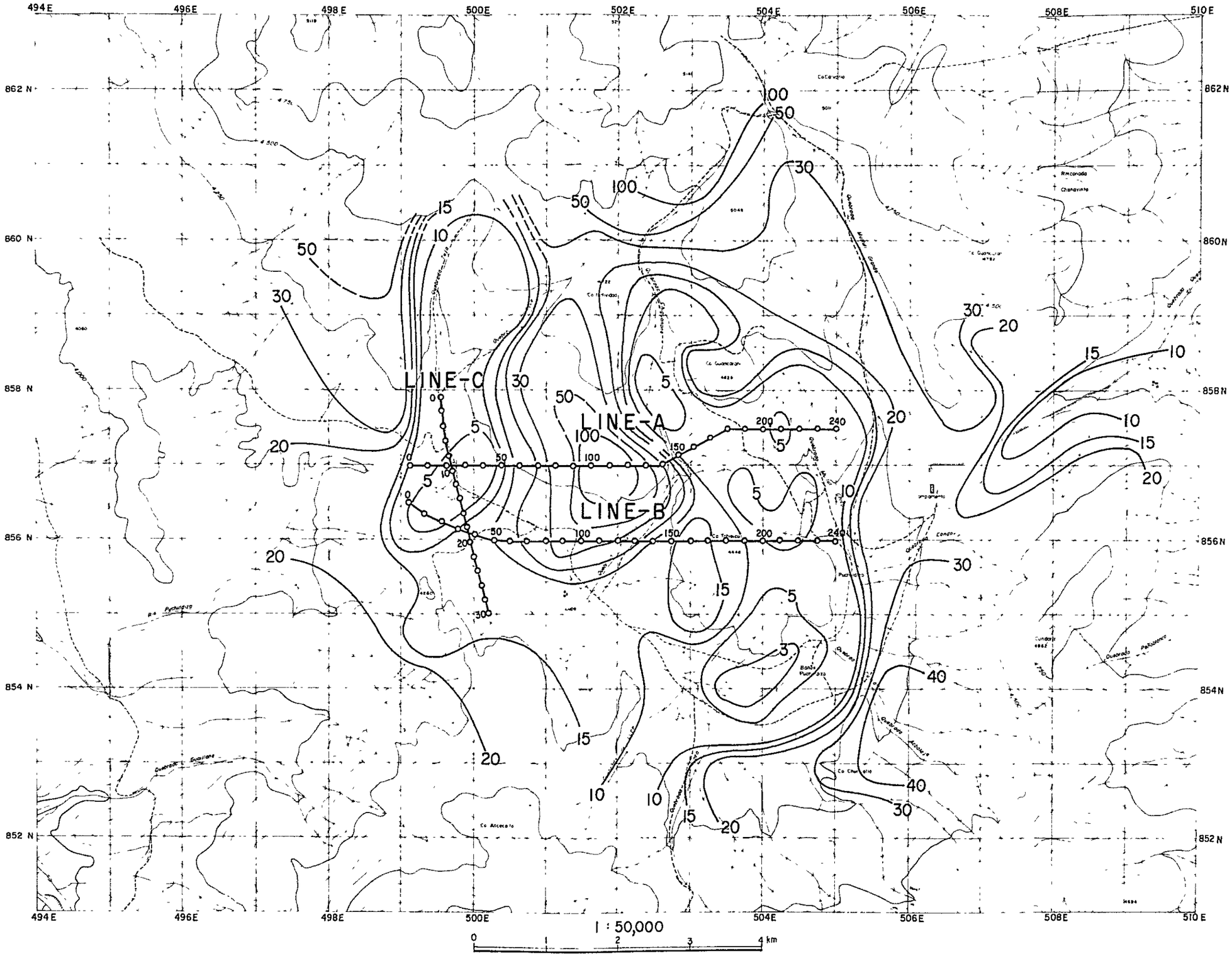

~·10
Contour Line of
Apparent Resistivity
Unit : Ωm

Geothermal Power Development Project
in Puchuldiza
the Republic of Chile

APPARENT RESISTIVITY MAP

AB / 2 = 500 m

1 : 50,000
0 1,000 2,000 m

Nov ~ Dec, 1978

Fig II-4-4

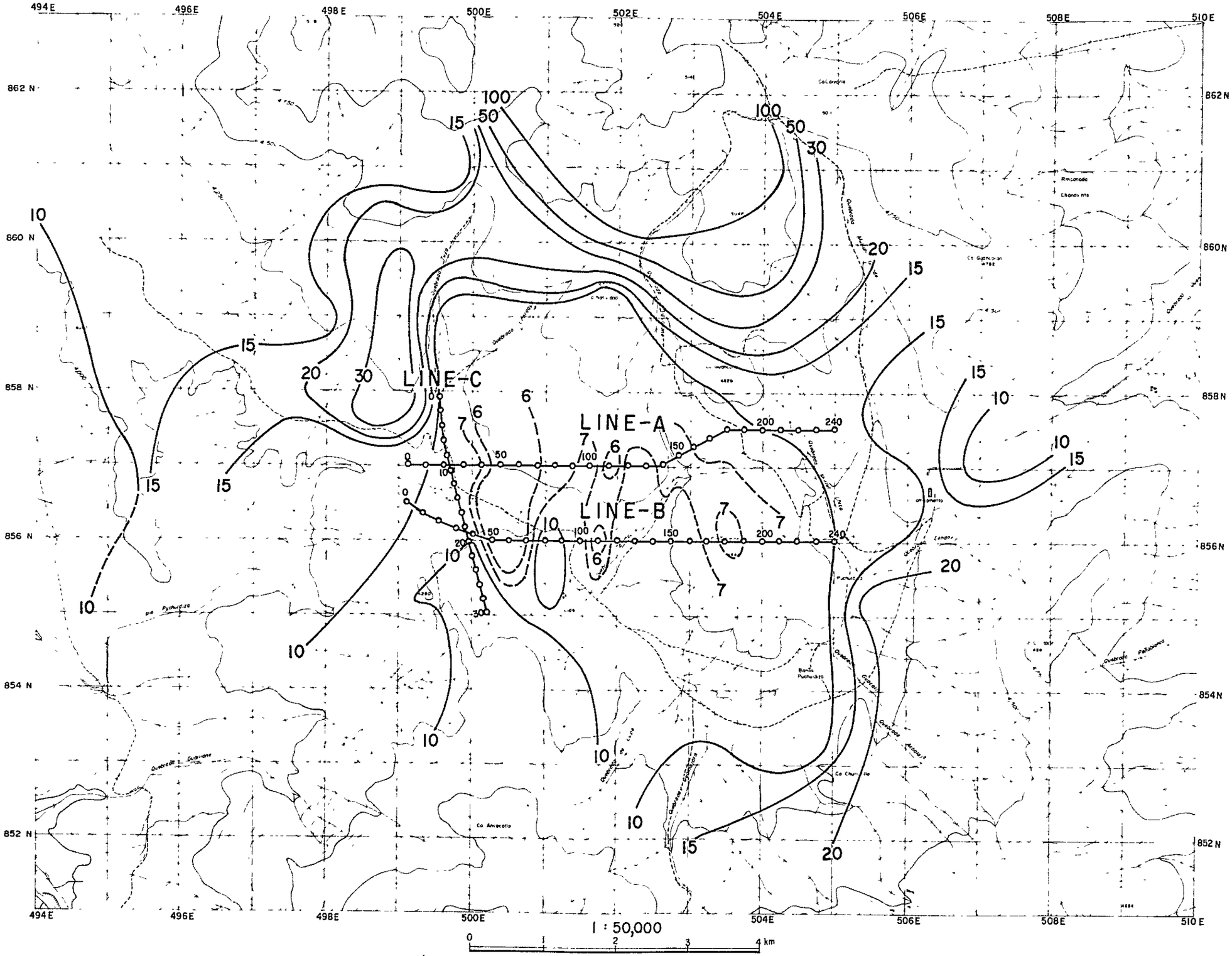

~10 Contour Line of Apparent Resistivity Unit : Ωm

Geothermal Power Development Project in Puchuldiza the Republic of Chile

APPARENT RESISTIVITY MAP

AB / 2 = 1,000m

1 : 50,000

0 1,000 2,000m

Nov~Dec, 1978

Fig II-4-5

From the list, the andesites indicate low porosity and high resistivity, while the tuffs indicate low resistivity. Both rocks may be separated by a boundary line of approximately 300 Ω m. However, it seems the resistivity may become low under the high temperature and high pressure in the depth and may become several Ω m in the geothermal reservoir because of the effect of hot saline water.

Resistivity of the surface water (Table II–4–2)

Location of the surface water and hot water, is shown in Fig. II–1–5. The results of the observation values were converted into 20°C as follows:

River water (containing hot water)	1.7 – 2.7 Ω m.
Flushing water of the exploratory wells	1.7 – 2.2 Ω m.
Well water	46 Ω m.

In this area, the resistivity of the river water does not change because the river water is almost the flushing type. The well water at the camp site is the surface water.

Furthermore, the resistivity of the surface water in the other area may become high because the Cl^- density of the well water is very low.

4–4–4 Resistivity Section

The resistivity and thickness of each resistivity layer were determined by the analysis of the VES curves observed in each station, and the resistivity section was made by plotting these evaluated data.

The resistivity is classified as the upper layer (high resistivity), the intermediate (low resistivity) and the lower (high resistivity), respectively. "Uncontinuous Resistivity Line" was drawn at part which indicated complete difference in the thickness and the resistivity both in lateral direction, compared with the neighboring stations.

A resistivity of the layer greatly varies with the rock condition (rock type, porosity, composition of layer-water, temperature, etc.). In most geothermal area, the location of the geothermal fluid corresponds to the low resistivity zone less than 10 Ω m.

Classification of the resistivity layer (Table II–4–3)

1) Upper layer (high-resistivity)

a–layer (1,000 – 3,000 Ω m)

This layer is distributed between No. 60 and No. 100 and near No. 180 on Line A, having the thickness of 0 to 200m. It corresponds to the Quaternary andesite (amphibole-biotite andesite).

b–layer (100 – 600 Ω m)

The layer is between No. 40 and No. 110, near No. 140 and No. 40, between No. 90 and No. 190 on Line B, its thickness is about 100m, and corresponds to the Quaternary andesite and Tertiary pyroxene andesite or the altered a–layer.

Table II-4-2 Resistivity of Surface Water

Instrument: Conductivity meter CM-1F TOA Electronics Co., Japan

Sample No.	Location	Observed value (Ω-m/°C)	Converted value (Ω-m/20°C)	Mean value (Ω-m/20°C)
a	Rio Tuja (above)	22.0/18	21.0	
b	" (middle)	5.2/31	6.2	River water
c	" (down)	1.7/31	2.4	1.7 - 2.7
d	Rio Puchuldiza (down)	1.7/21	1.7	
e	" (down, pool)	2.0/21	2.0	Above the river
f	" (middle)	1.7/21	1.7	20.0 - 35.0
g	" (above)	1.7/21	1.7	
h	" (middle)	20.0/21	20.0	
i	Q. Chulicollo (down)	1.8/17	1.7	
j	" (above)	1.6/45	2.6	
k	" (above, water fall)	1.0/81	2.7	
l	Q. Ancocollo (middle)	35.0/20	35.0	
m	Q. Chiguanane (down)	20.0/16	18.0	
n	" (")	20.0/21	19.9	
o	Pozo 1 (hot water)	1.7/21	1.7	Spouting hot water
p	" 2 (")	1.5/38	2.2	1.7 - 2.2
q	" 2 (")	2.2/21	2.2	Surface water
r	Campament (well water)	70.0/5.5	46.0	46.0

* Converted values into 20°C by means of the Schlumberger's relation curve between density of NaCl solution and resistivity.

Table II-4-3 Classification of VES curves (1)

Unit in Ω-m

LINE A						
STATION	TYPE	UPPER LAYER			MIDDLE LAYER	LOWER LAYER	REMARKS
10	2*		b 210		5.5		2*;two layer type
20	HK	c 43	5.0	72	4.0		----- : fault
30	HK	50	6.0	60	4.0		
40	QH	a	b 130	25	3.0	(35)	
50	H		260		3.0	(30)	
60	QH	1400 850	150		3.0		
70	QH	2500	300		4.0		
80	QH	2800	310		5.0	(20)	
90	QH	2300	400		6.0	(20)	
100	QH	3000	500		6.0		
110	KH		680		5.0		
120	H	1400			5.0		
130	H	1400			4.0		
140	HK	b 330 110	420		4.0		
150	QH		240	c 60	5.0	(20)	
160	H		600		5.0	(25)	
170	QH	c	43	40	6.0	(20)	
180	H	a	4300		5.0	(20)	
190	QH		780	87	6.0	(20)	
200	QH		1200	13	4.0	(40)	
210	Q		30	8	4.0		
220	Q	b	410	c 22	4.0	(12)	
230	Q		160	32	3.5		

Resistivity Classification		Resistivity(Ω-m)	Thickness (m)
I	Upper L.	a 1,000 - 3,000	0 - 200
		b 100 - 600	100±
		c 20 - 90	100 - 400
II	Middle L.	3 - 6	500 - 700
III	Lower L.	15 <	

Table Ⅱ-4-3 Classification of VES curves (2)

Unit in Ω-m

LINE B						
STATION	TYPE	UPPER LAYER			MIDDLE LAYER	LOWER LAYER	REMARKS
10	H	c		50	2.5		
20	2*			25	2.0		2* : two layer
30	2*			22	3.0		type
40	Q	b	220	23	3.0		
50	H			45	2.5	(25)	----- : fault
60	H			30	2.5	(30)	
70	H			25	2.7	(30)	
80	Q		55	30	2.5		
90	QH	b	220	44	4.0		
100	QH		200	30	3.5	(30)	
110	QH		200	50	3.5		
120	KQH		160	35	3.5		
130	QH		170	45	4.0		
140	H			70	4.0	(30)	
150	H			75	4.0	(25)	
160	H	b	100		4.0	(35)	
170	H		100		4.0	(30)	
180	H		150		4.0	(25)	
190	KH		140		4.0	(25)	
200	H	c		80	3.0	(20)	
210	H			75	3.0	(20)	
220	QH		50	25	2.5	(15)	
230	2*			25	(3.0)		

Resistivity Classification		Resistivity (Ω-m)	Thickness (m)
I	Upper L.	b 100 - 400	100+
		c 20 - 90	100 - 400
II	Middle L.	2 - 4	500 - 700
III	Lower L.	15 <	

c–layer (20 – 80 Ω m)

The distribution of c–layer is in Tuja altered zone between No. 20 and No. 40 of Line A, and on the east side of No. 140 of Line A, and between No. 20 and No. 150 of Line B and on the east side of No. 200 of Line B. Its thickness range from about 100 to 400 m, and corresponds to andesitic welded tuff of upper Puchuldiza formation.

2) Middle layer (low-resistivity) 2 – 6 Ω m

It distributes thickly under both survey lines. In Tuja and Puchuldiza, near the end of survey lines, the resistivity is lowest between No. 90 and No. 100 in Line B. Its thickness is about 500 to 700m and corresponds to andesitic welded tuff of Puchuldiza formation, dacitic welded tuff of Condoriri formation, and green sand stone of Chojña Chaya formation.

According to the calculated effective porosity as shown in the Table III–2–1, the resistivity of Condoriri formation is presumed to be the lowest with the tendency to gradually increase, proportional to high depth increment.

3) Lower layer (high-resistivity) 15 Ω m<

The basement layer is detected from the rising of the VES curve. Here, the resistivity is higher than upper layer, but the resistivity values could not be determined exactly.

In both survey lines, it grows shallow on the east side and deep on the west, and not detectable at the west ends of these lines. This seems to correspond to rhyolitic welded tuff of Utayane formation, but the thickness is not calculated.

The presumed resistivity values from the cores of well No.4 and No.5 are also a little high. The drainage of wells in the Puchuldiza area occur mainly in this layer.

Line A (Fig. II–4–6)

In the Upper layer (high-resistivity), a and b–layers, more than 600 Ω m has been covered between No. 40 and No. 130. It corresponds to the Quaternary andesites and the Tertiary pyroxene andesites, having the thickness of 100 to 200m. It may be thin at the top of Mt. Tahipicollo, but is not recognized on the east side of Chiguanane swamp. The low resistivity zone of the surface at No. 170, No. 190 and No. 210, coincide with the surface altered zone.

Between No. 40 and No. 60, and at No. 210, the middle layer (low-resistivity), which has the resistivity of less than 5 Ω m, was detected. At the depth of about 400m in No. 40 to No. 50, geothermal fluid associated with low resistivity may be expected. However, the lower layer exists comparatively at the shallow part but then its depth becomes deeper toward the east. At No. 210, the notable low

resistivity exists from the surface. Thus it seems that the geothermal fluid exist in a considerably shallow part.

The low resistivity layer between No. 70 and No. 130 has a thickness of about 800m. It may be cut by the uncontinuous resistivity line which is presumed to be on the west side of Chiguanane swamp.

The Resistivity values are also comparatively high between 5 to 6 Ω m to the east of No. 140. The thickness of the low resistivity layer may decrease to about 500m, and there is a tendency for the layer to become shallower toward the east based on the topography.

The lower high-resistivity layer to the east of No. 80 corresponds to Utayane formation but it may be slightly altered on the upper layer. In the lower high-resistivity layer, it seems that the portion where a lot gaps exist in may be a promising reservoir.

Line B (Fig. II–4–6)

Compared to Line A, a–layer does not exist but c–layer, having the resistivity of 20 to 80 Ω m, is distributed thickly. On the southern portion of Tuja, at the western edge of the survey line, on the west side of the fault between No. 20 and No. 30, a notable low resistivity zone of 2Ωm was delineated. This resistivity is lower than that of Tuja springs and was confirmed by the thermally altered zone toward the south. An anticlinal structure exists between No. 60 and No. 70, and low resistivity values of 2.5 to 3 Ω m has been recorded indicating the presence of latent geothermal fluid at depths. This area is the most interesting along this line.

c–layer is discontinuous between No. 80 and No. 90, and a fault was assumed because the lower high-resistivity layer has not been detected at depth. To the east of No. 90, the middle low-resistivity layer becomes monotonously shallow toward the east, and at No. 220 in the eastern Tahipicollo, the reservoir may be detected at a shallow depth.

The exploratory well No. 2 is located approximately 1,200m due south while the exploratory wells No. 3 and No. 4 are located about 800m due north. A reservoir of hot water at the shallow depth of 300m existing continuously from south to north has been verified.

Line C

The additional survey line was carried out using the double dipole method in order to find out the N–S extension of Tuja altered zone. At the intersection with Line A, the resistivity is higher than 20 Ω m at shallow depth, becoming lower than 3 Ω m at depth below 200m. On the other hand, at the interesection with

LINE-A

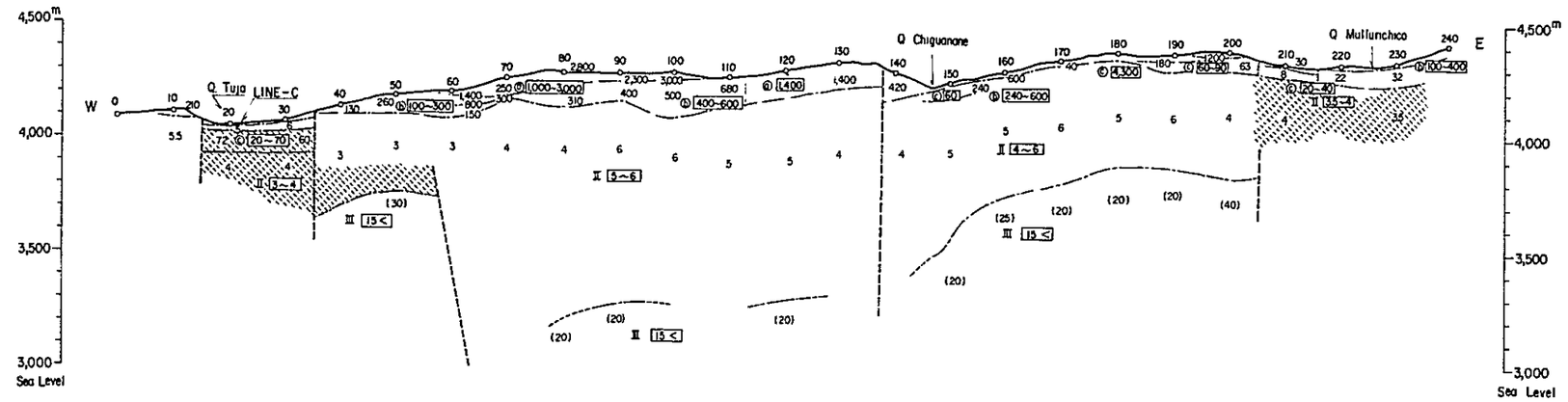

LINE-B

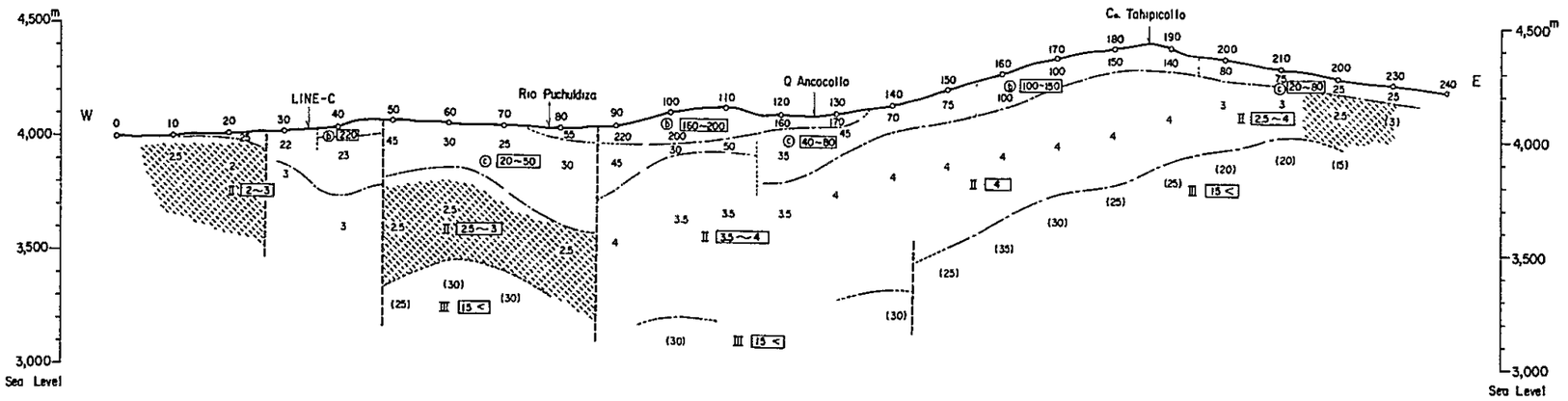

Geothermal Power Development Project
in Puchuldiza
the Republic of Chile

RESISTIVITY SECTION
(LINE-A,B)
(Unit Ω-m)

1 : 25,000

0 500 1,000 1,500 m

Nov ~ Dec, 1978

Fig II-4-6

Line B, the low resistivity values less than 3 Ω m was detected below 200m.

The resistivity changes very much, whereas to the south of line B low resistivity has not been detected.